

A thesis submitted to the Faculty of Civil Engineering of Graz University of Technology in partial
fulfilment of the requirements for the degree of Master of Science

The Stability Behaviour of Steel T-sections under Axial Compression

Master Thesis

Joshua P. Tapley B.Sc.

Graz University of Technology

Institute for Steel Structures

Head : Univ. Prof. DI Dr. Harald Unterweger

Supervisor:

Univ. Prof. DI Dr. Harald Unterweger

Assisting Supervisors:

Ass.Prof. Dipl.-Ing. Dr.techn. Andreas Taras

Dipl.-Ing. Dr. Markus Kettler

Graz, December 2013

Statutory Declaration

I declare that I have authored this thesis independently, that I have not used other than the declared sources / resources, and that I have explicitly marked all material which has been quoted either literally or by content from the used sources.

Graz, _____
Date

Signature

Abstract

Dimensioning of T-sections is usually carried out using methods originally developed for double symmetrical sections such as I-beams. This can lead to very conservative results for shorter length members. This becomes even more apparent when using Eurocode 3 to dimension T-sections prone to plate buckling (class 4 sections). According to the Eurocode, an effective section, rather than the gross section, must be used to calculate the dimensions of the section. In this case, an additional effective moment has to be considered which is due to the distance between the effective section's centre of gravity and that of the gross section.

This thesis looks at the stability behaviour of a number of sections under an axial compressive force. It looks at sections which are not prone to plate buckling (class 2) as well as sections which are (class 4). Single member finite element models were produced and used for geometrically and materially non-linear analyses with imperfections (GMNIA). Three class 2 sections and seven class 4 sections were analysed. The buckling resistance was obtained for all of the sections for a variety of different lengths. These results were then combined into a buckling curve for each section. The results from the GMNIA analyses were compared to the results from the current methods described in Eurocode 3.

The results of the analyses and the Eurocode 3 calculations showed that there was a large room for improvement. A proposal for the dimensioning of class 2 T-sections was suggested and then four proposals for the dimensioning of the class 4 sections. The proposals were compared and a proposal made.

The results for class 2 sections showed that these stockier sections can be described more appropriately already by a minor adjustment of the existing Ayrton-Perry formula in the Eurocode.

It was furthermore found that, for class 4 sections, the additional effective moment caused by the distance between the centroids of the gross and effective sections, could be ignored in design equations. This, as well as the finding for the class 2 sections, were combined to a suitable proposal for plate buckling prone T-sections.

A revision of the method described in Eurocode 3 is necessary. The sections under axial compression can be more economically dimensioned by the modifications to the design rules developed in this thesis. Further studies could look into T-sections under other types of load, such as a combined axial compression and additional moment.

Kurzfassung

Die Bemessung von T- Profilen erfolgt zurzeit an Anlehnung an das Bemessungskonzept für (doppelt- oder monosymmetrische) I- Profile. Dies führt zu sehr konservativen Ergebnissen bei kürzeren Bauteilen. Vor Allem bei T-Profilen, die anfällig gegenüber Plattenbeulen sind (Klasse 4), wird dieser Effekt bei Verwendung des Nachweiskonzeptes des EC-3 deutlich erkennbar. Laut EC-3 muss für die Bemessung - anstelle des Bruttoquerschnittes - ein effektiver Querschnitt verwendet werden. Unter Anwendung dieses effektiven Querschnittes muss ein zusätzliches Biegemoment berücksichtigt werden, welches aus dem Versatz des Schwerpunktes zwischen dem Brutto- und Nettoquerschnitt entsteht.

Diese Masterarbeit untersucht das Tragverhalten einiger T- Profile bezüglich Stabilität unter reiner zentrischer Druckbeanspruchung. Es wurden T-Profile untersucht, welche anfällig auf Plattenbeulen sind (Klasse 4), ebenso wie jene T-Profile, bei denen kein Plattenbeulen auftritt (Klasse 2). Finite Element Modelle für einzelne Stäbe wurden erstellt und geometrisch und materiell nichtlineare Analysen unter Ansatz von Imperfektionen (GMNIA) wurden durchgeführt. Von insgesamt 10 untersuchten T-Profilen sind drei in der Querschnittsklasse 2, die restlichen sieben sind Klasse 4. Es wurde die Traglast der Druckstäbe ermittelt, wobei deren Stablänge variierte. Aus diesen Ergebnissen wurden anschließend Knickspannungslinien für jedes Profil erstellt. Die aus den GMNIA Analysen erhaltenen Knickspannungslinien wurden dann mit dem EC-3 verglichen.

Die Ergebnisvergleiche der GMNIA Analysen und dem EC-3 zeigen auf, dass es einen Bedarf an Verbesserung des bisherigen Nachweiskonzeptes gibt. Es wurde ein Vorschlag für Klasse 2 Profile gemacht, sowie vier Vorschläge für Klasse 4 Profile.

Die Ergebnisse für Klasse 2 zeigten, dass bereits eine kleine Modifizierung der Ayrton-Perry Formel des Eurocodes deutlich bessere Ergebnisse für diese gedrunenen Querschnitte liefert. Es wurde zudem bewiesen, dass das zusätzliche Biegemoment infolge der Schwerpunktexzentrizität durch Berücksichtigung des effektiven Querschnittes für Klasse 4 Querschnitte bei der Stabilitätsbemessung vernachlässigt werden kann. Diese beiden Erkenntnisse wurden in einem endgültigen Vorschlag zusammengefasst.

Eine Verbesserung des Nachweiskonzeptes des Eurocode 3 in Anlehnung an die in dieser Masterarbeit entwickelten Vorschläge wäre notwendig, um eine wirtschaftliche Stabilitätsbemessung von T-Profilen durchführen zu können. Des Weiteren wären weitere Untersuchungen der T-Profile unter kombinierten Beanspruchungen, wie zentrischer Druck mit Biegemoment notwendig.

To
Martina,
Jessica,
Victoria
and
Tobias

Acknowledgements

It gives me great pleasure in acknowledging the support of both Professor Harald Unterweger and Assistant Professor Andreas Taras, both of whom have been influential in the contents of this thesis as well as my education thus far. Their willingness to give their time and knowledge so generously to the planning and development of this research work is greatly appreciated.

Advice given by colleagues from the Institute of Steel Construction at the Graz Technical University especially Dr Markus Kettler and DI Friedrich Novak was greatly appreciated.

I would like to acknowledge the support of Martina Tapley and Lydia Tapley as well as the rest of both my Austrian and English families without whom this thesis and the rest of my further education, would not have been possible. They were my “restraints”.

“No pressure, no diamonds!” - Thomas Carlyle, Scottish essayist and philosopher

Contents

Abstract.....	ii
Kurzfassung	iii
Acknowledgements	v
Contents	vi
List of Symbols.....	ix
1 Introduction	1
2 Selection of Investigated Cross-Sections	4
2.1 Studied cross sections.....	4
2.2 Classification of the cross-sections.....	6
3 Defining the Effective Dimensions and Properties	10
3.1 Eurocode 3, part 1-5 - Method of effective width	11
3.1.1 General remarks	11
3.1.2 Determination of $W_{y, eff}, 5M$ for isolated bending.....	12
3.1.3 Determination of $A_{eff}, 5N$ for isolated compression.....	16
3.2 Eurocode 3 Part 1-3 method of effective thickness	17
3.2.1 Determination of $W_{y, eff}, 3M$ for isolated bending.....	18
3.2.2 Determination of $A_{eff}, 3N$ for isolated compression.....	20
3.3 The reduced stress method.....	20
3.4 Comparison of the different methods.....	21
3.5 Defining the effective sections used in this thesis.....	25
3.5.1 Axial compression and moment due to centroid shift	25
4 FEM Model for GMNIA Analyses.....	28
4.1 System	28
4.2 FEM model	29

4.3	Imperfections	32
4.4	Residual Stress.....	36
5	Buckling Strength of Class 2 Sections.....	42
5.1	Studied class 2 section.....	42
5.2	Section properties.....	43
5.3	ABAQUS results.....	44
5.4	Results and comparison with Eurocode 3.....	45
5.5	Proposed hypothesis from Taras et al.....	49
5.6	Further sections	51
6	Class 4 Buckling Strength - General Eurocode 3 Rules	55
6.1	Lateral-torsional buckling around the y-y axis - Equ.(1).....	56
6.2	Torsional-flexural buckling around the z-z axis - Equ.(3)	61
6.3	Torsional-flexural buckling - Equ.(2)	62
6.4	ABAQUS calculations	64
6.4.1	Results for the IPE 300 section	65
6.4.2	Results for the IPE 400 section	69
6.4.3	Results for the IPE 500 section	73
6.4.4	Results for the IPE 600 section	74
6.4.5	Results for the HE-A 500 section	77
6.4.6	Results for the modified IPE 500 wide section	80
6.4.7	Results for the modified IPE 500 thin section	83
7	Development and verification of alternative design proposals for Class 4 sections	86
7.1	Proposal 1.....	86
7.2	Proposal 2.....	95
7.3	Proposal 3.....	101
7.4	Proposal 4.....	108
8	Conclusion	116

Appendix A. Results - reduction factor against torsional-flexural slenderness	119
Bibliography	134

List of Symbols

b	Width of the gross section
d	Gross width of the web which has a constant thickness
h	Height of the gross section
G	Centre of gravity
r	Fillet radius
t_w	Gross thickness of the web
t_f	Gross thickness of the flange
z_s	Z coordinates of the gross section's centre of gravity ($z = 0$ at the top of the flange)
A	Gross cross-section area
f_y	Yield Strength
ε	Yield strength coefficient
k_σ	Coefficient for plate buckling
ψ	Stress ratio
e_N	Distance between the centre of gravity of the gross and effective cross-sections
σ_1	Stress at the free end of the web
σ_2	Stress at the fixed end of the web

$A_{eff,5N}$	Final effective area according to EC 1993-1-5 due to axial compression according to EC1993-1-5
$W_{y,eff,5M(s)}$	Elastic section modulus, y-y axis, to the bottom of the web free end for the effective cross-section due to a pure bending moment according to EC1993-1-5
A_{eff}	Final effective area according to EC 1993-1-5 due to both axial compression and the bending from the centroid shift.
$W_{y,eff(s)}$	Elastic section modulus, y-y axis, to the bottom of the effective web's free due to both axial compression and bending from the centroid shift.
ΔM	Additional moment induced through the distance between the gross and effective cross-section centres of gravity
$d_{eff,3M}$	Effective width of the web according to EC 1993-1-3 under bending
$d_{eff,3N}$	Effective width of the web according to EC 1993-1-3 under axial compression
$d_{eff,5}^*$	Effective width of the web during the iteration according to EC 1993-1-5
$d_{eff,5M}$	Final effective width of the web according to EC 1993-1-5 under to bending
$d_{eff,5N}$	Final effective width of the web according to EC 1993-1-5 under to axial compression
d_{eff}	Final effective width of the web according to EC 1993-1-5 under to axial compression and bending
$A_{eff,5N}$	Final effective area according to EC 1993-1-5 due to axial compression
A_{eff}	Final effective area according to EC 1993-1-5 due to both axial compression and bending
$\bar{\lambda}_w$	Equivalent compression web slenderness
ρ	Buckling reduction factor

e_N^*	Centroid shift between the gross section and the current iteration centroid
$z_{s,eff}^*$	Position of the centroid for the current iteration cross-section
$z_{s,eff}$	Position of the centroid for the final effective cross according to EC 1993-1-3 due to bending and axial compression
$z_{s,eff,3}$	Position of the centroid for the effective cross section according to EC 1993-1-3 due to bending
$z_{s,eff,5M}$	Position of the centroid for the effective cross section according to EC 1993-1-5 due to bending
$z_{s,eff,5N}$	Position of the centroid for the effective cross section according to EC 1993-1-5 due to axial compression
A_{eff}^*	The effective area of the current iteration
N^*	Effective compression force for the current iteration
$M_{RS,I}$	Moment due to the initial residual stress after bisecting the I beam
λ_1	Slenderness value to calculate the relative slenderness
E	Modulus of elasticity
L_{cr}	Critical length
$\bar{\lambda}_z$	Relative bending slenderness around the weak z-z axis
i_z	Radius of gyration around the z-z axis
I_z	Gross sections second moment of area about the z-z axis
A_{fi}	Combined area of the two fillets
$I_{T,fi}$	Torsional constant of the fillet
I_T	Torsional constant of the gross section

$I_{T,rep}$	Torsional constant of the replacement box for the fillet
a_{rep}	Width of the fillet replacement box
t_{rep}	Thickness of the replacement box
A_{rep}	Torsional constant of the replacement box for the fillet
m	The number of half sine wave due to local imperfections along the test object
$e_{0,glob}$	Global imperfection
$e_{0,loc}$	Local imperfection
L	Length of the member
N_{pl}	Characteristic plastic resistance for the gross section
$N_{cr,z}$	Critical elastic force for the gross section when considering flexural buckling around the z-z axis
I_y	Gross sections second moment of area about the y-y axis
$I_{y,eff}$	Final effective second moment of area about the y-y axis according to EC 1993-1-5 due to both axial compression and bending Effective sections
i_y	Radius of gyration around the y-y axis
z_0	Distance between the gross centre of gravity and the shear point
$N_{cr,T}$	Critical elastic force for the gross section when considering torsional buckling
$N_{cr,TF}$	Critical elastic force for the gross section when considering torsional-flexural buckling
Φ_{TF}	Value for determining the torsional-flexural buckling factor
$\bar{\lambda}_{TF}$	Torsional-flexural slenderness

χ_{TF}	Reduction factor for torsional flexural buckling
G	Shear modulus
b_{e0}	Depth of the effective web which has web thickness equal to t_w (due to bending moment)
$t_{w,eff}$	Reduced web thickness for the effective cross-section
b_t	Depth of web found in tension (due to bending moments)
N_{Ed}	Design value for the axial force
N_{Rd}	Design value for the resistance to axial forces
χ_y	Reduction factor for flexural buckling around the y-y axis
χ_z	Reduction factor for flexural buckling around the z-z axis
$\chi_{LT(s)}$	Reduction factor for lateral torsional buckling relative to the web free end
$\chi_{LT(l)}$	Reduction factor for lateral torsional buckling relative to the flange
γ_{M0}	Partial factor for the resistance of cross-sections
Φ_y	Value for determining the flexural buckling factor around the y-y axis
Φ_z	Value for determining the flexural buckling factor around the z-z axis
Φ_{LT}	Value for determining the lateral-torsional buckling factor
$N_{cr,y}$	Critical elastic force for the gross section when considering the bending slenderness around the y-y axis
$N_{cr,LT}$	Critical elastic force for the gross section when considering lateral-torsional buckling
n_y	Coefficient to calculate the interaction coefficient in the y direction

n_z	Coefficient to calculate the interaction coefficient in the z direction
ψ_{cm}	The bending moment ratio at the ends of the member element
$W_{y,eff(l)}$	Elastic section modulus, y-y axis, to the top edge of the flange for the effective cross-section
z_j	Coefficient for mono symmetrical members to calculate M_{cr}
ψ_f	Flange ratio for the calculation of M_{cr}
I_{fc}	Second moment of area of a compressed flange around the z-z axis
I_{ft}	Second moment of area of a flange in tension around the z-z axis
h_s	The height of the section
φ	Rotation of a plane around the x-x axis

1 Introduction

Although the behaviour of double symmetric sections has been investigated thoroughly and has been effectively incorporated into Eurocode 3 for steel structures [1], mono-symmetrical sections are an area where more work is required. The design for axial compression members is based on the buckling curves obtained through numerical and experimental studies carried out on double symmetric cross-sections.

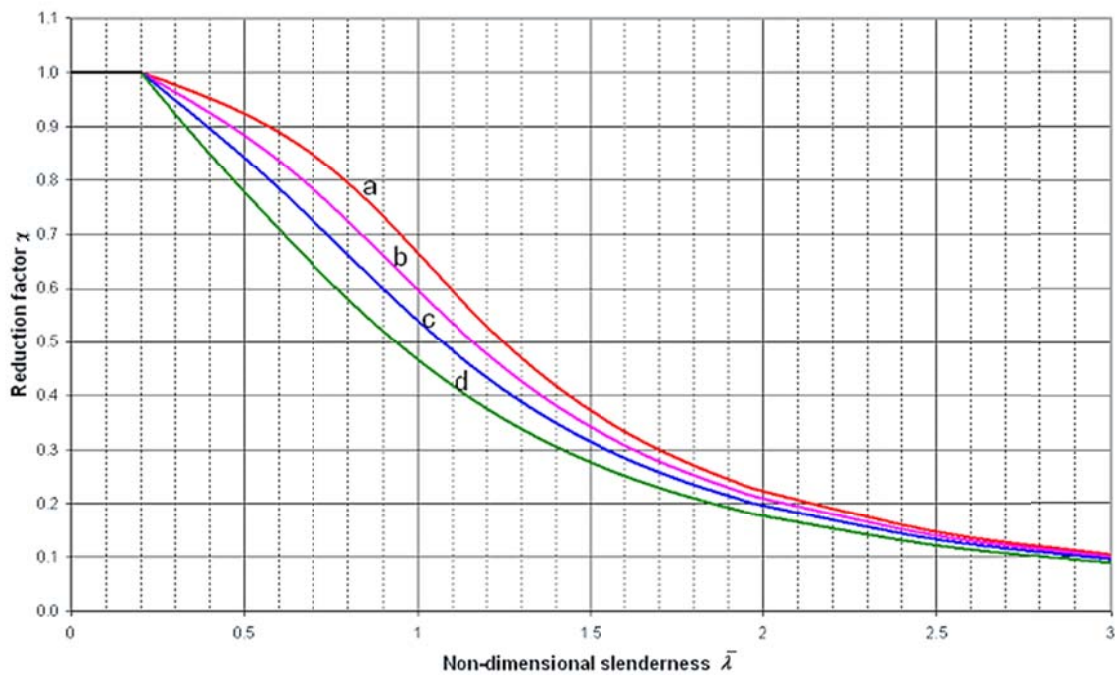


Figure 1 : Buckling curve

Taras, Greiner and Puig, among other researchers, have carried out numerical studies into the behaviour of mono-symmetrical I beam-columns[2]. Other sections still have to be investigated, such as T-sections. The failure of these sections subjected to axial compression can occur in a number of ways, including global mechanisms such as torsional-flexural failure (Figure 2) and flexural failure, as well as local buckling.

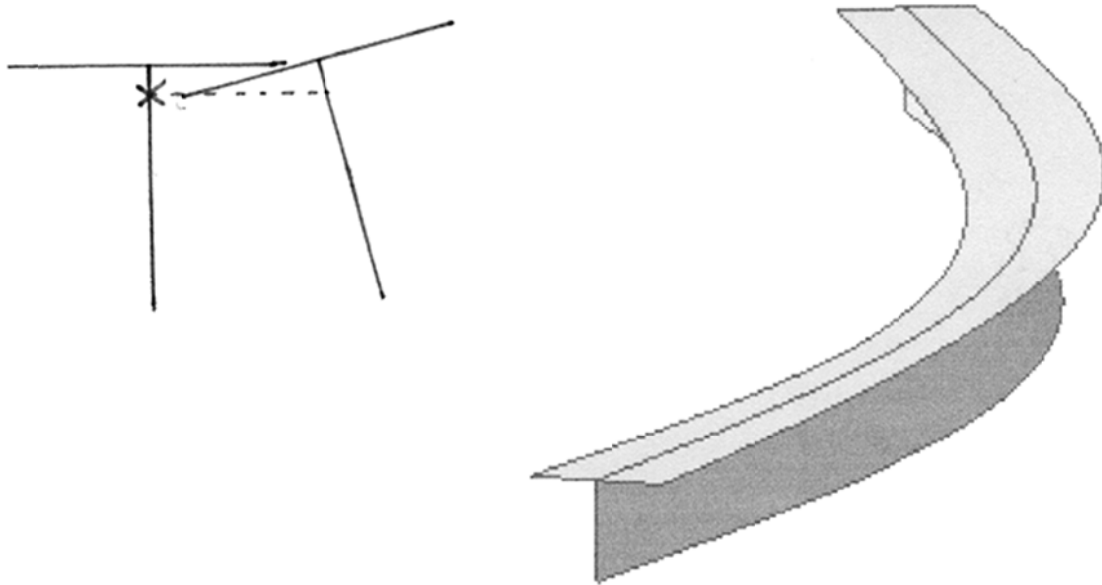


Figure 2: Torsional-flexural failure of a T-section under axial compression force

T-sections produced by bisecting double-T or H-section beams provide a low cost method for producing the chord of a truss. In these applications, the top chords usually find themselves in a state of axial compression (Figure 3).

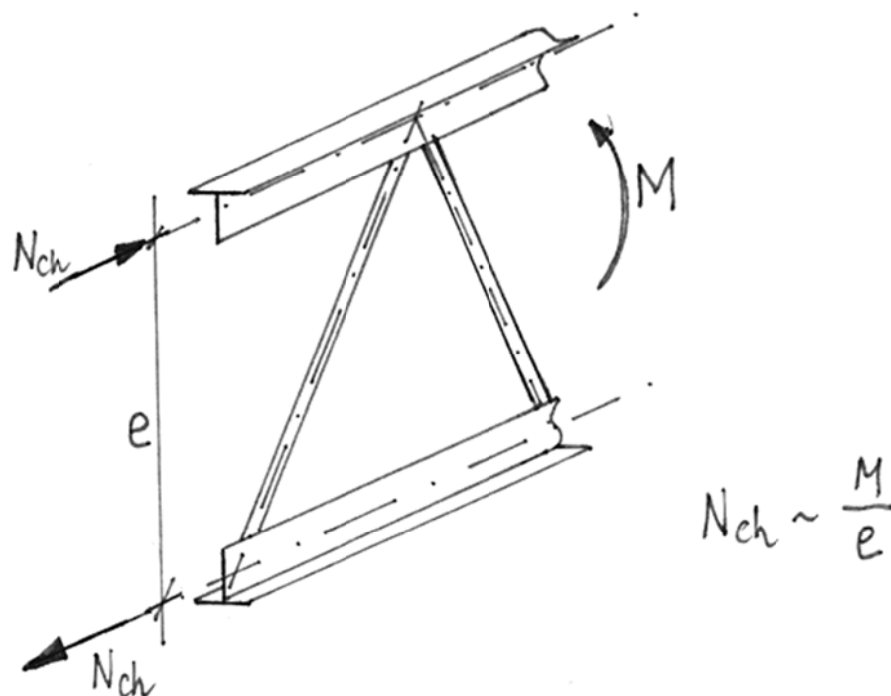


Figure 3: An example of a T-section truss (schematic representation of the diagonals)

This thesis will look into stability behaviour specifically for Eurocode classes 2 and 4 sections under axial compression. GMNIA buckling load calculations (geometrical and material non linear analyses with imperfections) will be carried out on a variety of T-section sections of different lengths. The *ABAQUS standard* finite element program will be used for these calculations.

The T-section members will be pin ended as the Eurocode is also based on pin ended columns. The buckling load results of the numerical experiments and the buckling loads suggested by the current Eurocode 3 will be compared. Preliminary studies have shown that columns with a low value of global slenderness and slender cross section(class 3,4), will have a much higher buckling load than the value described in the Eurocode; these findings should be corroborated and expanded in this thesis. Finally, suggestions will be posed as to how the Eurocode 3 could be adapted to incorporate the new findings.

In summary the questions that will be answered are:

- What are realistic buckling loads for double pinned T-sections under the influence of an axial compressive load?
- How does the section's class affect the calculation method?
- How do these results compare to the Eurocode 3 values?
- How can we calculate an accurate value for the buckling strength so that cross-sections are then economically dimensioned?

2 Selection of Investigated Cross-Sections

2.1 Studied cross sections

For this thesis, investigations were carried out on seven different class 4 T-sections and three class 2 sections. All were bisected I-beams, H beams or modified versions thereof, made of structural steel grade S235 with yield strength of 23.5 kN/cm².

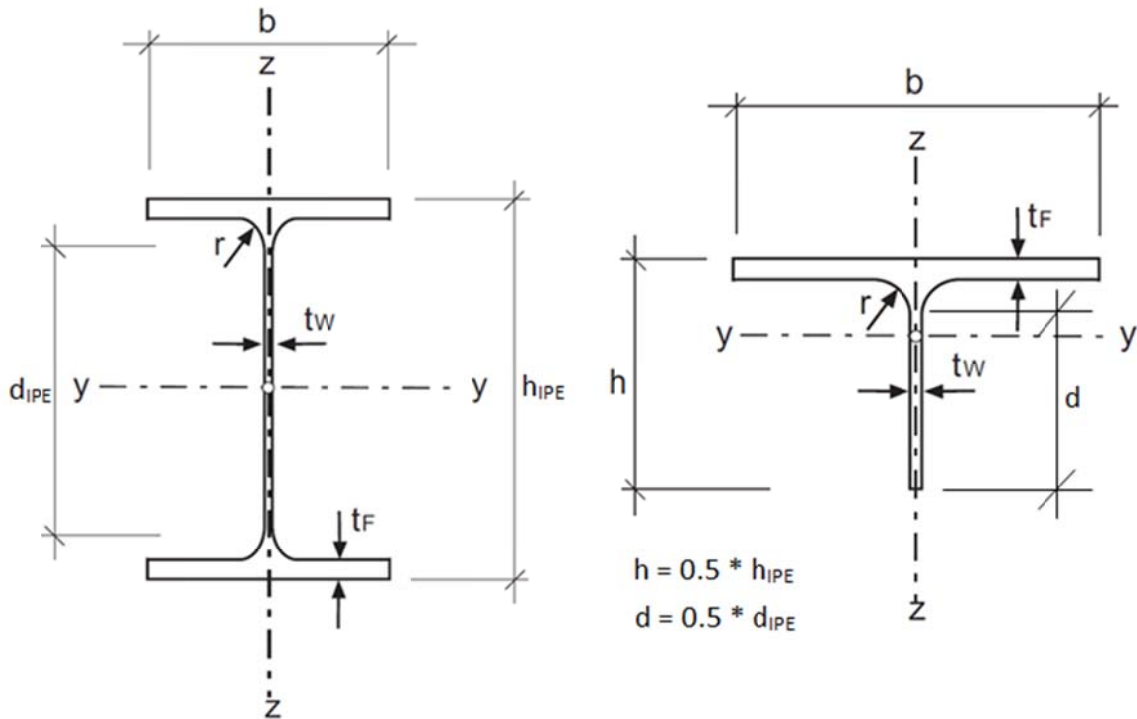


Figure 4: Examples of an IPE and a bisected IPE [3]

Four bisected standard IPE beams were selected as a basis for the class 4 calculations. These were the IPE 300, IPE 400, IPE 500 and IPE 600. It was taken into account that these were made from S235 steel only. Once they were (theoretically) bisected, the centre of gravity for all of these sections was in the web.

A bisected HE-A 500 was also selected. There the centre of gravity lay close to the flange. Also, two modified IPE 500 sections, one where the flange had a reduced width of 100 mm

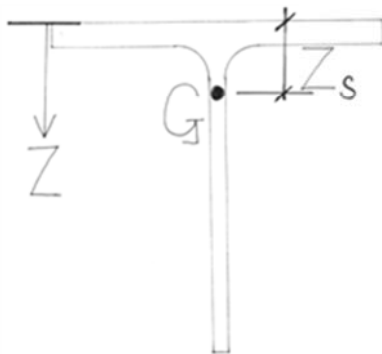
(named IPE 500-t in this thesis) and the other where the flange width was increased to 300 mm (named IPE 500-w), were investigated.

Cross Section	Height h (mm)	Width b (mm)	Web thickness t_w (mm)	Flange thickness t_f (mm)	Fillet radius r (mm)
1/2 IPE 300	150	150	7.1	10.7	15
1/2 IPE 400	200	180	8.6	13.5	21
1/2 IPE 500	250	200	10.2	16	21
1/2 IPE 500 - thin	250	100	10.2	16	21
1/2 IPE 500 - wide	250	300	10.2	16	21
1/2 IPE 600	300	220	12	19	24
1/2 HEA 500	245	300	12	23	27

Table 1: Dimensions of the chosen cross-sections

The shift in the centre of gravity plays a large role in the Eurocode 3 calculations for class 4 sections, as the Eurocode 3 design results are based on the method of the effective widths, which will be explained later. The position of the centre of gravity z_s relative to the top flange was calculated as follows. Here A_i was the area and z_i the z coordinate of the centre of gravity for each part of the section (i.e. flange, web and fillets).

$$z_s = \frac{\sum A_i * z_i}{\sum A_i}$$



Cross Section	Area A (cm ²)	Position of the centroid z_s (mm)
1/2 IPE 300	26.9	33.2
1/2 IPE 400	42.2	45.2
1/2 IPE 500	57.8	60.1
1/2 IPE 500 - thin	41.8	80.0
1/2 IPE 500 - wide	73.8	48.8
1/2 IPE 600	78	74.8
1/2 HEA 500	98.8	45.1

Table 2: Position of the centre of gravity (centroid) and area of each section

The cross-section values and the position of the centre of gravity are shown in Table 2. As this thesis deals mainly with class 4 sections the chosen sections had to be checked using Eurocode 3 classification rules to make sure they were in fact class 4 sections.

N.B. class 4 sections are sections with slender plate elements, which are affected by local buckling.

2.2 Classification of the cross-sections

Classification of the cross-sections was necessary to define how the resistance and rotation capacity was inhibited by local buckling. In the case of axial compression, every part of the section is subjected to compression. The class of every part of the sections needed to be identified individually. The classification of the section is then defined by the highest classed part.

Outstand flanges						
		Rolled sections		Welded sections		
Class	Part subject to compression	Part subject to bending and compression				
		Tip in compression		Tip in tension		
1	$c/t \leq 9\epsilon$	$c/t \leq \frac{9\epsilon}{\alpha}$	$c/t \leq \frac{9\epsilon}{\alpha\sqrt{\alpha}}$			
2	$c/t \leq 10\epsilon$	$c/t \leq \frac{10\epsilon}{\alpha}$	$c/t \leq \frac{10\epsilon}{\alpha\sqrt{\alpha}}$			
3	$c/t \leq 14\epsilon$	$c/t \leq 21\epsilon\sqrt{k_\sigma}$				
For k_σ see EN 1993-1-5						
$\epsilon = \sqrt{235/f_y}$	f_y	235	275	355	420	460
	ϵ	1.00	0.92	0.81	0.75	0.71

Table 3: Classification of outstand flanges [1] (excerpt from Eurocode 3, part 1-1)

The Eurocode classes range from 1 - 4 and differentiate as described in the following:

- Class 1 and 2 - The plastic resistance can be used for member design.
- Class 3 - The elastic resistance can be used for design purposes.
- Class 4 - A reduced cross section needs to be used to calculate the resistance. The reduction takes into account that parts of the section are likely to buckle locally and therefore reduce the elastic resistance.

A S235 steel was used so $\varepsilon = 1$ was used for the calculations (see Table 3). As stated in Table 3, the plate buckling coefficient, k_σ , was calculated using Eurocode 3, part 1-5. Two cases were considered:

- Pure axial compression ($\psi = 1$)
- Pure bending - even though axial compression is the only *external* load case considered in this thesis, the bending case was also of relevance because a nominal bending moment of $M = N * e_N$ had to be considered in the design calculations according to Eurocode 3, due to the shift of the centre of gravity, e_N .

In the bending case, it was first assumed that the maximum compression stress σ_1 , occurred at the free end of the web and $\sigma = 0$ at the centre of gravity of the gross section. Therefore, σ_2 was calculated according to Figure 5 and finally, the stress ratio, ψ , was calculated using the results from σ_2 .

$$\sigma_2 = \frac{\sigma_1}{h - z_s} * (z_s - t_f - r)$$

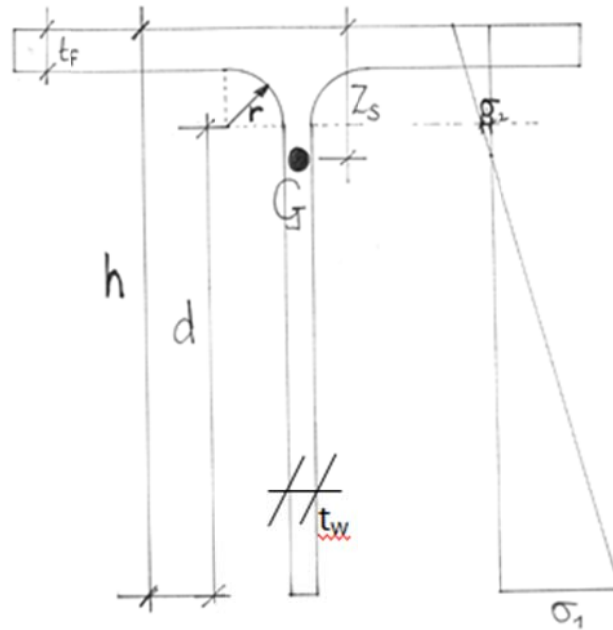


Figure 5: Diagram to calculate σ_2

To obtain ψ the following formula was used;

$$\psi = \frac{\sigma_2}{\sigma_1}$$

So,

$$\psi = \frac{(z_s - t_f - r)}{h - z_s}$$

Based on ψ , the plate buckling coefficient, k_σ , for the web was calculated using this formula from EC 1993-1-5;

$$k_\sigma = 0,57 - 0,21\psi + 0,07\psi^2$$

Just the webs were considered first as it was believed that in every case the web would define the class of the cross section.

Cross Section	d [mm]	$Z_s - t_f - r$ [mm]	ψ Stress Ratio (-)	k_σ Bending (-)	$\sqrt{k_\sigma}$ Bending (-)
1/2 IPE 300	124.30	7.50	-0.06	0.58	0.76
1/2 IPE 400	165.50	10.70	-0.07	0.58	0.76
1/2 IPE 500	213.00	23.10	-0.12	0.60	0.77
1/2 IPE 500 - thin	213.00	43.02	-0.25	0.63	0.79
1/2 IPE 500 - wide	213.00	11.77	-0.06	0.58	0.76
1/2 IPE 600	257.00	31.80	-0.14	0.60	0.78
1/2 HEA 500	195.00	-4.90	0.02	0.56	0.75

Table 4: T-section under bending - calculation of k_σ

In Table 5 it can be seen that these sections were all class 4 whether fully compressed (only N acting) or bent (only M acting). This means that it was no longer necessary to consider the flanges for classification of the cross section as the value for the web had defined the section.

Cross Section	d/t_w (-)	$21\varepsilon\sqrt{k_\sigma}$ (-)	Bending Class (-)	14ε (-)	Compression Class (-)
1/2 IPE 300	17.51	16.05	4	14.00	4
1/2 IPE 400	19.24	16.06	4	14.00	4
1/2 IPE 500	20.88	16.22	4	14.00	4
1/2 IPE 500 - thin	20.88	16.64	4	14.00	4
1/2 IPE 500 - wide	20.88	16.03	4	14.00	4
1/2 IPE 600	21.42	16.28	4	14.00	4
1/2 HEA 500	16.25	15.78	4	14.00	4

Table 5: Class definition of the T-sections under M and N respectively

In both cases, bending and compression, all of the sections were class 4 and therefore prone to local plate buckling. This meant the effective cross section needed to be defined as well as the effective attributes. This was carried out as described in chapter 3 “Defining the Effective Dimensions and Properties”.

3 Defining the Effective Dimensions and Properties

According to EN 1993-1-1, the strength of a slender (class 4) section shall be determined using the so-called “Effective Width Method” of EN 1993-1-5 [4], which prescribes reduction factors and rules for the determination of remaining, effective width of sections that are prone to local buckling. In addition, EN 1993-1-1 states “*Where a class 4 cross section is subjected to an axial force, the method given in EN 1993-1-5 should be used to determine the possible shift e_N of the centroid of the effective area A_{eff} relative to the centre of gravity of the gross cross section and resulting additional moment*”, which means that an additional bending moment, ΔM , must be considered in design calculations, the magnitude of which depends on the precise definition and geometry of the remaining, effective cross-section ($\Delta M = N * e_N$).

There is also an alternative “Effective Thickness Method” that is described in Eurocode 3 part 1-3 [5]. This method is usually used for cold formed steel sections with a thickness of less than 3mm. In contrast to EN 1993-1-5, in this method the total depth of the effective cross-section remains equal to the depth of the gross section, which means that in both cases (N and M) the actual, physical outer-most fibre in the cross-section describes the design-critical point.

In Eurocode 3 part 1-5, it is not clearly stated if, in the case of outstanding plates, such as the web of a T-section, the elastic modulus of the effective section, $W_{y,eff5M(s)}$ should be defined by the distance to the outermost fibre of the gross or the effective section. The latter one seems to be the more accurate one, because a definition of the stresses outside of a section is not used in practice.

EN 1993-1-1, section 6.2.9.3 (2) states that, for ease, the effective area A_{eff} and the effective section moduli, $W_{y,eff(s)}$ and $W_{y,eff(l)}$, may be calculated independently for an isolated compression force and an isolated bending moment, respectively. However, it is also possible – and more accurate – to calculate the effective cross-sectional properties for

the combined stress state; this however requires an iterative process and was used in the old DIN code (in this thesis these values are named A_{eff} , $W_{y,eff(s)}$ and $W_{y,eff(l)}$).

In the following, a comparison of the “Effective Thickness Method” and the “Effective Width Method” was made. For the sake of completeness the method of effective stress is also looked at briefly.

3.1 Eurocode 3, part 1-5 - Method of effective width

3.1.1 General remarks

The effective width method defines an effective section to replace the gross section by altogether removing certain “ineffective” parts of the cross-section. This effective section takes into account the local buckling and the loss of strength due to buckling. It allows the user to perform all the usual design checks - based on elastic stresses - replacing the gross section values with those of the reduced section. The theoretical removal of parts of the section also means that there is an extra moment that occurs when under axial compression. This is due to the eccentricity between the real centre of gravity and that of the effective section, and the fact that the external axial compressive force continues to act in the centroid of the gross section. The Eurocode states that this extra moment cannot be neglected.

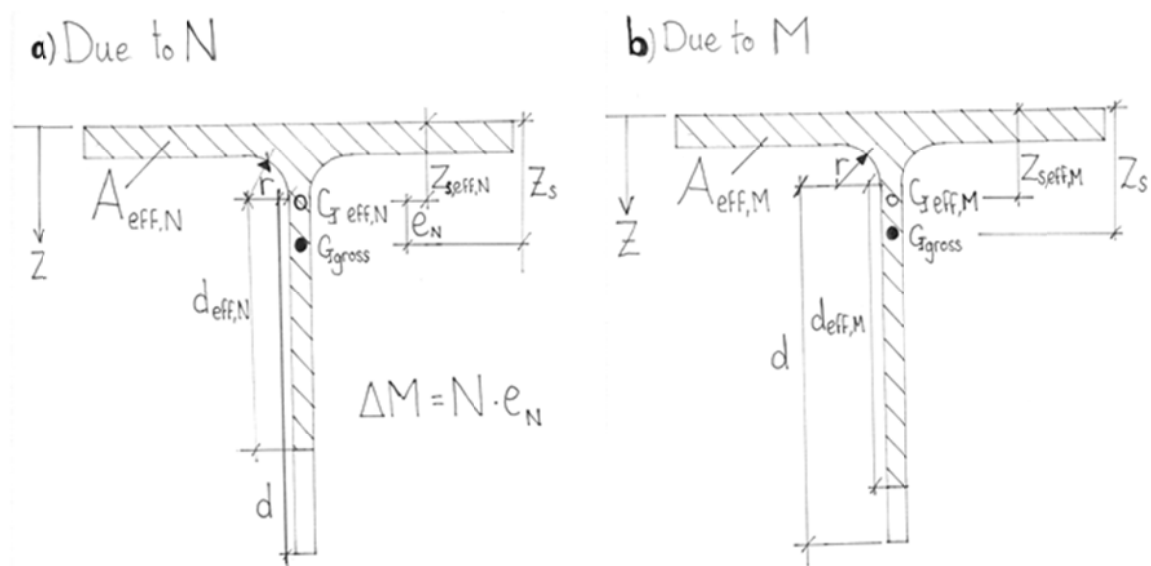


Figure 6 : Change in area and centroid position

3.1.2 Determination of $W_{y,eff,5M}$ for isolated bending

For pure bending, but also due to $\Delta M = N * e_N$, the “method of effective widths” described in Eurocode 3 part 1-5 is an iterative process, as the reduction in width causes the stress distribution to change and the stress distribution defines the width that is used as basis for the calculation of the area reductions. This means that the definition of an effective section is dependent on the applied moment and appropriate stress gradient.

The calculation of the initial stress ratio, ψ , and the starting plate buckling coefficient, k_σ , for the first iteration of pure bending has already been calculated in chapter 2.2 “Classification of the cross-sections”.

As the centre of gravity was in the fillet for the HE-A 500, ψ was positive (only compression stresses in the web). For all of the other sections ψ was negative because the centroid of the gross-section is in the web, and thus the two extremities of the web plate are subjected to stresses of opposite sign. This means that all of the values for the IPE sections had to be calculated using the second row in Table 6 and for the HE-A using the first row.

It is very important to note that Eurocode 3, part 1-5 very clearly makes use of the “fictitious” stress at the outermost fibre of the slender outstanding plate (in the case of T-sections: mainly the web) for the determination of ψ - i.e. a stress that is “outside” of the effective cross-section, in all iteration steps except the very first one (when the gross section is still active).

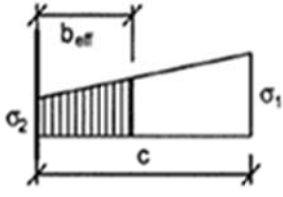
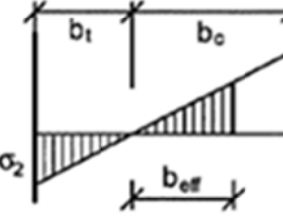
Stress distribution		Effective width		
		$1 \geq \psi \geq 0$ $b_{\text{eff}} = \rho c$		
		$\psi < 0$ $b_{\text{eff}} = \rho b_c = \rho c(1 - \psi)$		
$\psi = \sigma_2/\sigma_1$	1	0	-1	$1 \geq \psi \geq -3$
Buckling coefficient, k_σ	0,43	0,57	0,85	$0,57 - 0,21 \psi + 0,07 \psi^2$

Table 6: Effective widths for outstand compression elements acc. to EN 1993-1-5

N.B. The symbol d is used instead of c shown in Table 6.

The equivalent compression web slenderness, $\bar{\lambda}_w$, was calculated for the web.

$$\bar{\lambda}_w = \frac{d/t_w}{28.4\epsilon\sqrt{k_\sigma}}$$

And from that the buckling reduction factor, ρ , is defined using the following two formula.

When $\bar{\lambda}_w \leq 0.748$ then

$$\rho = 1.0$$

And when $\bar{\lambda}_w > 0.748$ then

$$\rho = \frac{\bar{\lambda}_w - 0.188}{\bar{\lambda}_w^2}$$

Once the reduction factor was calculated, the effective width of the web was calculated, based on Table 6.

The IPE cross-sections were calculated using the formula in the second row of Table 6

$$b_{eff,5M}^* = \rho * d / (1 - \psi)$$

The HE-A cross-section was calculated using the formula in the first row of Table 6.

$$b_{eff,5M}^* = \rho * d$$

As stated above the method in EC 1993-1-5 is an iterative process. Using the value $b_{eff,5M}^*$ (index “5” here to show that it is calculated as defined in Eurocode 3 part 1-5) the centroid of this effective cross-section was calculated and from that the new ψ , based on the stress at the bottom of the gross section’s web. The process was then carried out repeatedly, until the value $b_{eff,5M}^*$ converged to an answer. This defined the effective cross-section dimensions.

Cross Section	$b_{eff,5M}^*$	$b_{eff,5M}^*$	$b_{eff,5M}^*$	$b_{eff,5M}^*$	$b_{eff,5M}^*$	ψ
	1 st iteration (cm)	2 nd iteration (cm)	3 rd iteration (cm)	4 th iteration (cm)	5 th iteration (cm)	Stress Ratio
1/2 IPE 300	11.10	11.24	11.25	11.25	11.25	-0.04781
1/2 IPE 400	13.76	14.16	14.19	14.19	14.19	-0.03140
1/2 IPE 500	16.01	16.70	16.76	16.77	16.77	-0.06157
1/2 IPE 500 - thin	14.60	15.29	15.38	15.39	15.39	-0.17598
1/2 IPE 500 - wide	16.81	17.44	17.49	17.49	17.49	-0.01046
1/2 IPE 600	18.68	19.57	19.66	19.67	19.67	-0.07284
1/2 HEA 500	19.29	19.28	19.28	19.28	19.28	0.02709

Table 7: The effective depth, $b_{eff,5M}^*$, of the web after each iteration EC 3 part 1-5

With the new dimensions, the effective properties for the bending cross-section were calculated. They are shown in Table 8.

$W_{y,eff,5M}$ can then be calculated as follows

$$W_{y,eff,5M} = \frac{I_{eff,5M}}{z_{b,eff}}$$

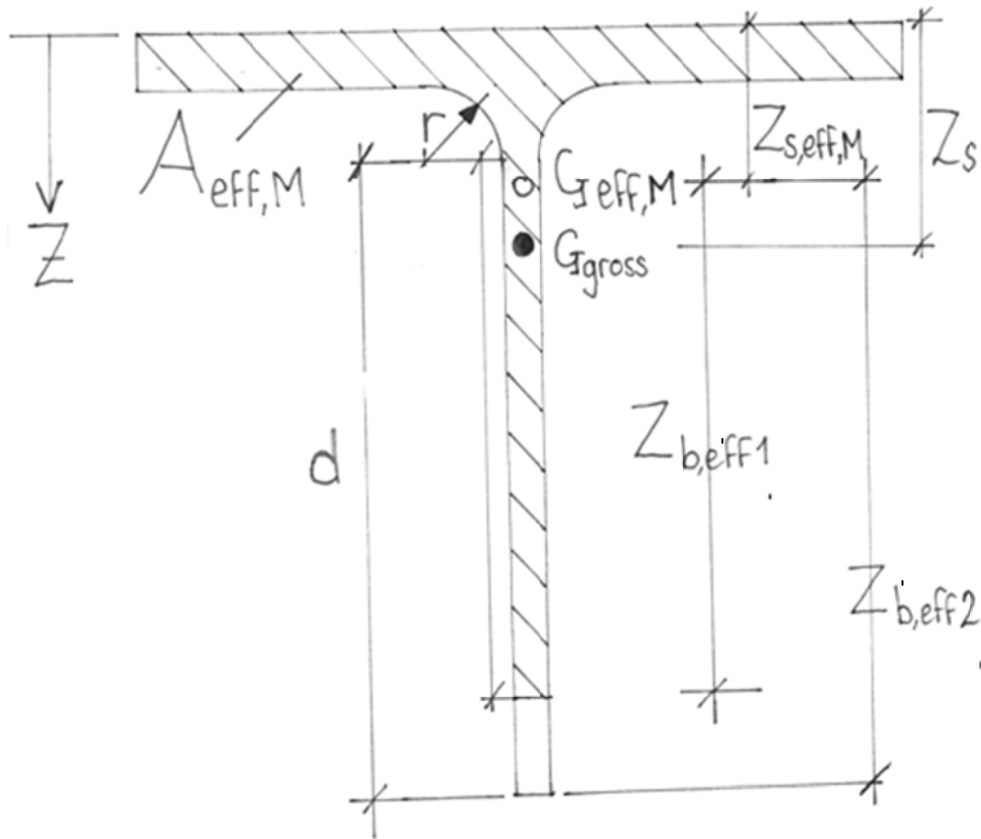


Figure 7: Shows the difference between $z_{b,eff1}$ and $z_{b,eff2}$

It is however unclear at the moment whether the distance $z_{b,eff}$ should be considered to be the distance from the effective section's centroid to the bottom of the gross section, $z_{b,eff,2}$, or the distance from the effective section's centroid to the bottom of the effective section, $z_{b,eff,1}$ (see Figure 7). In the chapter 3.4 the two results obtained here for $W_{y,eff,5M}$ will be compared to the results from the effective thickness method and the correct value for $z_{b,eff}$ can then be deduced.

$$M_{Rd} = W * f_y$$

Cross Section	$b_{eff,SM}$ [cm]	$d_{eff,SM}$ [cm]	$I_{y,eff}$ [cm ⁴]	$z_{b,eff,1}$ [cm]	$W_{eff,SM,1}$ [cm ³]	$M_{Rd,SM,1}$ [kNcm]	$z_{b,eff,2}$ [cm]	$W_{eff,SM,2}$ [cm ³]	$M_{Rd,SM,2}$ [kNcm]
1/2 IPE 300	11.3	11.8	453	10.7	42	995	11.9	38	897
1/2 IPE 400	14.2	12.6	1099	13.7	80	1887	16.1	68	1610
1/2 IPE 500	16.8	18.4	2187	15.5	141	3308	20.1	109	2561
1/2 IPE 500 - thin	15.4	19.0	1930	12.2	158	3718	18.1	107	2504
1/2 IPE 500 - wide	17.5	18.1	2309	17.3	134	3141	21.1	110	2574
1/2 IPE 600	19.7	25.7	4205	17.9	235	5512	24.0	176	4125
1/2 HEA 500	19.3	23.1	3916	19.8	198	4642	20.0	195	4591

Table 8: Method of effective widths - effective section properties EC 3 part 1-5

N.B. In Table 8 $W_{eff,5M,1}$ and $W_{eff,5M,2}$ refer to the y direction

3.1.3 Determination of $A_{eff,5N}$ for isolated compression

When using the simplified method of EN 1993-1-1 6.2.9.3 (2), the effective section for isolated axial compression can easily be calculated: this is not an iterative process and the values are obtained when ψ is equal to 1.0.

When considering pure axial compression k_σ is equal to 0.43.

N.B. again in the following the symbol d is used instead of c shown in Table 6.

The equivalent compression web slenderness, $\bar{\lambda}_w$, was calculated for the web.

$$\bar{\lambda}_w = \frac{d/t_w}{28.4\epsilon\sqrt{k_\sigma}}$$

Then that the buckling reduction factor, ρ , was obtained using the following two formula.

When $\bar{\lambda}_w \leq 0.748$ then

$$\rho = 1.0$$

And when $\bar{\lambda}_w > 0.748$ then

$$\rho = \frac{\bar{\lambda}_w - 0.188}{\bar{\lambda}_w^2}$$

The effective width of the web

$$b_{eff,5N} = \rho * d$$

In the case of pure axial compression $b_{eff,5N}$ is equal to $d_{eff,5N}$

In the case of a bisected S235 IPE 300 section,

$$\bar{\lambda}_w = \frac{12.43/0.71}{28.4 * 1.0 * \sqrt{0.43}} = 0.94$$

$$\rho = \frac{0.94 - 0.188}{0.94^2} = 0.851$$

$$b_{eff,5N} = 0.851 * 12.43 = 10.578$$

The effective area could then be calculated.

The results for the studied sections are shown in Table 9.

$$N_{Rd} = A_{eff,5N} * f_y$$

Cross Section	$A_{eff,5N}$ [cm ²]	Yield Strength f_y [kN/cm ²]	N_{Rd} [kN]
1/2 IPE 300	25.6	23.5	602
1/2 IPE 400	39.3	23.5	924
1/2 IPE 500	52.2	23.5	1227
1/2 IPE 500 - thin	36.2	23.5	851
1/2 IPE 500 - wide	68.2	23.5	1603
1/2 IPE 600	69.6	23.5	1636
1/2 HEA 500	96.4	23.5	2265

Table 9: Effective width method - pure axial compression

3.2 Eurocode 3 Part 1-3 method of effective thickness

The method of effective thickness is carried out using the stresses acting on the *gross* section. Therefore, for the investigated T-sections under axial force N only the effective

section properties for $\psi = 1$ (only N) must be calculated. For our comparison the values for isolated bending will also be considered.

3.2.1 Determination of $W_{y,eff,3M}$ for isolated bending

Unlike the method of effective widths, the method of effective thicknesses in EN 1993-1-3 Annex D is not an iterative process, because ψ is always defined by the stresses of the gross section. It has one step that needs to be carried out. These values were calculated to compare them with the values obtained from the Eurocode 3 part 1-5.

Maximum compression at free longitudinal edge		
Stress distribution	Effective width and thickness	Buckling factor
	$1 \geq \psi \geq 0$ $b_{e0} = 0,42b_p$ $t_{eff} = (1,75\rho - 0,75)t$	$1 \geq \psi \geq -2$ $k_\sigma = \frac{1,7}{3 + \psi}$
	$\psi < 0$ $b_{e0} = \frac{0,42b_p}{(1 - \psi)} + b_t < b_p$ $b_t = \frac{\psi b_p}{(\psi - 1)}$ $t_{eff} = (1,75\rho - 0,75 - 0,15\psi)t$	$-2 > \psi \geq -3$ $k_\sigma = 3,3(1 + \psi) + 1,25\psi^2$
		$\psi < -3$ $k_\sigma = 0,29(1 - \psi)^2$

Table 10: Outstand compression elements - Method of effective thickness

In this case of bending without an axial compression the value for ψ had already been calculated (see chapter 2.2). The second row from Table 10 was used for calculating the 1/2 IPE cross-sections and the first row for the 1/2 HE-A. In all cases, ψ was between 1 and -2. This meant that the buckling coefficient was calculated using this formula;

$$k_\sigma = \frac{1,7}{3 + \psi}$$

The equivalent compression web slenderness, $\bar{\lambda}_w$ and the buckling reduction factor, ρ for the web were all calculated as in 3.1 "Eurocode 3, part 1-5".

N.B. here b_p is replaced with d .

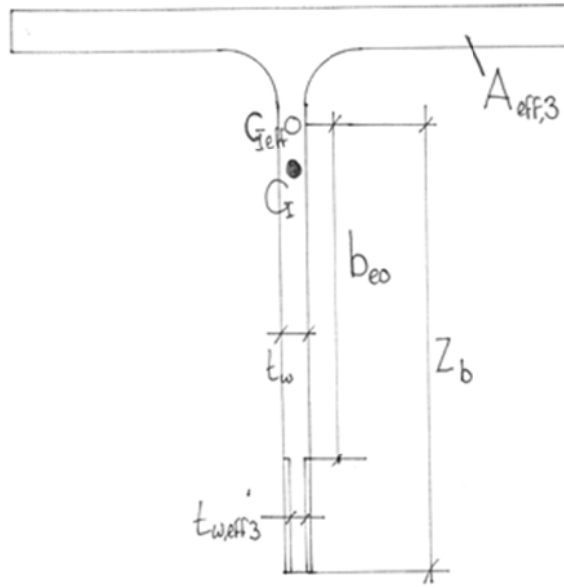


Figure 8: Values for effective thickness method

Based on Table 10 the length with tension becomes:

$$b_t = \frac{\psi * d}{(\psi - 1)}$$

$$b_{e0} = \frac{0.42 * d}{(1 - \psi)} + d_t < d$$

$$t_{w,eff} = (1.75 * \rho - 0.75 - 0.15 * \psi)t_w$$

The final dimensions needed to define the effective cross section can be seen in Table 11.

Cross Section	b_t [cm]	b_{e0} [cm]	$t_{w,eff3}$ [cm]	z_b [cm]	$W_{eff,3M}$ [cm ³]	$M_{Rd,3M}$ [kNcm]
1/2 IPE 300	0.8	5.7	0.65	11.8	41	968
1/2 IPE 400	1.1	7.6	0.70	15.9	81	1911
1/2 IPE 500	2.3	10.3	0.75	19.7	141	3302
1/2 IPE 500 - thin	4.3	11.4	0.80	17.7	136	3191
1/2 IPE 500 - wide	1.2	9.6	0.73	20.8	141	3323
1/2 IPE 600	3.2	12.6	0.86	23.5	232	5459
1/2 HEA 500	0.0	8.2	1.17	20.0	198	4649

Table 11: Method effective thicknesses - effective section properties under bending

3.2.2 Determination of $A_{eff,3N}$ for isolated compression

These values which would be more relevant for the investigated sections are also defined.

This was also not an iterative process and the values are obtained when ψ is equal to 1.0.

Cross Section	$A_{eff,3N}$ [cm ²]	Yield Strength f_y [kN/cm ²]	N_{Rd} [kN]
1/2 IPE 300	25.5	23.5	600
1/2 IPE 400	39.2	23.5	920
1/2 IPE 500	52.0	23.5	1222
1/2 IPE 500 - thin	36.0	23.5	846
1/2 IPE 500 - wide	68.0	23.5	1598
1/2 IPE 600	69.4	23.5	1630
1/2 HEA 500	96.3	23.5	2263

Table 12: Results for $A_{eff,3N}$ using the effective thickness method

3.3 The reduced stress method

For the purpose of completeness another variation was also considered. This was the method of reduced stress. This involved taking the value for ρ as calculated in 3.1 “Eurocode 3, part 1-5 - Method of effective width” and multiplying it with the yield strength, f_y . In the case of these cross sections $f_y = 23.5$ kN/cm². This reduced stress $\rho * f_y$ defines the maximum compression stress. For the calculation of stresses the gross cross-section values are used.

N.B. There is a difference here between ρ_M and ρ_N

With this method, instead of saying that a specific area did not have any strength, it said that that the entire area of the cross-section had a reduced value of strength. It was simply another way of showing the loss of strength due to local buckling suggested in Eurocode 3.

It was known that there would be discrepancies between this method and the other two, as ρ is quadratic in the calculation of the elastic section modulus with the other methods and here it was not.

Cross Section	A [cm ²]	ρ_N	Yield Strength - f_y [kN/cm ²]	N_{Rd} [kN]
1/2 IPE 300	26.9	0.85	19.98	537
1/2 IPE 400	42.2	0.79	18.52	781
1/2 IPE 500	57.8	0.74	17.37	1004
1/2 IPE 500 - thin	41.8	0.74	17.37	725
1/2 IPE 500 - wide	73.8	0.74	17.37	1281
1/2 IPE 600	78	0.73	17.08	1333
1/2 HEA 500	98.8	0.90	21.13	2087

Table 13: Results for N_{Rd} using the reduced stress method

Cross Section	I_y [cm ⁴]	W_s [cm ³]	ρ_M	Reduced Yield Strength - $f_y * \rho_M$ [kN/cm ²]	M_{Rd} [kNcm]
1/2 IPE 300	509	44	0.95	22.28	971
1/2 IPE 400	1450	94	0.89	20.82	1950
1/2 IPE 500	3260	172	0.84	19.74	3389
1/2 IPE 500 - thin	2660	156	0.86	20.09	3144
1/2 IPE 500 - wide	3606	179	0.83	19.58	3508
1/2 IPE 600	6500	289	0.83	19.41	5603
1/2 HEA 500	4020	201	0.99	23.22	4669

Table 14: Results for M_{Rd} using the reduced stress method

3.4 Comparison of the different methods

The comparison that was made looked at the cross-section resistances and didn't include any global stability effects. The N_{Rk} and the M_{Rk} values for the isolated axial force and bending moment, respectively, were looked at.

$$N_{Rk} = A_{eff} * f_y$$

$$M_{Rk} = W_{eff} * f_y$$

3 Defining the Effective Dimensions and Properties

Four different variants were considered.

Variation 1: The method of effective widths and the distance for the elastic section modulus from the centroid to the end of the effective web is used.

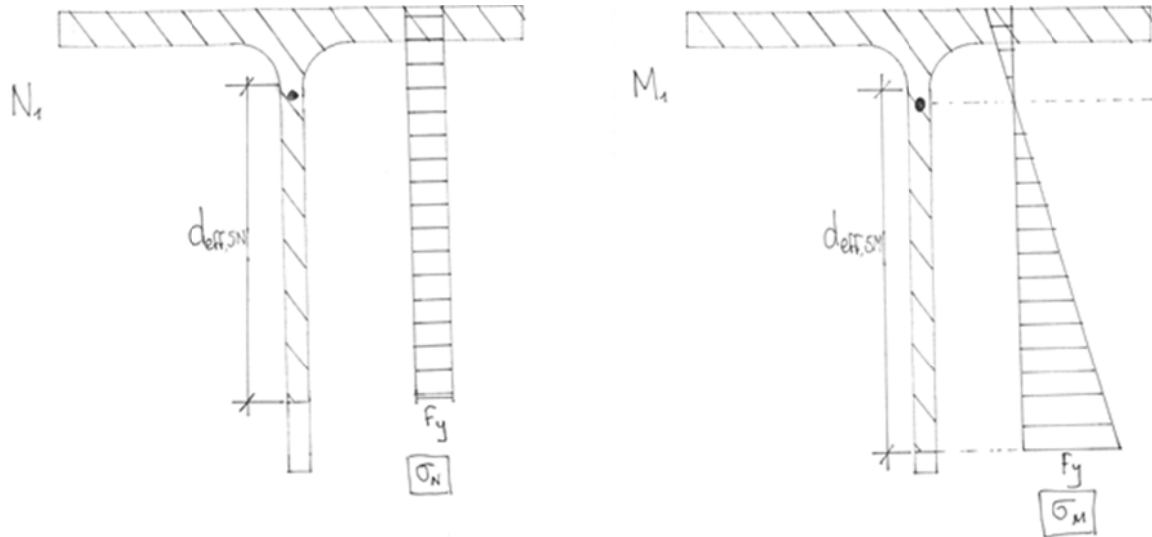


Figure 9: Variation 1

Variation 2: The method of effective widths and the distance for the elastic section modulus from the centroid to the end of the gross web.

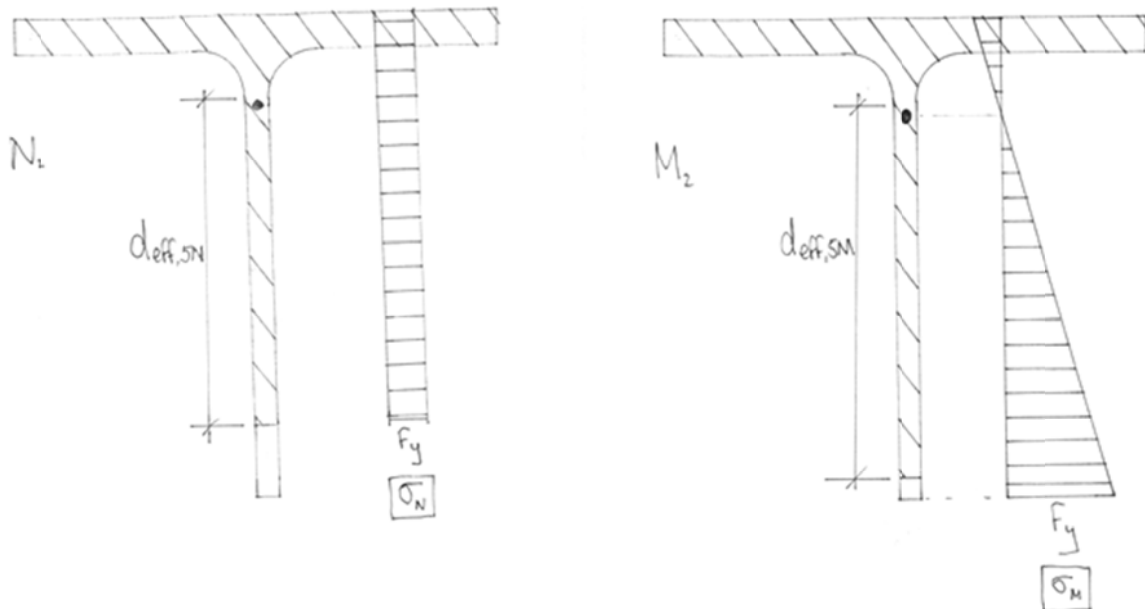


Figure 10: Variation 2

Variation 3: The method of effective thickness and the distance for the elastic section modulus from the centroid to the end of the gross web.

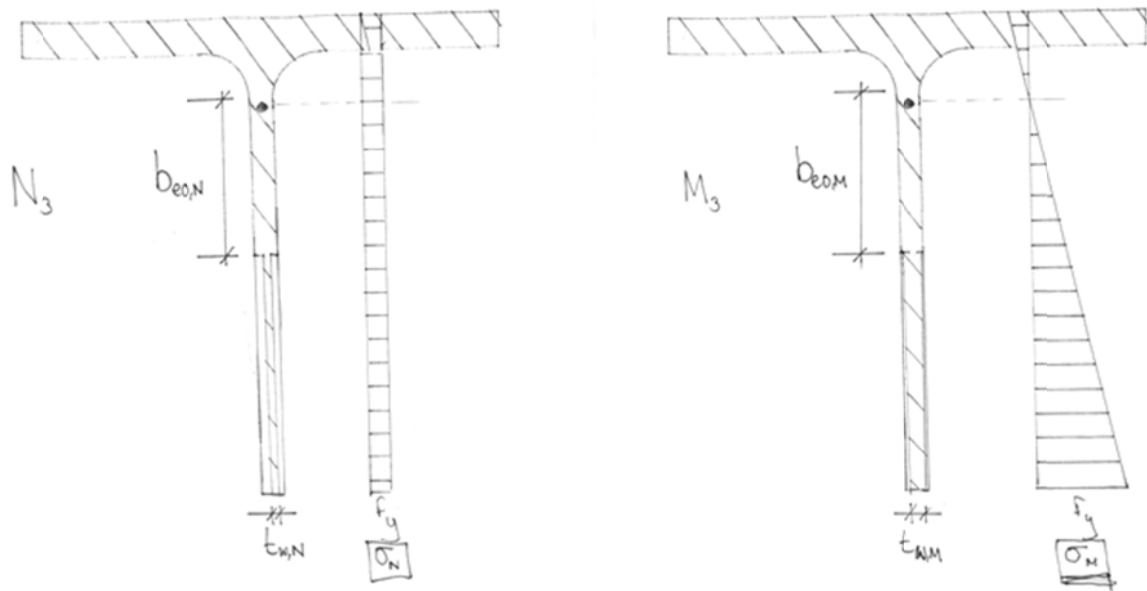


Figure 11: Variation 3

Variation 4: The method of reduced strength using the gross cross-section values and the reduced strength.

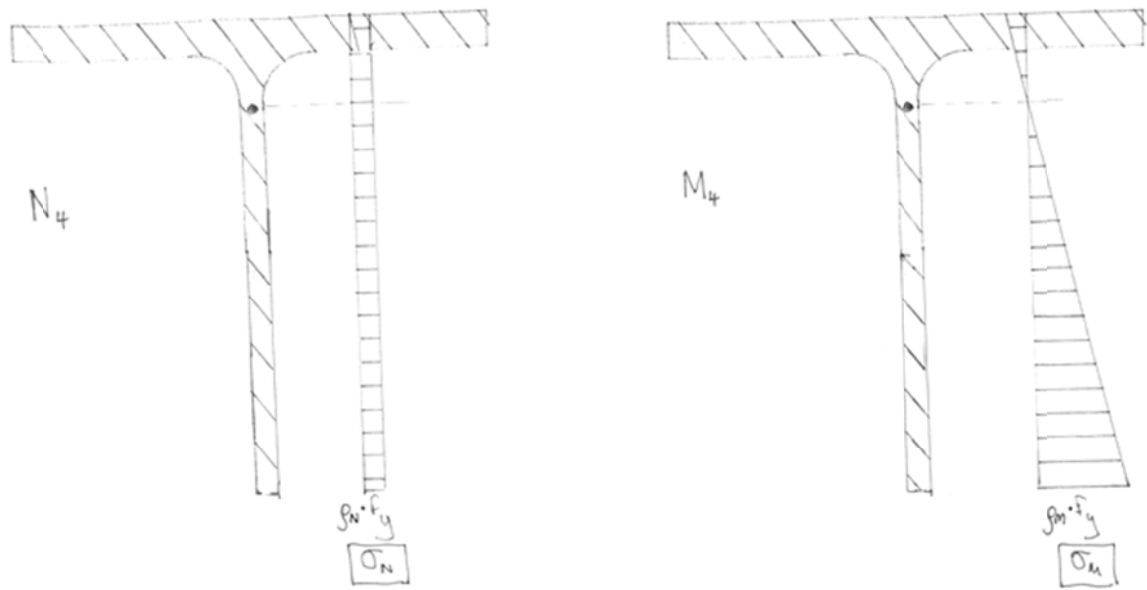


Figure 12: Variation 4

The values for N_{Rd} under compression have been calculated earlier in this chapter. Here are the results combined together:

Cross Section	N_{Rd} - Var 1 [kN]	N_{Rd} - Var 2 [kN]	N_{Rd} - Var 3 [kN]	N_{Rd} - Var 4 [kN]
1/2 IPE 300	602	602	600	537
1/2 IPE 400	924	924	920	781
1/2 IPE 500	1227	1227	1222	1004
1/2 IPE 500 - thin	851	851	846	725
1/2 IPE 500 - wide	1603	1603	1598	1281
1/2 IPE 600	1636	1636	1630	1333
1/2 HEA 500	2265	2265	2263	2087

Table 15: Comparison pure compressive resistance N_{Rd} for variations 1, 2, 3 and 4

From the results shown in Table 15, it was clear that the values for variations 1 and 2 were essentially identical to variation 3, which they must be in this case. The reduced stress method, variation 4, is always conservative, as expected.

The values for M_{Rd} under pure bending have also been calculated earlier in this chapter. Here are the results combined together:

Cross Section	M_{Rd} - Var 1 [kNcm]	M_{Rd} - Var 2 [kNcm]	M_{Rd} - Var 3 [kNcm]	M_{Rd} - Var 4 [kNcm]
1/2 IPE 300	995	897	968	971
1/2 IPE 400	1887	1610	1911	1950
1/2 IPE 500	3308	2561	3302	3389
1/2 IPE 500 - thin	3718	2504	3191	3144
1/2 IPE 500 - wide	3141	2574	3323	3508
1/2 IPE 600	5512	4125	5459	5603
1/2 HEA 500	4642	4591	4649	4669

Table 16: M_{Rd} for variations 1, 2, 3 and 4

From the results shown in Table 16 it was clear that the values for variations 1 and 3 were very similar, while variation 2 leads to very conservative results. This meant that the correct interpretation of the effective width method from EC 3 part 1-5 was where the stress values

were assumed at the extremity of the effective and *not* the gross section. Interestingly, variation 4 was not always the most conservative method.

3.5 Defining the effective sections used in this thesis

For this thesis it was decided that the *two* effective sections for the isolated loading conditions (N and M) would *not* be used - the more accurate iterative method based on the combined stress state due to N and $\Delta M = N * e_N$ was used instead (N.B. The shift e_n was also calculated for the combined stresses due to $N + \Delta M$). This method used to obtain an effective section for both the axial compression as well as the bending due to the centroid shift is explained in 3.5.1 “Axial compression and moment due to centroid shift”.

3.5.1 Axial compression and moment due to centroid shift

Using EC 3, part 1-5, this procedure was carried out for all of the sections under axial compression. The starting point for these calculations was a stress ratio of $\psi = 1$. For the first iteration, the shift in the centroid between the gross section and the new effective section (based on $\psi = 1$) was calculated, e_N^* .

$$e_N^* = z_s - z_{s,eff^*}$$

Next the force present in the first iteration N^* was calculated so that the moment that was induced through the centroid shift could be taken into account. It was assumed that the stress at the free end of the effective web was equal to the yield strength, f_y . The criterion used to calculate the force was

$$\frac{N^*}{A_{eff}^*} + \frac{N^* * e_N^* * (h^* - z_{s,eff^*})}{I_{y,eff}^*} = f_y$$

From here N^* was calculated.

$$N^* = \frac{f_y}{\frac{1}{A_{eff}^*} + \frac{e_N^* * (h^* - z_{s,eff^*})}{I_{y,eff}^*}}$$

Before the accurate stress ratio ψ could be calculated, σ_1 and σ_2 had to be calculated.

3 Defining the Effective Dimensions and Properties

$$\sigma_2 = \frac{N^*}{A_{eff}^*} - \frac{N^* * e_N^* * (t_f + r - z_{s,eff}^*)}{I_{y,eff}^*}$$

$$\sigma_1 = \frac{N^*}{A_{eff}^*} - \frac{N^* * e_N^* * (h - z_{s,eff}^*)}{I_{y,eff}^*}$$

It must be noted that here σ_1 is a theoretical stress value that was larger than the yield strength.

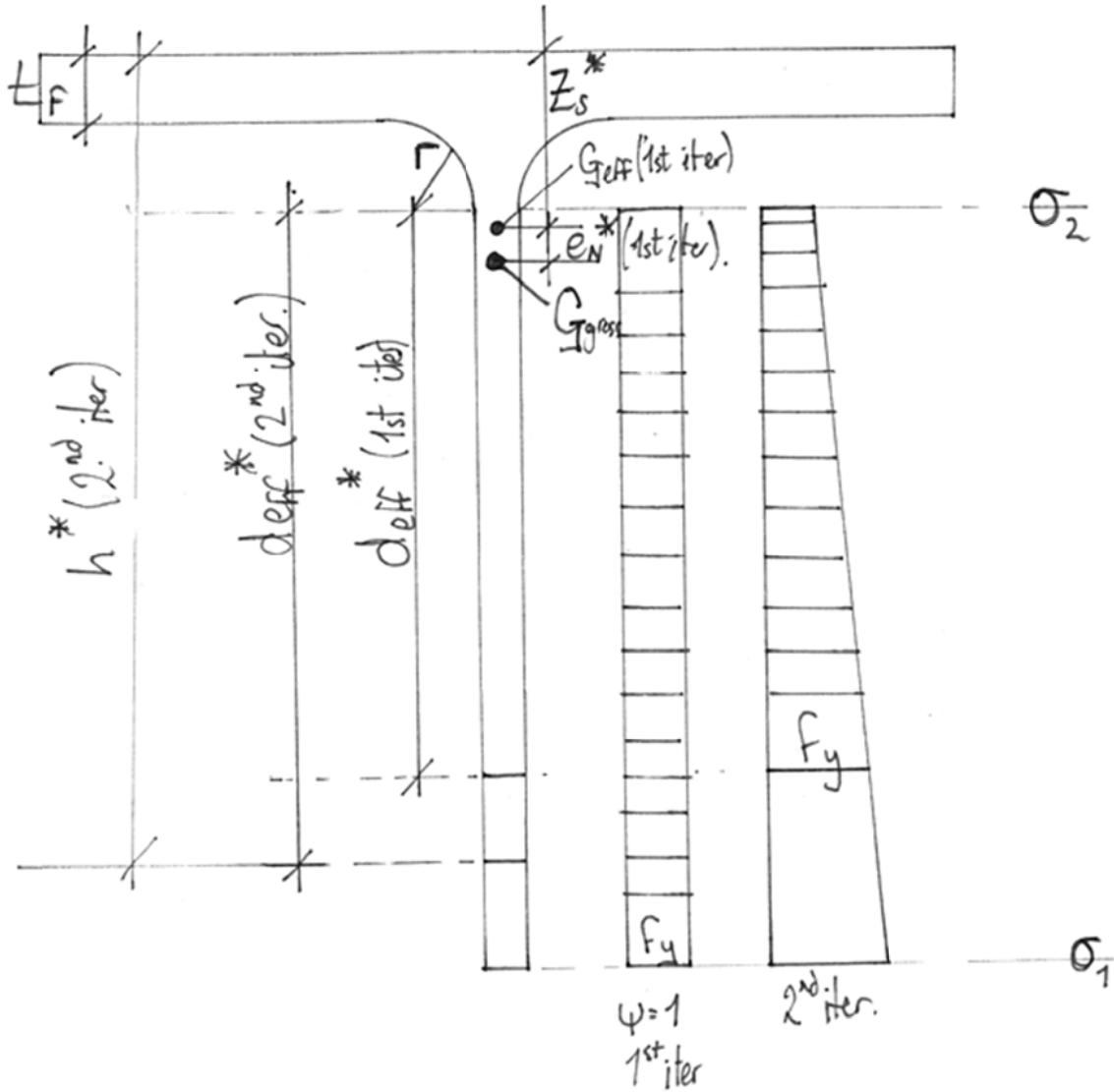


Figure 13: Effective width method for combined N and M

The stress ratio, ψ , buckling coefficient, k_σ , the equivalent compression web slenderness, $\bar{\lambda}_w$, the buckling reduction factor, ρ and finally the effective width, $d_{eff,5}$ were all

3 Defining the Effective Dimensions and Properties

calculated the same way as for the HE-A 500 in chapter 3.1 “Eurocode 3, part 1-5 - Method of effective width”. These values were then used for the iteration until the result converged.

Cross Section	d_{eff}^{\cdot} 1 st iteration (cm)	d_{eff}^{\cdot} 2 nd iteration (cm)	d_{eff}^{\cdot} 3 rd iteration (cm)	d_{eff}^{\cdot} 4 th iteration (cm)	d_{eff}^{\cdot} 5 th iteration (cm)
1/2 IPE 300	10.58	10.85	10.80	10.81	10.81
1/2 IPE 400	13.10	13.61	13.53	13.54	13.54
1/2 IPE 500	15.81	16.59	16.47	16.49	16.49
1/2 IPE 500 - thin	15.81	16.50	16.40	16.42	16.41
1/2 IPE 500 - wide	15.81	16.64	16.50	16.53	16.52
1/2 IPE 600	18.69	19.68	19.52	19.55	19.54
1/2 HEA 500	17.53	17.83	17.78	17.79	17.79

Table 17: The effective depth of the web after each iteration - N and ΔM

Here are the results for the effective sections due to N and $\Delta M = N * e_N$ using the method of effective widths and iteration.

Cross Section	d_{eff} [cm]	Stress ratio	A_{eff} [cm ²]	$I_{y,eff}$ [cm ⁴]	W_{eff} [cm ³]	$z_{s,eff}$ [cm]	e_N [cm]
1/2 IPE 300	10.81	0.71	25.76	367.40	34.850588	2.84	0.49
1/2 IPE 400	13.54	0.61	39.64	909.39	67.9846403	3.61	0.91
1/2 IPE 500	16.49	0.53	52.85	1777.23	113.055456	4.47	1.54
1/2 IPE 500 - thin	16.41	0.57	36.78	1450.95	103.014872	6.03	1.97
1/2 IPE 500 - wide	16.52	0.51	68.89	1956.35	117.848597	3.62	1.25
1/2 IPE 600	19.54	0.51	70.60	3389.04	184.246881	5.45	2.03
1/2 HEA 500	17.79	0.79	96.71	3249.61	173.928433	4.10	0.41

Table 18: Method of effective widths - final effective section properties

N.B. These are the values that will be used for the rest of this thesis. All the values listed in the Table 18 are due to N and $\Delta M = N * e_N$. From this point on the indices “eff” means the same as “eff,M+N”.

In the rest of this thesis, if it is not otherwise stated, $W_{eff} = W_{y,eff,N+M(s)}$ and $W_{y,eff} = W_{y,eff,N+M(s)}$ where $W_{y,eff,N+M(s)}$ is the elastic section modulus, y-y axis, to the bottom of the web free end for the effective cross-section due to N and M according to EC1993-1-5.

4 FEM Model for GMNIA Analyses

Rather than carrying out lots of costly real experiments, appropriate finite element models were produced and buckling force calculations were carried out on these. This corresponds to the state-of-the-art in stability research for steel structures and is justified by the high degree of accuracy that can be achieved by numerical non-linear buckling analyses. The finite element program that was used was *ABAQUS standard 10.1*.

4.1 System

As in Eurocode 3, the calculations were carried out on a single member that was pinned at both ends and the axial compression was applied to the centroid of the gross cross section.

The calculations were carried out for 20 different member lengths for each of the cross sections. The length for each member was calculated using the bending slenderness in the z direction, $\bar{\lambda}_z$ for the gross section, as an input parameter, in order to make sure that lengths corresponding to comparable levels of buckling sensitivity were chosen for the different cross-sections.

The $\bar{\lambda}_z$ slenderness was varied in intervals of 0.1, (0.1, 0.2, 0.3, ... , 1.9) up to, 2.0 and using the following formula the real member length, L_{cr} , for each cross-section shape was then defined.

Based on

$$\bar{\lambda}_z = \frac{\lambda_z}{\lambda_1} = \frac{L_{cr}}{i_z * \lambda_1}$$

The member length L_{cr} was found:

$$\lambda_1 = \pi * \sqrt{\frac{E}{23.5}}$$

$$L_{cr} = \bar{\lambda}_z * i_z * \lambda_1$$

The radius of gyration around the z-z axis for the gross section was calculated.

$$i_z = \sqrt{\frac{I_z}{A}}$$

In Table 19 the final lengths that were considered for the IPE 300 are shown.

Cross Section	L_{cr} [cm]	Cross Section	L_{cr} [cm]
1/2 IPE 300	31	1/2 IPE 300	346
1/2 IPE 300	63	1/2 IPE 300	378
1/2 IPE 300	94	1/2 IPE 300	409
1/2 IPE 300	126	1/2 IPE 300	440
1/2 IPE 300	157	1/2 IPE 300	472
1/2 IPE 300	189	1/2 IPE 300	503
1/2 IPE 300	220	1/2 IPE 300	535
1/2 IPE 300	252	1/2 IPE 300	566
1/2 IPE 300	283	1/2 IPE 300	598
1/2 IPE 300	315	1/2 IPE 300	629

Table 19: Lengths, L_{cr} , calculated for the IPE 300 sections

4.2 FEM model

A finite element model for the T-sections was created. It consisted of 16 elements for the flange and 20 elements for the web in the cross section. The elements were modelled using shell elements. They were chosen from the ABAQUS library. The S4, which uses a linear function, was chosen as an appropriate element. The computational time was acceptable, the hourglass effect was not an issue and it prevented membrane and shear locking.

The model of the flange was created using an offset for the shell. This meant that the nodes on the middle line of the flange could coincide with the top edge of the web. The web was

modelled without an offset. It was decided that the models should be 100 elements long. This is independent from the total length. This means that an input file could be created for every cross-section and for every length and all would have the same number of elements and nodes. The input file generation was much faster using this method.

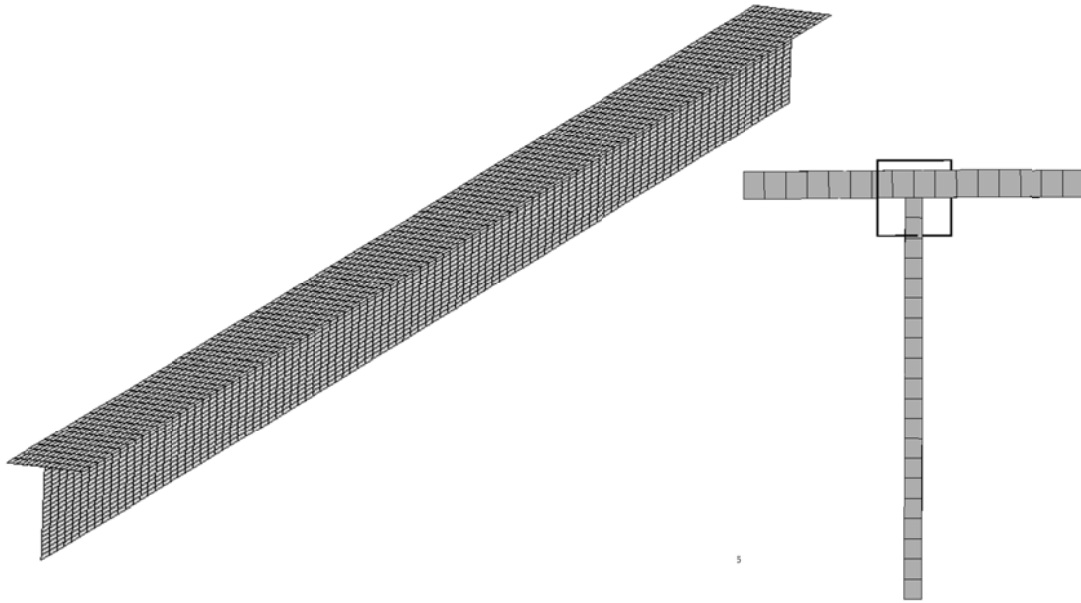


Figure 14: Elements of the finite element model

The fillets, between flange and web, also needed to be modelled. Both fillets were modelled using one beam element. It was important that the beam, which replaced the fillets, had as many of the same properties as possible. The fillets supply a large resistance to torsion. It also has an area which is important for the axial compression. It was important that the beam had the same area as the fillet and the same torsional constant.

A box beam element was used to model the fillets. Its centre of gravity coincided with point where the web shell and the flange shell met. This was the middle of the flange underside. The thickness of the walls and the distance between the walls were calculated so that they created the same effects as the fillets.

The area

$$A_{fi} = A - b * t_f - (h - t_f)t_w$$

and torsional constant were the same as the fillet's.

$$I_{T,fi} = I_T - \frac{1}{3}(b * t_f^3 + (h - t_f)t_w^3)$$

N.B. I_T is the torsional constant of the gross section “with fillets”

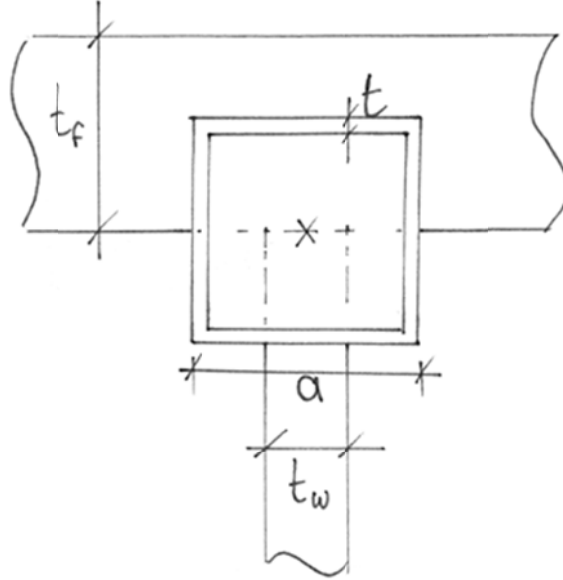


Figure 15: The fillet replacement - box beam element [3]

A and I_T define the total area and torsional constant of the gross T-section.

The torsion constant for a thin walled square that replaces the fillet is calculated as follows.

$$I_{T,rep} = a_{rep}^3 * t_{rep}$$

And the area

$$A_{rep} = 4 * a_{rep} * t_{rep}$$

From these formula and the calculated values of the real fillet we can calculate the thickness and the width of the replacement box.

$$a_{rep} = \sqrt{\frac{4 * I_{T,fi}}{A_{fi}}}$$

$$t_{rep} = \frac{I_{T,fi}}{a_{rep}^3}$$

4.3 Imperfections

Geometric imperfections were needed in the model for both local and global buckling failure modes. In Eurocode 3 part 1-5, Annex C, it is explained how finite element calculations should be modelled and carried out whenever the plate buckling phenomena needs to be considered. It states that either the local imperfection should be modelled at 100% and the global at 70%, or vice versa. The calculations were all carried out for both cases and the worst case scenario was then used to define the results.

A Linear Buckling Analysis (LBA) was first considered as a viable option to include relevant imperfection shapes into the GMNIA analysis, where the buckling mode would have been multiplied by the amplitude of the imperfection as in many other investigations that have been carried out at the TU-Graz. The problem involved here was that - for T-sections, where the global torsional-flexural mode strongly resembles a local buckling mode - the results from the LBA analysis did not make it possible to define the local and global failure modes independently and therefore made it difficult to apply the correct amplitudes.

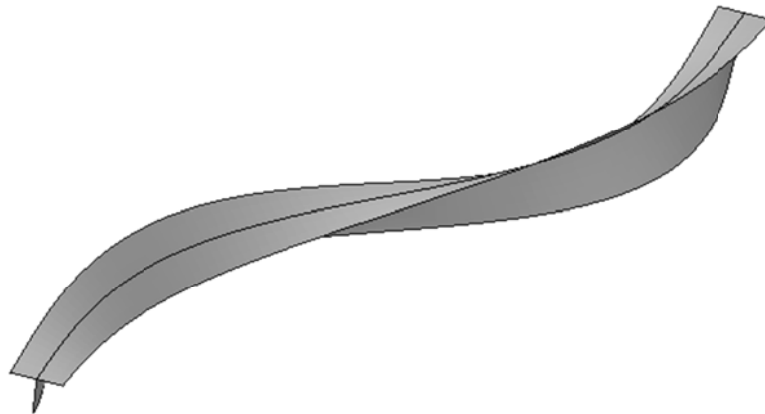


Table 20: Example of LBA results - always global and local modes involved.

Therefore it was decided to model the imperfections directly into the model. The global imperfection was taken as a half sine wave along the whole length of the member, either upwards, downwards or sideways with an amplitude equal to $L_{cr}/1000$, where L_{cr} is the member length.

$$e_{0,glob} = \frac{L_{cr}}{1000}$$

For the local imperfections a number of half sine waves were applied to the member. They were considered to be a rotation of the cross section around the centre of gravity of the gross section where the deflection of the end of the web was equal to the amplitude of the local imperfection. The number of waves was dependent on the length of the member L_{cr} and d , the depth of the web.

$$m = L_{cr}/d$$

m was then rounded to the nearest whole number and this was the number of half sine waves that were implemented for the local imperfections.

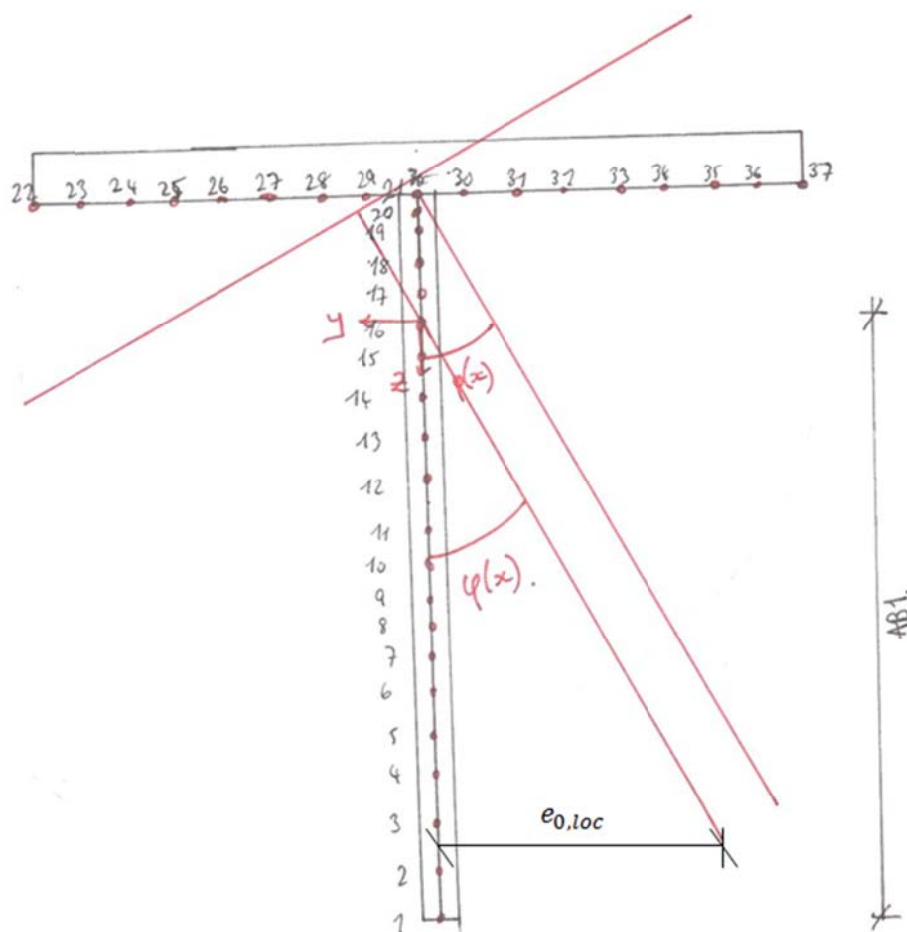


Figure 16: Rotation of the section due to local imperfections

The line through the member, along the sections centre of gravity, would therefore only experience a global imperfection in the shape of a half sine wave and no local imperfection. The maximal amplitude of the local imperfections was set as explained in Eurocode 3, part

1-5, Annex C, the local imperfection amplitude, $e_{0,loc}$, was 80% of the manufacturing tolerance.

$$e_{0,loc} = \frac{d}{150} * 80\%$$

The position of every node, for each of the situations was calculated. All the possible situations were considered and a model made for each. For example, a member with 100% global imperfection sideways and 70% local imperfection where the first half sin wave deflection is in the same direction as the global deflection.

As all of the calculation members were 100 elements long, it was very simple to add the global imperfection. It was simply dependent on the amplitude which was dependent on the direction of the imperfection and whether the global imperfection was the main imperfection.

The position of every node could then be calculated depending on the node plane number, i , along the length of the member.

$$e_{0,glob,i} = e_{0,glob} * \sin\left(\frac{i * \pi}{100}\right) \quad \text{for } 0 \leq i \leq 100$$

The local imperfection, as previously stated, was considered to be a rotation around the centre of gravity (Figure 16). The final starting coordinates of the nodes were dependent on;

- the number of half sine waves along the length of the member.
- the dominant imperfection (local or global).
- the distance from the end of the member.
- the size of the imperfection.
- the distance of the node from the centre of gravity.

The rotation of the section at each node plane i was first calculated dependent on the size of the largest local imperfection and in which plane along the x axis the section was to be found.

$$\varphi = \frac{e_{0,loc}}{AB1} * \sin\left(\frac{i * \pi * m}{100}\right) \quad \text{for } 0 \leq i \leq 100$$

Once the rotation had been defined it was possible to define the coordinates of every node of each section. The original coordinates of the nodes were needed, \bar{P} .

$$\bar{P}' = \bar{T} \cdot \bar{P}$$

The transformation matrix, \bar{T} , is a simple rotation matrix. It is different for a clockwise and an anticlockwise rotation.

$$\bar{T} = \begin{bmatrix} \cos\left(\frac{e_{0,loc}}{AB1} * \sin\left(\frac{i * \pi * m}{100}\right)\right) & -\sin\left(\frac{e_{0,loc}}{AB1} * \sin\left(\frac{i * \pi * m}{100}\right)\right) \\ \sin\left(\frac{e_{0,loc}}{AB1} * \sin\left(\frac{i * \pi * m}{100}\right)\right) & \cos\left(\frac{e_{0,loc}}{AB1} * \sin\left(\frac{i * \pi * m}{100}\right)\right) \end{bmatrix}$$

In the other direction it looks like this

$$\bar{T} = \begin{bmatrix} \cos\left(\frac{e_{0,loc}}{AB1} * \sin\left(\frac{i * \pi * m}{100}\right)\right) & \sin\left(\frac{e_{0,loc}}{AB1} * \sin\left(\frac{i * \pi * m}{100}\right)\right) \\ -\sin\left(\frac{e_{0,loc}}{AB1} * \sin\left(\frac{i * \pi * m}{100}\right)\right) & \cos\left(\frac{e_{0,loc}}{AB1} * \sin\left(\frac{i * \pi * m}{100}\right)\right) \end{bmatrix}$$

The vector for the global imperfection is dependent on the direction of the imperfection. Either it curves upwards, downwards or laterally.

$$\bar{G} = \left[e_{0,glob} * \sin\left(\frac{i * \pi}{100}\right) \right] * \begin{bmatrix} 1 \\ 0 \end{bmatrix} \quad \text{sideways}$$

$$\bar{G} = \left[e_{0,glob} * \sin\left(\frac{i * \pi}{100}\right) \right] * \begin{bmatrix} 0 \\ \pm 1 \end{bmatrix} \quad \text{vertical}$$

From the global and the local imperfections, the final starting coordinates were calculated for each of the nodes. The final starting positions of the nodes are given using these formulae:

$$\bar{P}' = \bar{P} + \bar{G} + 0.7 * \bar{T} \cdot \bar{P}$$

$$\bar{P}' = \bar{P} + 0.7 * \bar{G} + \bar{T} \cdot \bar{P}$$

Due to the different imperfection combinations and the fact that either the global or the local imperfection was dominant, 240 input files were produced for each section. 12 Files for each of the 20 lengths.

4.4 Residual Stress

Residual stresses are present in rolled or welded sections even when there are no loads or actions acting on the member. In the case of T-sections, the residual stresses caused by the method of manufacture are particularly complex, and little studied.

The T-sections that were investigated were bisected I sections. It was assumed that the production of these T-sections was as follows:

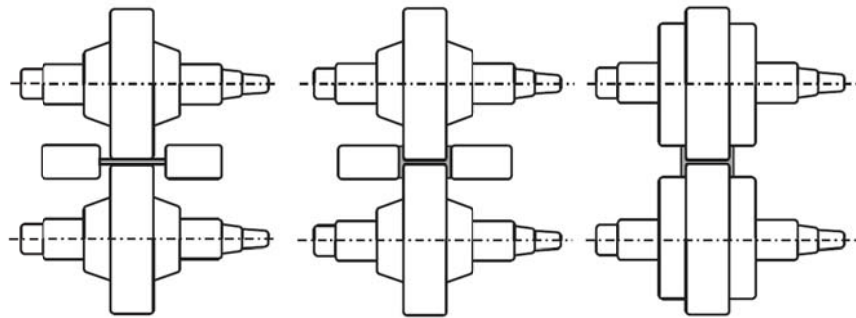


Figure 17 : The process of hot rolling to produce an I section [3]

The original sections were hot rolled. The hot rolling process happened in several steps at temperatures between 900-1200°C [3]. After the section had been formed, it cooled. The cooling of the section parts occurred at different speeds. The outer parts of the flanges cooled relatively quickly whereas the centre of the fillet cooled very slowly. This caused residual stresses in the IPE/HE-A sections.



Figure 18 : A bisected I beam into two T-sections [6]

After the sections had cooled, they were bisected. This can be seen in Figure 18. It was assumed that the cutting process did not cause the residual stresses to change. It did however cause the member to bend. The sections were then bent in the opposite direction until a straight beam was produced.

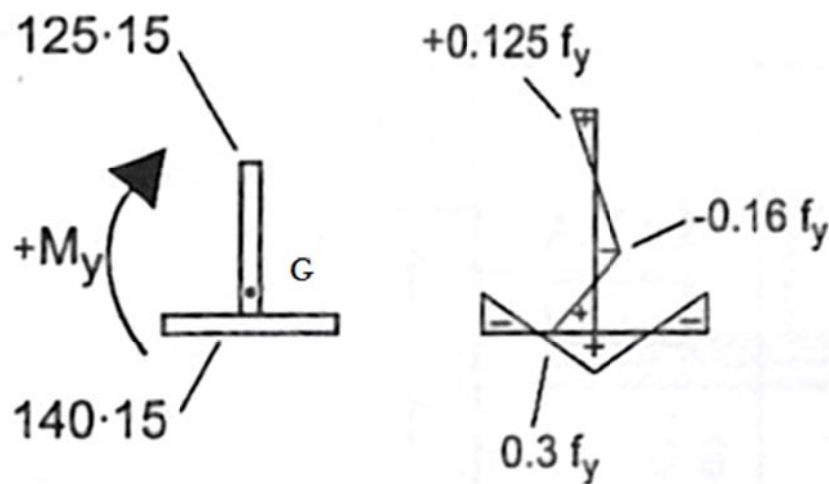


Figure 19 : Residual stress, T-section - as proposed by Peter Kaim[7]

Peter Kaim, in his dissertation [7], suggested a distribution for the residual stresses within the T-sections. This distribution can be seen in Figure 19. The method he used to arrive at this distribution is unfortunately not clear: with the given distribution of stresses, depending on different assumptions regarding the lengths of the segments under tension or compression, the sections must invariably be either slightly out of equilibrium, either for axial forces or for bending moments. Thus, a different solution was found by analytical

means, which could then be more easily translated onto every cross-section that was investigated without having to artificially compensate for an initial lack of equilibrium.

This alternative state of residual stress was determined as follows: the residual stresses for a double symmetric I beam were used as the initial situation of the T-sections. It was assumed that the T-sections were then created by a “cold” cutting technique, which induces no additional thermal stresses. This situation would lead to an imbalance of moments within the two sections leading to a resulting moment and corresponding vertical deformations (Figure 20). The latter ones can also be observed in real fabrication processes as an outward “bent” of cut specimens, see the following figure, which shows the curvature induced by (thermal) cutting during the fabrication of cellular beams (Figure 21).

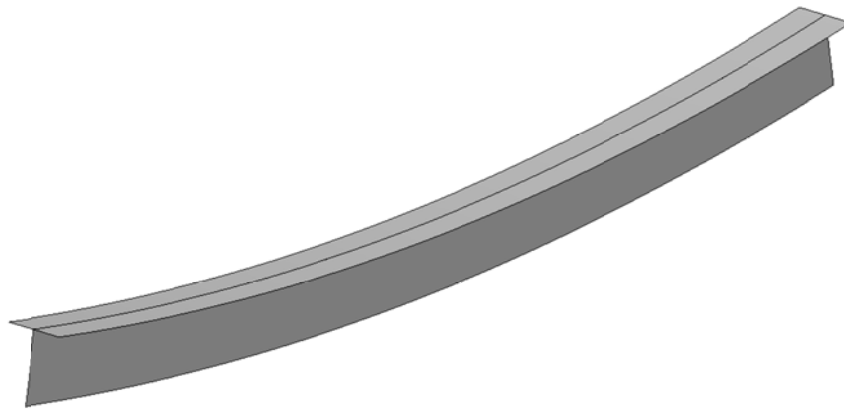


Figure 20: Curvature after bisecting an IPE 500 beam (amplified 100 times)

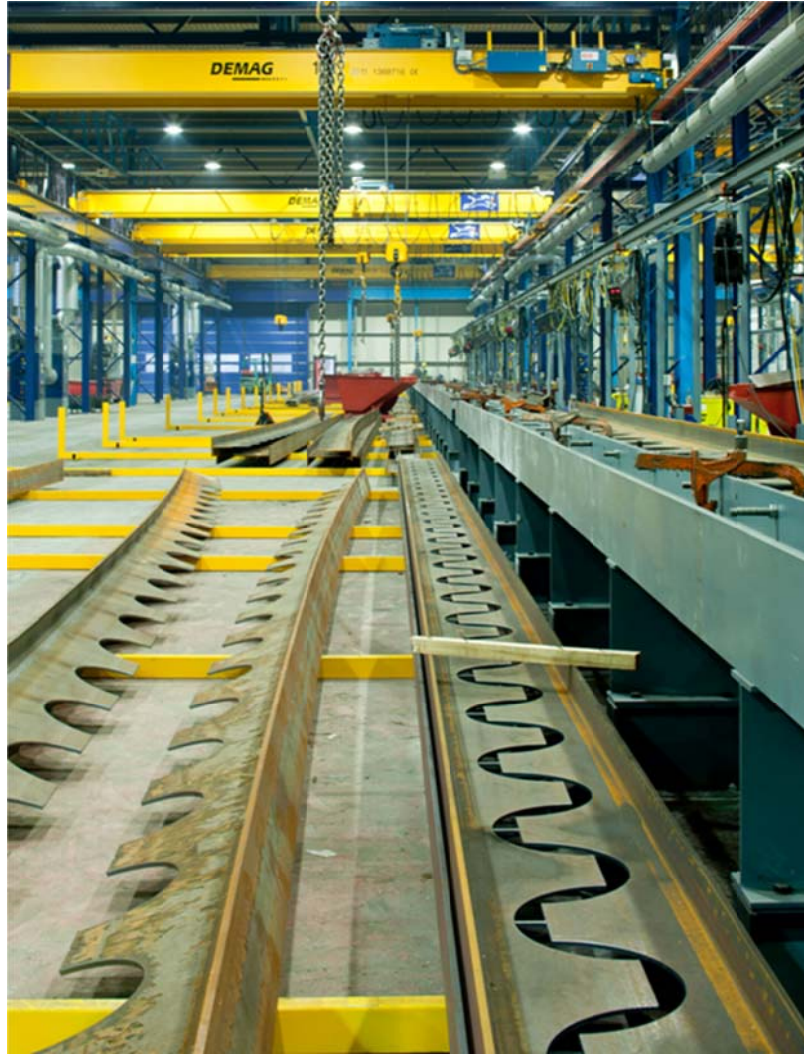


Figure 21: Cut beams for the production of cellular beam[8]

The moment caused from this stress distribution was then calculated. The forces in the flange before cutting were in equilibrium and therefore did not influence the moment. Thus, only the elastic section modulus and the stress distribution over the web were considered.

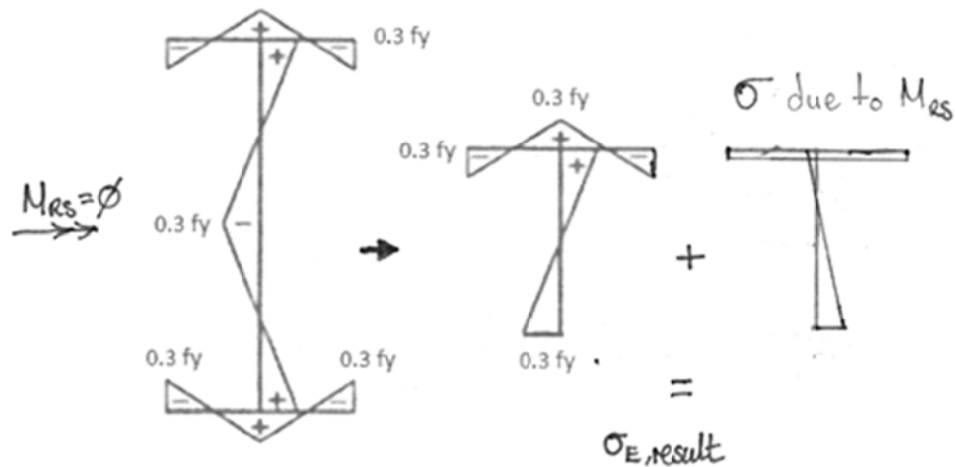


Figure 22: Residual stresses for an I beam transposed onto a T-section

The moment caused by the stress distribution in the web, shown in Figure 22, was calculated. The gross elastic section properties were used for these calculations as the yield strength was not reached at any point on the section. The moment that was needed to counteract the bending induced by the “imbalanced” residual stress distribution immediately after cutting was then calculated.

$$M_{RS,I} = \frac{0.3 * f_y * t_w * (h - t_f)^2}{6}$$

This moment was then applied to the gross T-section but not on the FEM model. The resulting stress distribution based on an elastic stress calculation, was then added to the initial stress distribution of the I-section. This combination of stresses was then considered to be the residual stress situation for the T-sections in the FEM model. The final distribution of an IPE500 section can be seen in Figure 23.

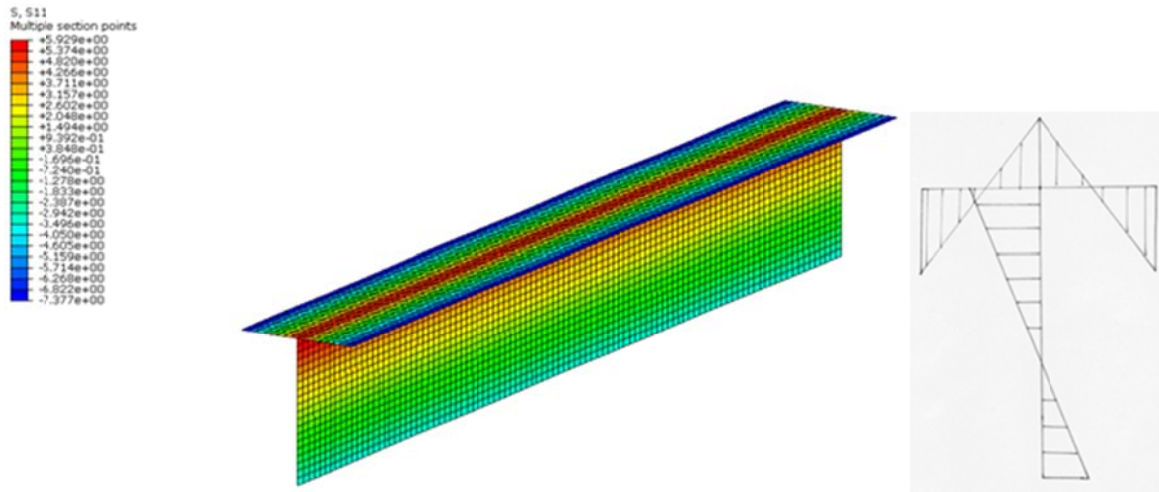


Figure 23: Residual stress distribution for an IPE 500 with $[\text{kN/cm}^2]$

This assumption for residual stresses does not depict the real residual stress distribution perfectly: it does not consider the more common thermal cutting processes, which would induce new thermal residual stresses into the section, and also omits the effects of any straightening of the members, which would include some plastic deformations and thus, additional redistributions of the internal (residual) stresses. It was however considered to be a good and slightly conservative approximation, especially because the increased compression stresses in the flange. To obtain the real residual stress distribution more research would be necessary and there would probably be a need for real experiments to be carried out. This would return other results.

5 Buckling Strength of Class 2 Sections

As stated in the introduction, the main focus of this thesis is put on slender class 4 sections. However, in order to understand the interaction problem for class 4 sections and the appropriate torsional-flexural and lateral-torsional effects, it was decided that class 2 sections should be looked at first, allowing for a clearer separation of the global (torsional-flexural) buckling phenomenon from the interactive global-local buckling phenomenon. The difference between class 2 sections and the class 4 sections is that for the first ones there is no danger of local buckling accelerating the loss in stability. This means, also, that there will be no moment M_y present when the T-section is loaded in the centre of gravity and therefore only lateral buckling and torsion-flexural buckling modes are possible when loaded with an axial compression force.

5.1 Studied class 2 section

Initially, a single class 2 section was considered for the calculations concerned with class 2 sections. For this, a modified IPE 500 was used. The web thickness was increased until it was a class 2 section. As the section was to be made of S235 steel and loaded under an axial compression load, this meant that the d/t_w ratio had to be less than 10.

$$\frac{d}{t_w} < 10$$

As the depth of the section was kept the same the thickness was calculated.

$$d = h - t_f - r$$

$$d = 25 - 1.6 - 2.1 = 21.3 \text{ cm}$$

$$t_w > \frac{21.3}{10} = 2.13 \text{ cm}$$

A thickness of 2.2 cm was chosen.

The class of the flange also needed to be obtained

$$10 > \frac{b - t_w}{2} - r$$

$$10 > \frac{20 - 2.2}{2} - 2.1 = 6.8$$

As the flange is class 1 in all cases, the section is defined by the web. This section is a valid class 2 section.

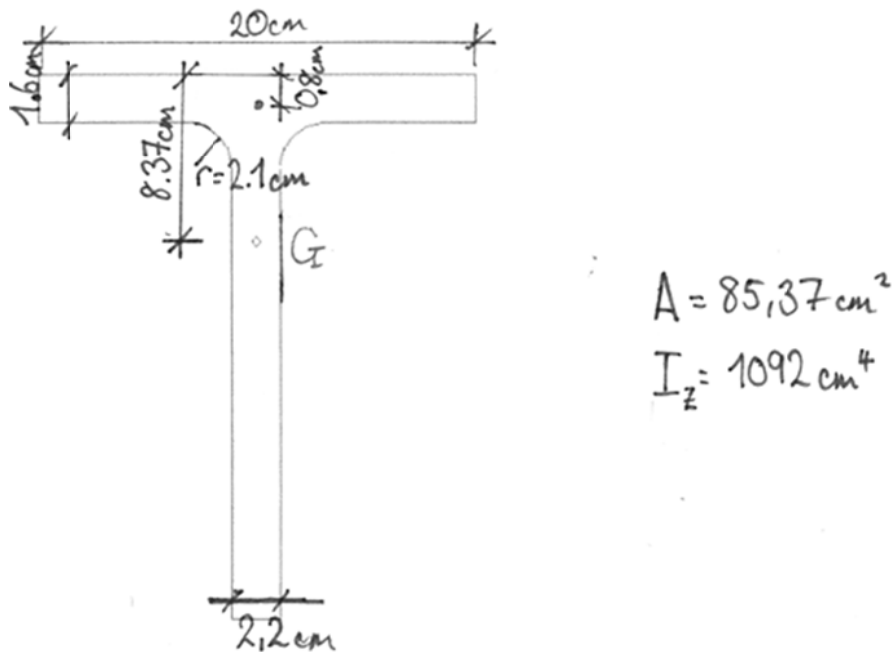


Figure 24: Modified IPE 500 with a thick class 2 web

5.2 Section properties

The characteristic plastic resistance for the section was calculated and this value was the basis for the ABAQUS calculations. This was simply the area of the section multiplied by the yield strength.

$$N_{pl} = A * f_y$$

Twenty members were calculated, each with a different length. The lengths of the members were selected as described in 4.1 “System”. Here is an example for this section shown in Figure 24 and based on a dimensionless slenderness of 0.6.

$$L = \bar{\lambda}_z * \pi * \sqrt{\frac{E}{f_y} * \frac{I_z}{A}} = 0.6 * \pi * \sqrt{\frac{21000}{23.5} * \frac{1092.800}{85.3728}} = 202 \text{ cm}$$

The members with these lengths were then analysed in ABAQUS. The members were calculated taking into account the modelled local and global imperfections. From the 12 results for each length, the smallest was taken as the defining value.

5.3 ABAQUS results

The results were obtained from ABAQUS by seeing at which step the calculations aborted. If the calculation had not aborted and continued to the end then the full resistance had been achieved. These results were then plotted as a graph of the reduction factor against the slenderness $\bar{\lambda}_{TF}$, which will be given in chapter 5.4. This can be seen in Figure 25.

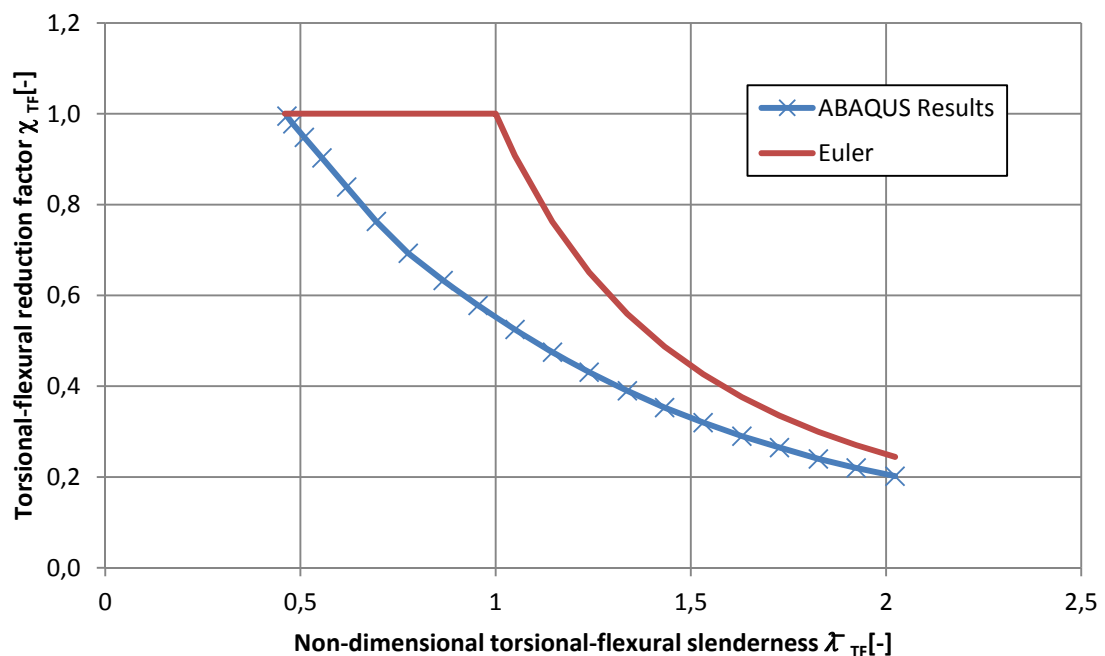


Figure 25: GMNIA results for a class 2 T-section

The comparison to the Euler critical load was also made. This is the maximum critical load that an ideal column can carry. An ideal column is a perfectly straight, homogenous column that does not contain any residual stress [9]. The section is 100% identical along its entire length.

5.4 Results and comparison with Eurocode 3

The resistance to an axial force according to Eurocode 3 was then calculated.

The value of the cross-section capacity N_{pl} was used that had previously been calculated in 5.2 “Section properties”. The critical elastic torsional force $N_{cr,T}$ and the critical elastic torsional-flexural force, $N_{cr,TF}$ were calculated as stated in the dissertation from Peter Kaim [7].

$$N_{cr,z} = \frac{\pi^2 * E * I_z}{L^2}$$

$$i_y = \sqrt{\frac{I_y}{A}}$$

$$i_z = \sqrt{\frac{I_z}{A}}$$

$$z_0 = z_s - \frac{t_f}{2}$$

The i_0 is defined

$$i_0^2 = i_y^2 + i_z^2 + z_0^2$$

$$N_{cr,T} = \frac{1}{i_0^2} * G * I_T$$

$$N_{cr,TF} = \frac{N_{cr,z}}{2 * \left(1 - \frac{z_0^2}{i_0^2}\right)} \left[1 + \frac{N_{cr,T}}{N_{cr,z}} - \sqrt{\left(1 - \frac{N_{cr,T}}{N_{cr,z}}\right)^2 + 4 * \left(\frac{z_0^2}{i_0^2}\right) * \frac{N_{cr,T}}{N_{cr,z}}}\right]$$

The relative torsional-flexural slenderness was calculated.

$$\bar{\lambda}_{TF} = \sqrt{\frac{N_{pl}}{N_{cr,TF}}}$$

The buckling curve for bisected IPE or HE-A sections is not stated in Eurocode. As one can see in Table 21, the T-section that is shown in Eurocode 3 does not have the same shape as the members that are being dealt with in this thesis.

Cross section		Limits	Buckling about axis	Buckling curve	
				S 235 S 275 S 355 S 420	S 460
Rolled sections		$h/b > 1,2$	$t_f \leq 40 \text{ mm}$	y-y z-z	a a ₀
			$40 \text{ mm} < t_f \leq 100$	y-y z-z	b a
		$h/b \leq 1,2$	$t_f \leq 100 \text{ mm}$	y-y z-z	b a
			$t_f > 100 \text{ mm}$	y-y z-z	d c
Welded I-sections		$t_f \leq 40 \text{ mm}$	y-y z-z	b c	
		$t_f > 40 \text{ mm}$	y-y z-z	c d	
Hollow sections		hot finished	any	a	a ₀
		cold formed	any	c	c
Welded box sections		generally (except as below)	any	b	b
		thick welds: $a > 0,5t_f$ $b/t_f < 30$ $h/t_w < 30$	any	c	c
U-, T- and solid sections			any	c	c
L-sections			any	b	b

Table 21: Buckling curve definition for different sections

As it was not clear which curve should be applied, both the b and the c curves were investigated for the studied T-section.

The coefficients for calculating the reduction factors were calculated for both buckling curves using $\alpha_z = 0.49$ for buckling curve c and $\alpha_z = 0.34$ for buckling curve b.

$$\Phi_{TF} = 0.5[1 + \alpha_z(\bar{\lambda}_{TF} - 0.2) + \bar{\lambda}_{TF}^2]$$

Then the reduction factors for torsional-flexural buckling were calculated.

$$\chi_{TF} = \frac{1}{\Phi_{TF} + \sqrt{\Phi_{TF}^2 - \bar{\lambda}_{TF}^2}} \leq 1.0$$

Length [cm]	$\bar{\lambda}_{TF}$	Φ_{TF} curve c	χ_{TF} curve c	Φ_{TF} curve b	χ_{TF} curve b
0	0.4605467	0.6699	0.8648	0.6503	0.9013
34	0.46537879	0.6733	0.8622	0.6534	0.8992
67	0.4804819	0.6841	0.8538	0.6631	0.8928
101	0.50999822	0.7060	0.8374	0.6827	0.8798
134	0.55518391	0.7411	0.8116	0.7145	0.8589
168	0.61836713	0.7937	0.7744	0.7623	0.8277
202	0.69434784	0.8622	0.7282	0.8251	0.7869
235	0.77603107	0.9422	0.6772	0.8990	0.7391
269	0.86525326	1.0373	0.6213	0.9874	0.6834
302	0.95495839	1.1409	0.5665	1.0843	0.6258
336	1.04947499	1.2588	0.5118	1.1951	0.5660
370	1.14544072	1.3877	0.4606	1.3167	0.5086
403	1.23956558	1.5230	0.4153	1.4450	0.4571
437	1.33728386	1.6728	0.3734	1.5875	0.4093
470	1.43267197	1.8283	0.3374	1.7358	0.3682
504	1.53138353	1.9988	0.3046	1.8989	0.3309
538	1.63044171	2.1796	0.2758	2.0723	0.2984
571	1.72685255	2.3651	0.2512	2.2506	0.2707
605	1.82640856	2.5664	0.2289	2.4444	0.2458
638	1.92321619	2.7716	0.2098	2.6423	0.2245
672	2.02311227	2.9932	0.1923	2.8564	0.2052

Table 22: Non-dimensional torsional-flexural reduction factors for buckling curves b and c for the modified 1/2 IPE 500 section

In Table 22 the results for both buckling curves can be seen. These needed to be plotted against the previous FEM results and the Euler curve.

As the curves in Eurocode 3 are all based on the relative slenderness, the results were plotted as slenderness against the reduction factor so that they could be directly compared with the Eurocode 3 buckling curves. Both curves were plotted in the same diagram and can be seen in Figure 26.

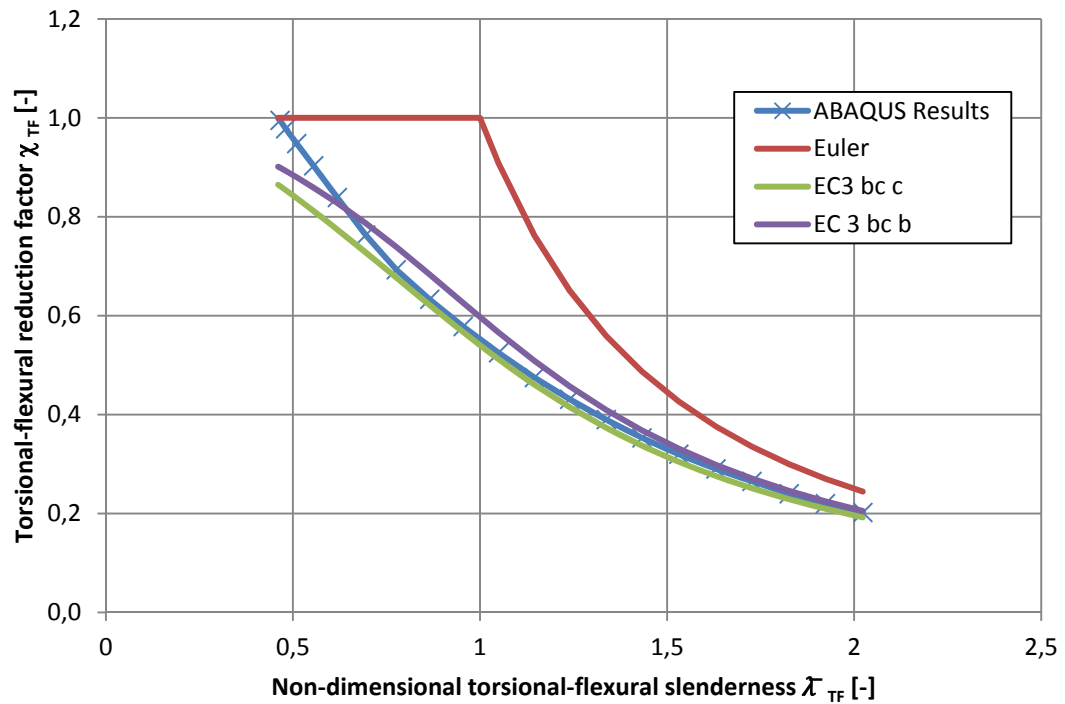


Figure 26: Modified 1/2 IPE 500 under compression - Comparison with buckling curves b and c

It can be seen that buckling curve b seems to be inaccurate and non-conservative for this section. Largely, this may be due to the relatively large compressive residual stresses in the flange that have been assumed. More work would be needed to check the real residual stress distribution. Buckling curve c, however, had a margin of safety and never returns an unsafe value.

Buckling curve c was assumed to be the more appropriate curve and further calculations were then based on this curve.

The most interesting finding in these plots, however, is that there is a very high margin of safety for the less slender members. It can be seen that the results for the c curve, at a

slenderness of 0.5 are conservative. A value of 0.85 is calculated where as the ABAQUS calculations returned a value of around 1.0. Most strikingly, all buckling curves start at a value of $\bar{\lambda}_{TF}$ equal to about 0.5, even when the members have a length of practically 0 cm. This is due to the fact that the non-dimensional torsional-flexural slenderness is not zero for T-section members with zero length.

The limit for the slenderness can be explained.

$$\bar{\lambda}_{TF,L=0} = \sqrt{\frac{N_{pl}}{N_{cr,TF,L=0}}}$$

At zero length, $N_{cr,TF}$ converges towards $N_{cr,T}$:

$$N_{cr,TF} = \frac{N_{cr,z}}{2 * \left(1 - \frac{z_0^2}{i_0^2}\right)} \left[1 + \frac{N_{cr,T}}{N_{cr,z}} - \sqrt{\left(1 - \frac{N_{cr,T}}{N_{cr,z}}\right)^2 + 4 * \left(\frac{z_0^2}{i_0^2}\right) * \frac{N_{cr,T}}{N_{cr,z}}}\right]$$

$$\rightarrow L = 0 \rightarrow N_{cr,TF} \sim N_{cr,T}$$

It is thus clear that the torsional-flexural slenderness will tend towards: -

$$\bar{\lambda}_{TF,L=0} = \sqrt{\frac{N_{pl} * i_0^2}{G * I_T}} = \sqrt{\frac{N_{pl}}{N_{cr,T}}}$$

In summary, although buckling curve b was not suitable, buckling curve c was too conservative. For all members with a slenderness value, $\bar{\lambda}_{TF}$, less than 0.75 the dimensioning would be very conservative. This meant that maybe there would be a better buckling curve or reduction formula which is not yet incorporated into Eurocode 3.

5.5 Proposed hypothesis from Taras et al

During the development of this thesis, it was proposed (Taras et al., 2014) that the real behaviour could better be described when amending the buckling reduction formula in a way that considers not only the torsional-flexural slenderness but - for the term related to the “generalized imperfection amplitude α ” of the buckling curve - also to the buckling

slenderness around the z-z axis. The proposal was that the coefficient for the reduction factor should be calculated as follows:

$$\Phi_{TF} = 0.5[1 + \alpha_z(\bar{\lambda}_z - 0.2) + \bar{\lambda}_{TF}^2]$$

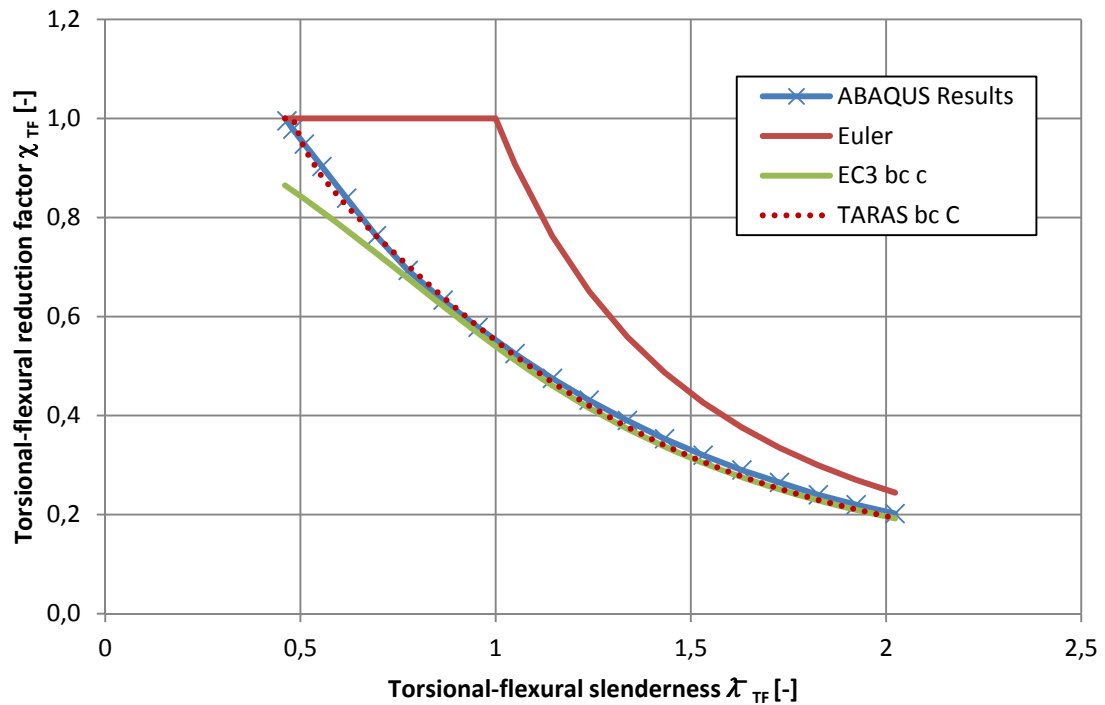


Figure 27: New proposal (Taras et al.) and FEM comparison - plotted over the torsional-flexural slenderness

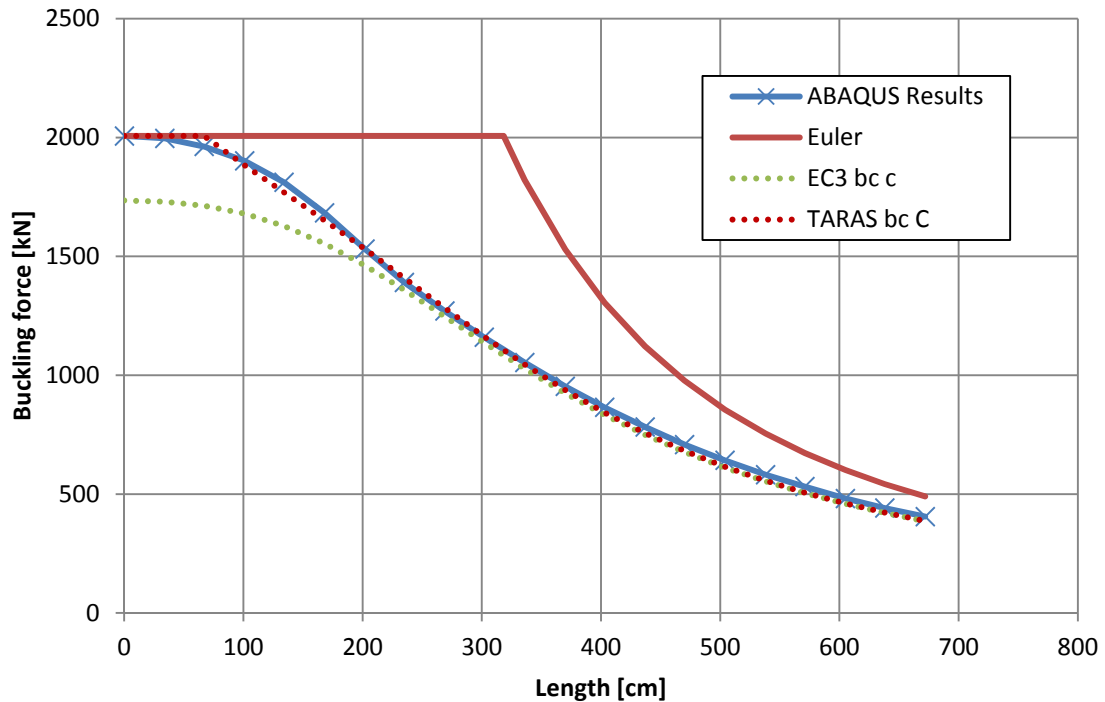


Figure 28: New proposal (Taras et al.) and FEM comparison - plotted over the member length

This hypothesis fits very well with the results obtained from the ABAQUS calculations.

As one can see the new proposal was always closer to the calculations than the Eurocode 3 results. This meant that it was more favourable and economic to use for the dimensioning of T-sections than the current Eurocode rule. The results were mostly slightly conservative and had a maximum “un-conservative” error of -2.2% when the slenderness was around 0.5. This can be considered to be a negligible inaccuracy.

5.6 Further sections

In order to further confirm the accuracy and validity of the proposed new formulation for flexural-torsional buckling of class 2 T-sections, the same methods and calculations as above were carried out for a section that was right on the boundary of Eurocode classes 1 and 2, this was named IPE 500-12 (N.B. 12 = class 1, class 2), as well as another section on the boundary of classes 2 and 3, which was named IPE 500-23 (N.B. 23 = class 2, class 3).

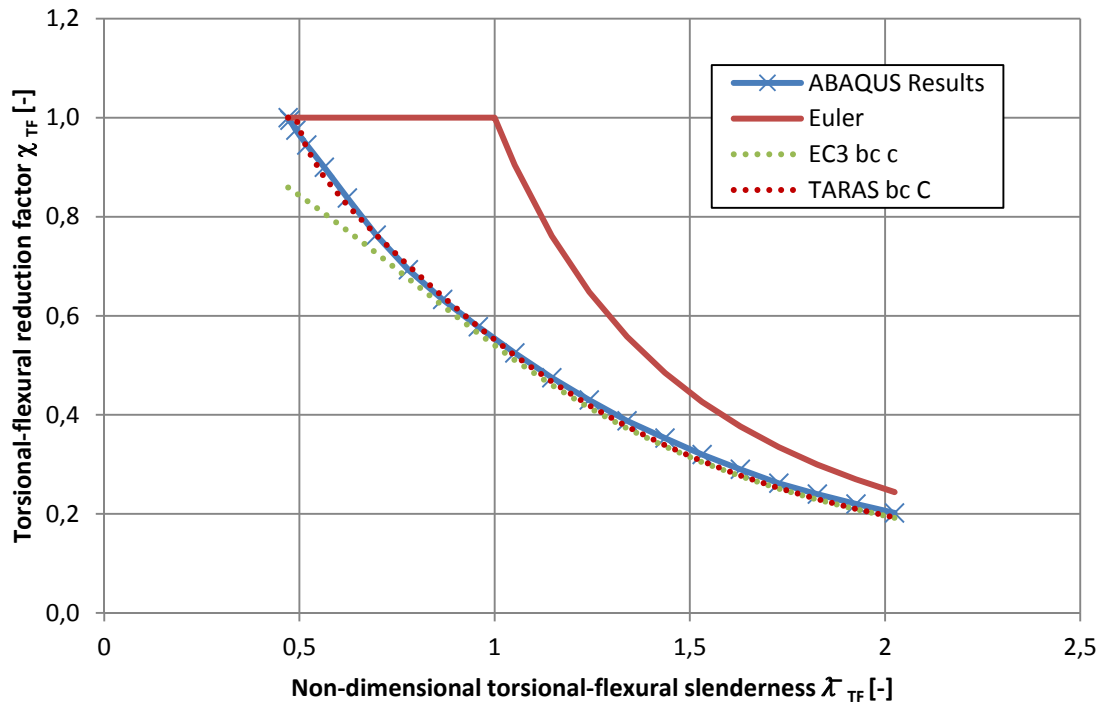


Figure 29: IPE 500-23 comparison new proposal and Eurocode 3 - plotted over slenderness

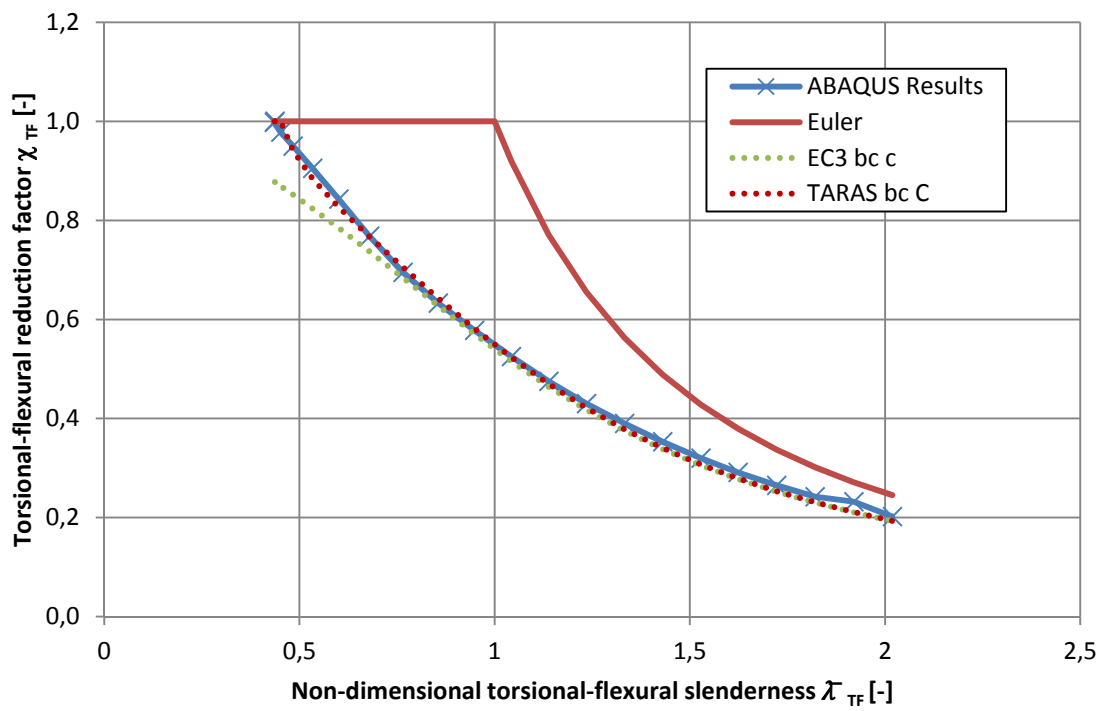


Figure 30: IPE 500-21 comparison new proposal and Eurocode 3 - plotted over slenderness

The basis for these specimens was again the IPE 500 section. The web was made thicker/thinner so as to obtain the aforementioned class 2 sections. The dimensions of the flange were not changed. The depth of the web was still 21.3 cm. The thickness of IPE 500-12 web was 2.36 cm and the thickness of the IPE 500-23 was 2.13 cm.

The results can be seen as the reduction factor plotted against the torsional-flexural slenderness in Figure 29 and Figure 30 whereas the results are plotted as the buckling force against the length in Figure 31 and Figure 32. The results showed that in both of these cases the Eurocode 3 method of dimensioning was extremely inaccurate for shorter lengths. It seemed that the results for these two sections were just as accurate as with the first section, if not better. Obviously, as the maximum force was only dependent on the area of the section, this value was higher for the IPE 500-12 and lower for the IPE 500-23. The results stayed on the conservative side of the ABAQUS results for a larger portion of the plot for the IPE 500-23.

In both cases the first portion of the line showed that there was room for improvement in the Eurocode method of calculation. It also showed that the proposal from Taras et al seemed to fit the results almost perfectly.

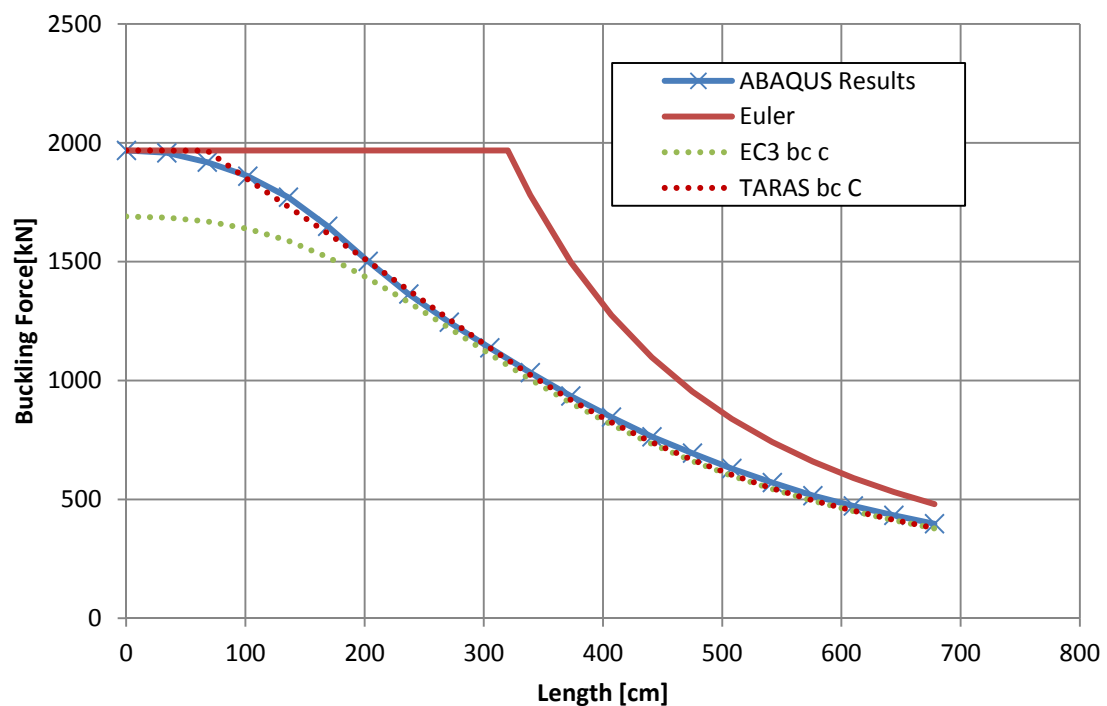


Figure 31: IPE 500-23 comparison new proposal and Eurocode 3 -plotted over length

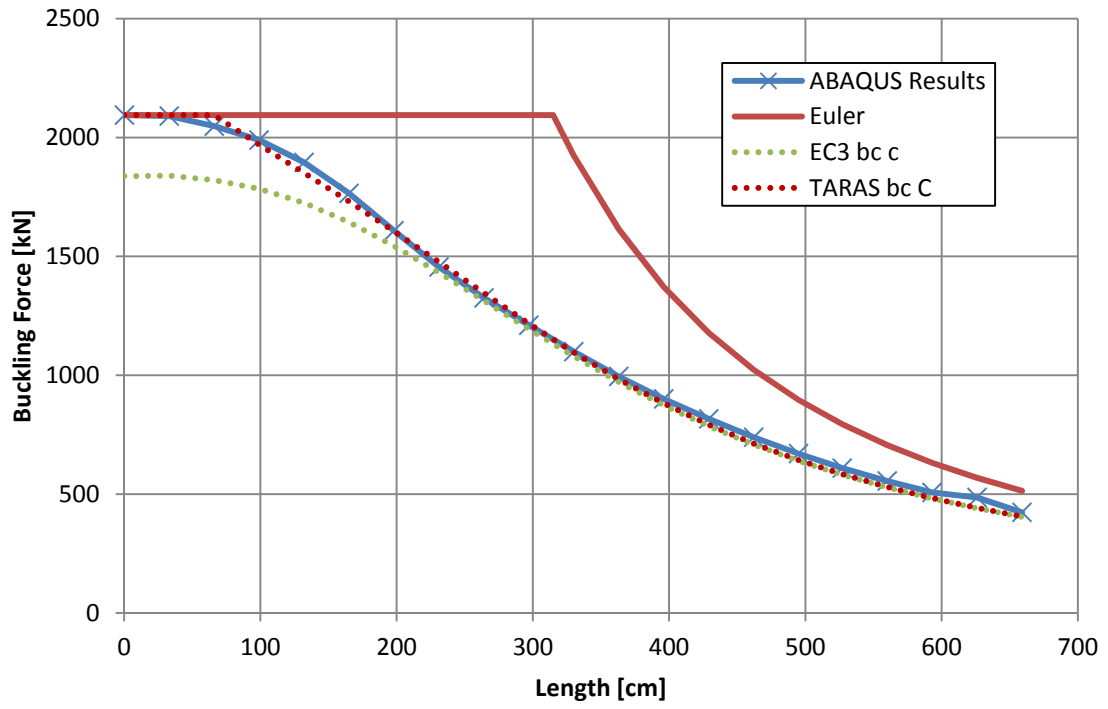


Figure 32: IPE 500-21 comparison new proposal and Eurocode 3 -plotted over length

6 Class 4 Buckling Strength - General Eurocode 3 Rules

To start the specific investigations for T-sections, it was necessary to see how the Eurocode 3 buckling strength is calculated for class four sections. Due to the shift of centroid that needs to be considered in class 4 T-sections, the treatment of the interactive global-local buckling behaviour of class 4 T-sections according to the Eurocode is very complex, and always requires the consideration of bending moments. In the original EN-version of EC3-1-1, this would not be (easily) possible, since the interaction formulae given for members in bending-compression (“beam-columns”) are only valid for double-symmetric sections; the only possibility given in this case would be the use of second-order based stress verifications.

A somewhat easier alternative is found in the Austrian national annex to the Eurocode 3 part 1-1[10] which contains specific rules for mono-symmetric sections. The interaction criteria for mono-symmetric sections that need to be fulfilled according to this document are as follows:

$$\frac{N_{Ed}}{\chi_y * N_{Rd}} + k_y \frac{C_{my} * M_{y,Ed}}{\chi_{LT(s)} * M_{y,Rd(s)}} \leq 1 \quad \text{Equ. (1)}$$

$$\frac{N_{Ed}}{\chi_{TF} * N_{Rd}} + k_{LT} \frac{M_{y,Ed}}{\chi_{LT(s)} * M_{y,Rd(s)}} \leq 1 \quad \text{Equ. (2)}$$

$$\frac{N_{Ed}}{\chi_z * N_{Rd}} - k_{LT} \frac{M_{y,Ed}}{\chi_{LT(l)} * M_{y,Rd(l)}} \leq 1 \quad \text{Equ. (3)}$$

In the case of the T-sections under axial compression, no additional external moment acts on the members. The only moment present is the one that occurs due to the shift in the centroid of the effective section ($M_{y,Ed} = N_{Ed} * e_N$). This leads to a uniform bending moment diagram in the beam column, meaning that $C_{my} = 1.0$.

The axial design resistances for the class 4 sections were calculated using the following formula.

$$N_{Rd} = \frac{A_{eff} * f_y}{\gamma_{M1}}$$

The partial factor γ_{M1} was 1.0 as stated in Eurocode 3 part 1-1. This means that the characteristic and design values are the same.

Thus the following equations can be used.

$$\frac{N_{Ed}}{\chi_y * A_{eff} * f_y} + k_y \frac{N_{Ed} * e_N}{\chi_{LT(s)} * M_{y,Rk(s)}} \leq 1 \quad Equ (1)$$

$$\frac{N_{Ed}}{\chi_{TF} * A_{eff} * f_y} + k_{LT} \frac{N_{Ed} * e_N}{\chi_{LT(s)} * M_{y,Rk(s)}} \leq 1 \quad Equ (2)$$

$$\frac{N_{Ed}}{\chi_z * A_{eff} * f_y} - k_{LT} \frac{N_{Ed} * e_N}{\chi_{LT(l)} * M_{y,Rk(l)}} \leq 1 \quad Equ (3)$$

To find the ultimate limit load, N_{Ed} was increased for each of the criteria until left side of the inequality was exactly equal to 1.0. When the equation was no longer true, the next criterion was checked. After all of the maximum values were obtained, the smallest was then the ultimate limit load according to Eurocode 3.

6.1 Lateral-torsional buckling around the y-y axis - Equ.(1)

The first criterion was checked and a value obtained like this. The value for χ_y was obtained using the Ayrton-Perry equations [3].

$$\chi_y = \frac{1}{\Phi_y + \sqrt{\Phi_y^2 - \bar{\lambda}_y^2}} \leq 1.0$$

The values for the reduction factor could not be bigger than 1.0. The value, Φ_y , to help calculate the reduction factor needed to be calculated.

$$\Phi_y = 0.5[1 + \alpha_y(\bar{\lambda}_y - 0.2) + \bar{\lambda}_y^2]$$

The α_y term is the imperfection factor. The imperfection factor takes into account the homogeneity errors in the material as well as residual stresses.

This term α_y was obtained using Table 21, that can be found in chapter 5.4 “Results and comparison with Eurocode 3” and Table 23 as a basis. These are found in Eurocode 3. In the case of a rolled T-section section the imperfection coefficient is 0.49 for buckling in both directions. It was therefore assumed that they would also be calculated using buckling curve c.

Buckling curve	a ₀	a	b	c	d
Imperfection factor α	0,13	0,21	0,34	0,49	0,76

Table 23: Imperfection coefficient dependent on buckling curve

Where $\bar{\lambda}_y$ was the bending slenderness of the effective section around the y-y axis.

$$\bar{\lambda}_y = \sqrt{\frac{A_{\text{eff}} * f_y}{N_{\text{cr},y}}}$$

The critical elastic force, $N_{\text{cr},y}$, is also sometimes referred to as the Euler force, was then obtained using the following formula.

$$N_{\text{cr},y} = \frac{\pi^2 * E * I_y}{l^2}$$

Next the interaction factor k_y needed to be obtained. This factor is responsible for applying an interaction between the compression and the bending moment present due to the eccentricity of the axial load in relation to the centroid of the effective cross-section.

$$k_y = 1 + 0.6 * \bar{\lambda}_y * n_y$$

$$n_y = \frac{N_{Ed}}{\chi_y * A_{eff} * f_y}$$

The moment around the y-y axis stayed the same for the cross sections all the way along the length of the member, therefore the value for C_{my} is always, in the cases dealt with in this thesis, 1.0.

The only part left to define from the first criterion was the resistance part of the moment term. The index (s) refers to the direction of the moment M_y , leading to compöression on the bottom of the web.

$$\chi_{LT(s)} * M_{y,Rk}$$

Cross-section	Limits	Buckling curve
Rolled I-sections	$h/b \leq 2$	a
	$h/b > 2$	b
Welded I-sections	$h/b \leq 2$	c
	$h/b > 2$	d
Other cross-sections	-	d

Table 24: Lateral-torsional buckling curve definition for different manufacture methods

The χ_{LT} term was calculated in a very similar way to χ_y . Firstly the buckling curve had to be defined using Table 24 (curve d). Then the lateral-torsional imperfection coefficient obtained from Table 25.

As can be seen the imperfection coefficient α_{LT} of 0.76 needed to be used instead of 0.49 that was used to calculate Φ_y .

Buckling curve	a	b	c	d
Imperfection factor α_{LT}	0,21	0,34	0,49	0,76

Table 25: Lateral-torsional imperfection coefficient dependent on buckling curve

To calculate the relative lateral-torsional slenderness, the elastic section modulus of the free end of the effective web for the effective cross-section needed to be calculated. These were already calculated in Chapter 3.4 “Comparison”. Here they are listed again in Table 26.

Cross Section	$W_{y,eff(s)}$ [cm ³]
1/2 IPE 300	35
1/2 IPE 400	68
1/2 IPE 500	113
1/2 IPE 500 - thin	103
1/2 IPE 500 - wide	118
1/2 IPE 600	184
1/2 HEA 500	174

Table 26: Table showing the elastic section moduli $W_{y,eff(s)}$

The elastic section modulus to the top edge of the effective cross-sections flange was also calculated as it was needed later (Equ. (3)).

$$W_{y,eff(l)} = \frac{I_{y,eff}}{z_{s,eff}}$$

$$W_{y,eff(s)} = \frac{I_{y,eff}}{(t_f + r + d_{eff} - z_{s,eff})}$$

The equation for the critical moment that was used is stated in the Austrian national extension to Eurocode 3, appendix B 1993-1-1 [10] for mono-symmetrical I sections. As there was a constant moment along the length of the member this simplified the equation used.

$$M_{cr} = \frac{\pi^2 * E * I_z}{L^2} * \sqrt{\frac{L^2 * G * I_T}{\pi^2 * E * I_z} + (-z_j)^2} - (-z_j)$$

It is important to note that the bending moment caused by the centroid shift is always “negative” according to the definition used in the national annex [10], meaning that the outer tip of the web is in compression due to this bending moment. This means that the flange of the T-section is in tension due to bending. This is important for the calculation of z_i , which was done in accordance with [10], as follows:

The second moment of area around the z-z axis was calculated for the flange, I_{ft} (index “t” for tension) as well as a substitute compression flange, I_{fc} (index “c” for compression),

which was entered in the formula with the width of the web and the height also equal to thickness of the web. With this information the flange ratio was acquired.

$$\psi_f = \frac{I_{fc} - I_{ft}}{I_{fc} + I_{ft}}$$

In the case of the T-sections, the flange was always in tension compared to the end of the web. This meant that ψ_f was always a bit larger than -1. For cases where ψ_f is smaller than zero the value for z_j is calculated as follows:

$$z_j = \psi_f * \frac{h_s}{2}$$

While for mono-symmetric I-sections the height h_s is equal to the distance between the centroids of the two flanges, for T-sections the total depth of the section was used. All of the other components for M_{cr} were known, so the critical moment was calculated using the formula above. From there the relative lateral-torsional slenderness was obtained.

$$\bar{\lambda}_{LT(s)} = \sqrt{\frac{W_{y,eff(s)} * f_y}{M_{cr}}}$$

Note that all the terms, i.e. the critical moment, the section modulus and the slenderness, relate to the “smaller flange” (index “s”), i.e. in the case of T-sections the outstanding tip of the web.

As before for the buckling around the y-y axis, the Ayrton-Perry equations were used. Next the value to help calculate the reduction factor was found.

$$\Phi_{LT} = 0.5[1 + \alpha_{LT}(\bar{\lambda}_{LT(s)} - 0.2) + \bar{\lambda}_{LT(s)}^2]$$

As stated before the value for α_{LT} was taken as 0.76 and then the reduction factor for lateral-torsional buckling was obtained.

$$\chi_{LT(s)} = \frac{1}{\Phi_{LT(s)} + \sqrt{\Phi_{LT(s)}^2 - \bar{\lambda}_{LT(s)}^2}} \leq 1.0$$

The final part of the equation that needed to be defined was the resistance to the bending moments around the y-y axis. This was very simple and shown in the next equation.

$$M_{y,Rk(s)} = \frac{W_{y,eff(s)} * f_y}{\gamma_{M1}}$$

With all of this information it was possible to calculate the buckling force resistance against lateral-torsional buckling due to bending around the y-y axis.

6.2 Torsional-flexural buckling around the z-z axis - Equ.(3)

Next the following criterion was considered;

$$\frac{N_{Ed}}{\chi_z * A_{eff} * f_y} - k_{LT} \frac{N_{Ed} * e_N}{\chi_{LT(l)} * M_{y,Rk(l)}} \leq 1.0$$

Note that this equation, which was specifically developed for mono-symmetric I-sections, requires the calculation of the resistance $M_{y,Rk(l)}$ - leading to compression stresses at the flange of the T-section. The equations that were used for the evaluation of this equation are listed here. Where they are analogue to the equations above, no explanation has been added.

$$\chi_z = \frac{1}{\Phi_z + \sqrt{\Phi_z^2 - \bar{\lambda}_z^2}} \leq 1.0$$

$$\Phi_z = 0.5[1 + \alpha_z(\bar{\lambda}_z - 0.2) + \bar{\lambda}_z^2]$$

The values for α_z were again taken from Table 21 and Table 23. These were the same as for the y direction, 0.49.

$$\bar{\lambda}_z = \sqrt{\frac{A_{eff} * f_y}{N_{cr,z}}}$$

$$N_{cr,z} = \frac{\pi^2 * E * I_z}{L^2}$$

$$n_z = \frac{N_{Ed}}{\chi_z * A_{eff} * f_y}$$

The factor n_z is needed for the interaction coefficients.

$$C_{MLT} = 0.6 + 0.4 * \psi_{cm} = 1.0$$

N.B. constant moment - $\psi_{cm} = 1.0$

$$k_{LT} = 1 - \frac{0.05 * \bar{\lambda}_z * n_z}{C_{MLT} - 0.25} \geq 1 - \frac{0.05 * n_z}{0.75}$$

The elastic section moduli were calculated earlier, $W_{y(l)}$.

$$\bar{\lambda}_{LT(l)} = \sqrt{\frac{W_{y,eff(l)} * f_y}{M_{cr}}}$$

$$\Phi_{LT} = 0.5[1 + \alpha_{LT}(\bar{\lambda}_{LT(l)} - 0.2) + \bar{\lambda}_{LT(l)}^2]$$

N.B. $\alpha_{LT} = 0.76$

$$\chi_{LT(l)} = \frac{1}{\Phi_{LT(l)} + \sqrt{\Phi_{LT(l)}^2 - \bar{\lambda}_{LT(l)}^2}} \leq 1.0$$

The value for M_{cr} was calculated earlier.

$$M_{y,Rk(l)} = \frac{W_{y,eff(l)} * f_y}{\gamma_{M1}}$$

With all of this information it was possible to calculate the buckling forces due to the lateral-torsional buckling around the z-z axis.

6.3 Torsional-flexural buckling - Equ.(2)

The final equation that needed to be fulfilled was

$$\frac{N_{Ed}}{\chi_{TF} * A_{eff} * f_y} + k_{LT} \frac{N_{Ed} * e_N}{\chi_{LT(s)} * M_{y,Rk(s)}} \leq 1$$

All the parts of this equation had already been defined except for the torsional flexural reduction factor. To define the reduction factor χ_{TF} it was necessary to use equations for $N_{cr,TF}$ - the ones reported in the dissertation from P. Kaim were used [7].

The critical torsion force was necessary to come to the critical torsional-flexural force and for this the radii of gyration, i_y , i_z and the difference between the position of the centre of gravity and the shear point, z_0 are necessary to know. (see figure describing Table 2)

$$i_y = \sqrt{\frac{I_y}{A}}$$

$$i_z = \sqrt{\frac{I_z}{A}}$$

$$z_0 = z_s - \frac{t_f}{2}$$

The i_0 is defined

$$i_0^2 = i_y^2 + i_z^2 + z_0^2$$

$$N_{cr,T} = \frac{1}{i_0^2} * G * I_T$$

Using $N_{cr,T}$ the value for $N_{cr,TF}$ could then be defined.

$$N_{cr,TF} = \frac{N_{cr,z}}{2 * \left(1 - \frac{z_0^2}{i_0^2}\right)} \left[1 + \frac{N_{cr,T}}{N_{cr,z}} - \sqrt{\left(1 - \frac{N_{cr,T}}{N_{cr,z}}\right)^2 + 4 * \left(\frac{z_0^2}{i_0^2}\right) * \frac{N_{cr,T}}{N_{cr,z}}}\right]$$

Once the critical force has been calculated the torsional-flexural slenderness was calculated.

$$\bar{\lambda}_{TF} = \sqrt{\frac{A_{eff} * f_y}{N_{cr,TF}}}$$

Then using the Ayrton-Perry formulae the reduction factor was calculated. The Eurocode states that for torsional flexural failure the imperfection factor α_{TF} is the same as α_z

$$\Phi_{TF} = 0.5[1 + \alpha_z(\bar{\lambda}_{TF} - 0.2) + \bar{\lambda}_{TF}^2]$$

N.B. $\alpha_z = 0.49$

$$\chi_{TF} = \frac{1}{\Phi_{TF} + \sqrt{\Phi_{TF}^2 - \bar{\lambda}_{TF}^2}} \leq 1.0$$

With all of this information it was possible to calculate the buckling force resistance due to the torsional-flexural buckling combined with the lateral-torsional one.

As the equation to calculate M_{cr} is based on mono-symmetrical I beams, the values were checked using the software LTBeam, for all of the possible lengths. LTBeam is a program where the smallest possible length that could be calculated was 100cm. The difference in the final results between using the equation and LTBeam are minimal. The calculations were therefore seen as optimal for the calculations.

The final buckling force resistance was the smallest value returned from these three equations.

6.4 ABAQUS calculations

The calculations were carried out in ABAQUS using the model described in chapter 4 “FEM Model”. The model was loaded with the cross sectional plastic capacity of the gross section as the reference load. This force was applied to the model in steps. The actual loading resistance for the model was then reached when the subject failed. The calculation returned the percentage of N_{pl} at which the member failed. This was the actual reduction factor.

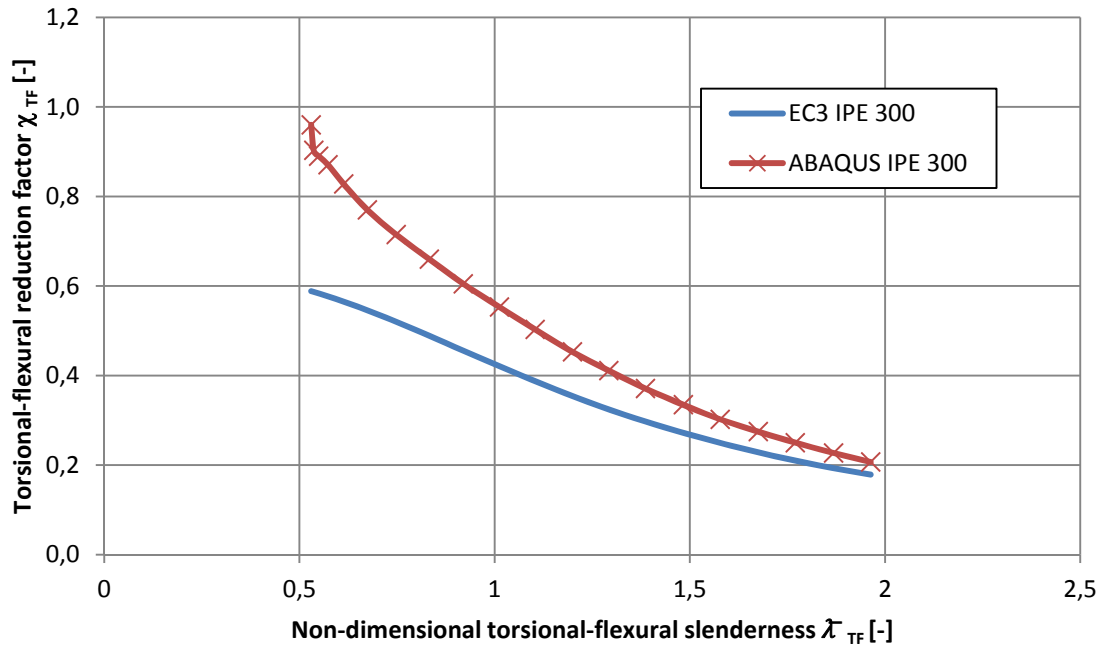
6.4.1 *Results for the IPE 300 section*

Figure 33: IPE 300 under compression - comparison between present Eurocode 3 and the ABAQUS calculations - plotted over the torsional-flexural slenderness

The Eurocode results plotted in these diagrams is the smallest value from the three equations explained earlier.

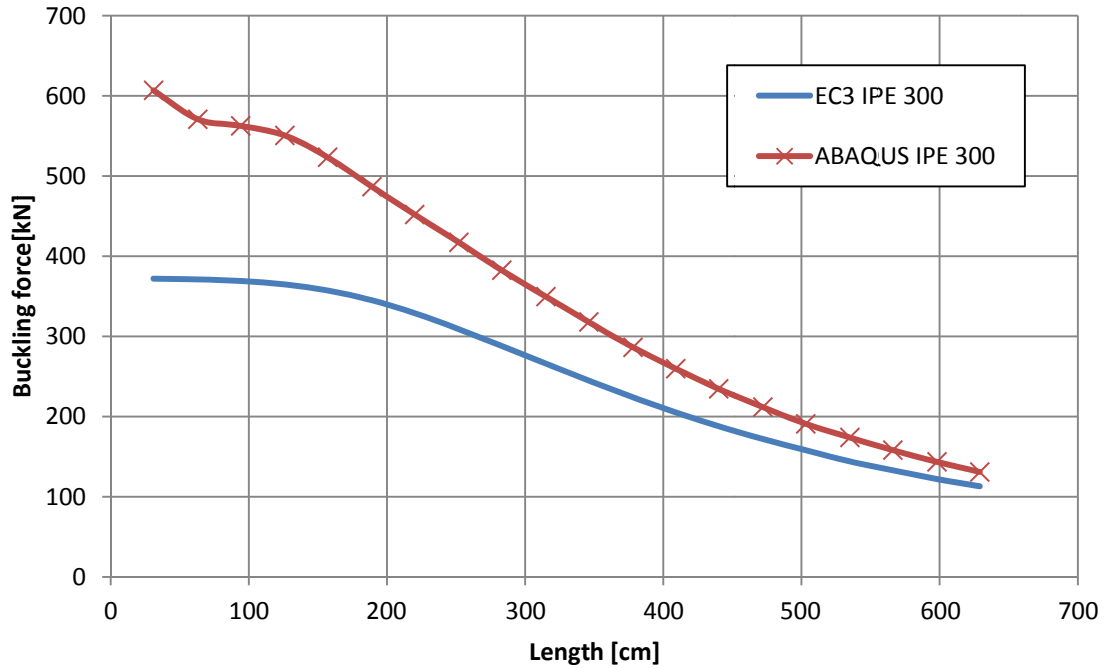


Figure 34: IPE 300 under compression - ABAQUS results and Eurocode 3 resistances - plotted over length

The failure of the member at smaller lengths was different to that at longer lengths. The first imperfection mode was when local imperfections were applied to 100% and the global imperfections were at 70% and in the vertical upward direction. This was the definitive imperfection mode up to a length of 126 cm. The imperfections/deformations, at zero load, can be seen in Figure 35 for a 1/2 IPE 300 with a length of 63 cm.

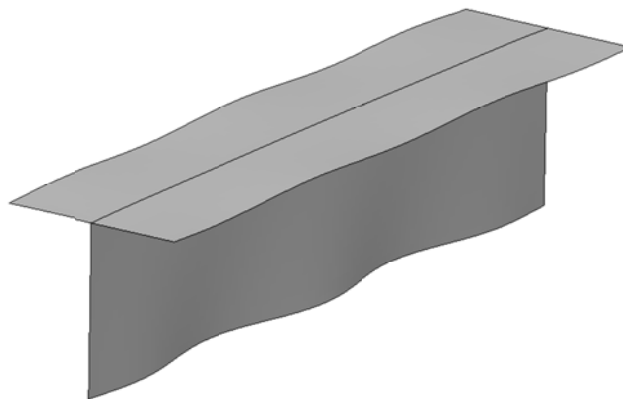


Figure 35: IPE 300, L=63cm 100% local and 70% upward global imperfection (amplified by factor 300)

The second defining imperfection constellation was when the global imperfections were set to 100% and the local imperfections to 70%. This was the case for the longer lengths (longer than 157cm). This starting situation can be seen, amplified, in Figure 36.

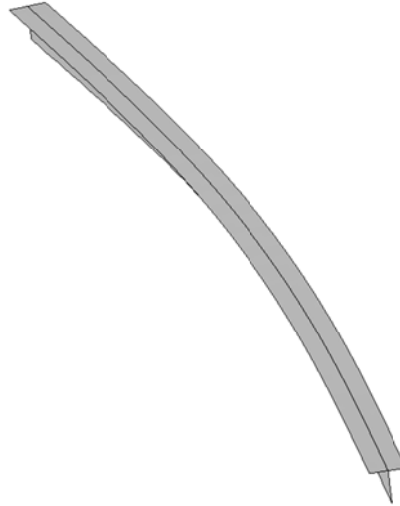


Figure 36: IPE 300, 629cm 70% local and 100% sideways global imperfection (amplified by factor 300)

In Figure 37 and Figure 38 the stresses at failure of the members can be seen. The first one being 63cm long and the second was over 6m long.

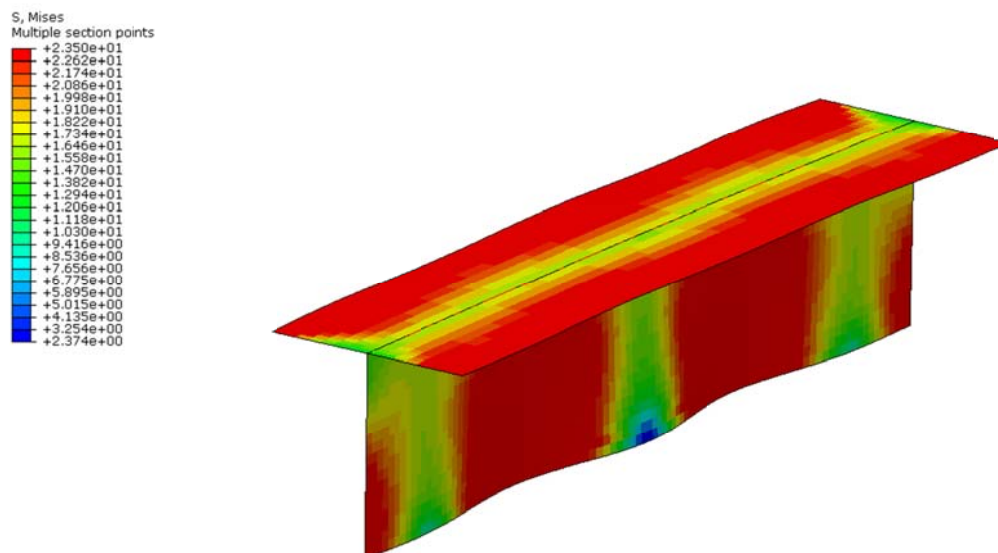


Figure 37 : Stress distribution at the point of failure IPE 300 length = 63cm

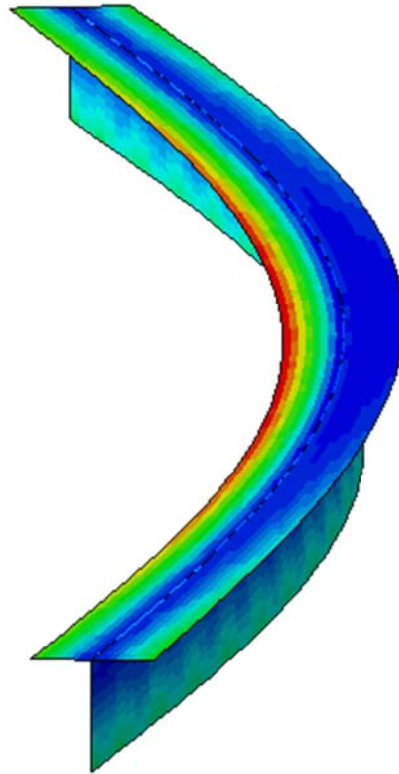


Figure 38: Stress distribution at the point of failure IPE 300 length = 600cm

The reduction factor was simply the real axial force N_{Rd} at buckling failure (according to either EC3 or ABAQUS) divided by the plastic section resistance. The plastic resistance (as opposed to the elastic resistance $N_{Rk,eff}$) was chosen for a simpler reference without additional distortion of the results.

$$\chi = \frac{N_{Rd}}{N_{pl}}$$

These results show that the Eurocode is extremely conservative in the case of the IPE 300. The safety in Figure 33 reaches a maximum with the smallest possible slenderness for torsional-flexural slenderness, at about 0.5. The finite element calculation returned a reduction factor value of over 0.98, whereas the Eurocode 3 returns a value well under 0.6. This meant that when a T-section such as this was dimensioned using the Eurocode 3 (and the Austrian national annex) under the influence of just an axial compression, it was more than 35% over-dimensioned.

6.4.2 Results for the IPE 400 section

The Eurocode 3 values for the buckling force and those that were obtained from the finite element calculations were also compared for the IPE 400. The results can be seen in Figure 39 and Figure 40.

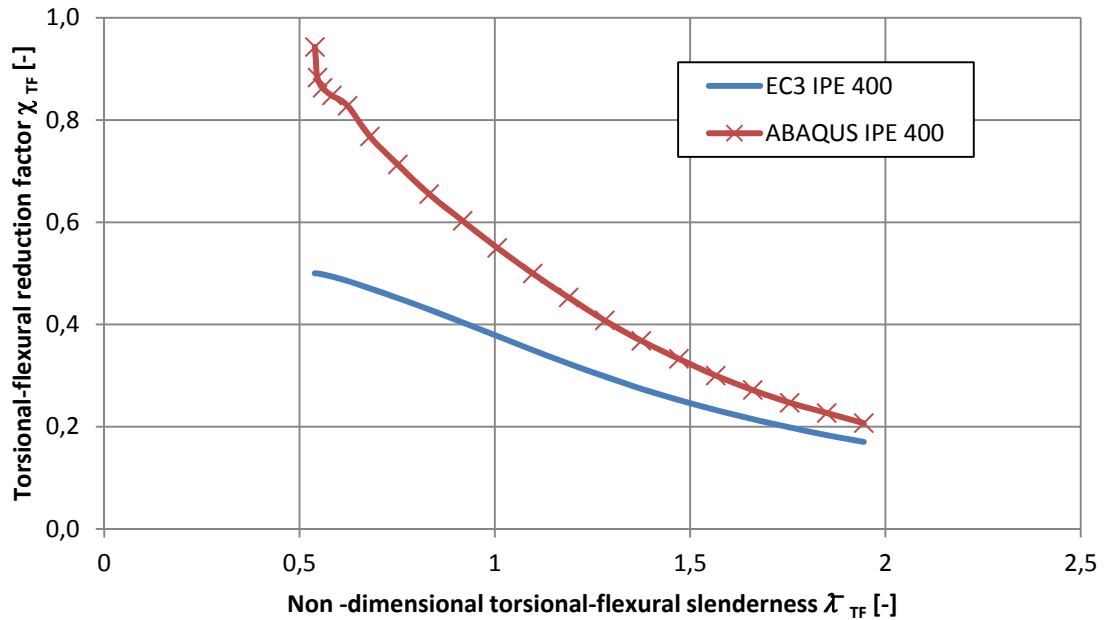


Figure 39: IPE 400 under compression - comparison between Eurocode 3 and the ABAQUS calculations - plotted over the torsional-flexural slenderness

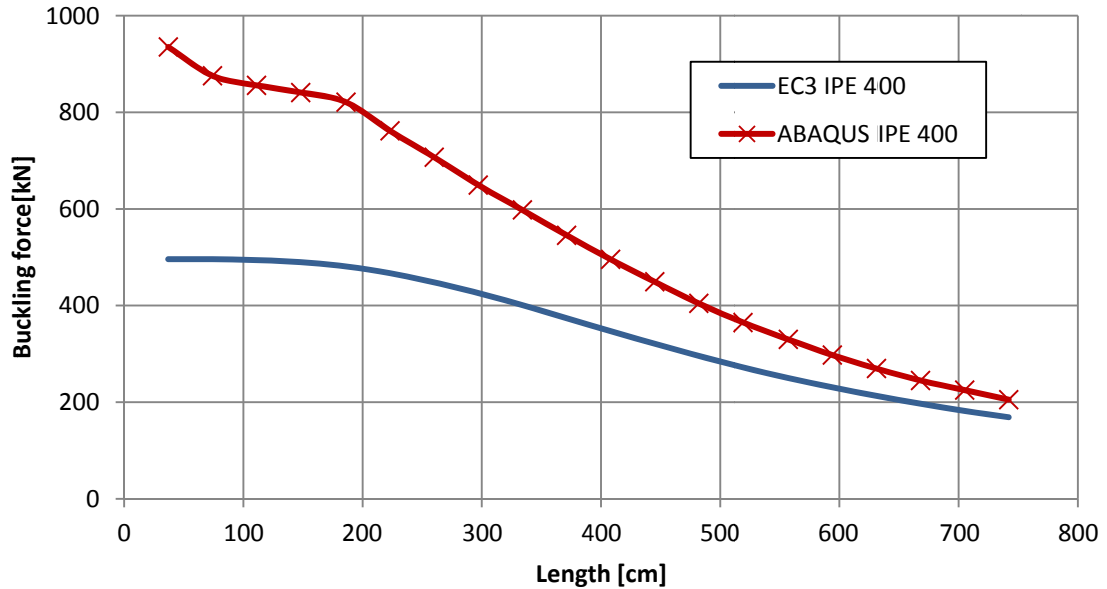


Figure 40: IPE 400 under compression - ABAQUS results and Eurocode 3 resistances - plotted over length

As with the IPE 300 the imperfection mode for the failure of the smaller length members was different to that at longer length members. This was observed in Figure 40. The difference between the IPE 400 and the IPE 300 was that the first member failed in the imperfection mode 100% local and 70% global for a larger range of lengths. In the case of the IPE 400 the first defining mode was the same as the IPE 300 and occurred when the local imperfections were applied to 100% and the global upwards imperfection was set to 70%. The starting configuration can be seen in Figure 41.

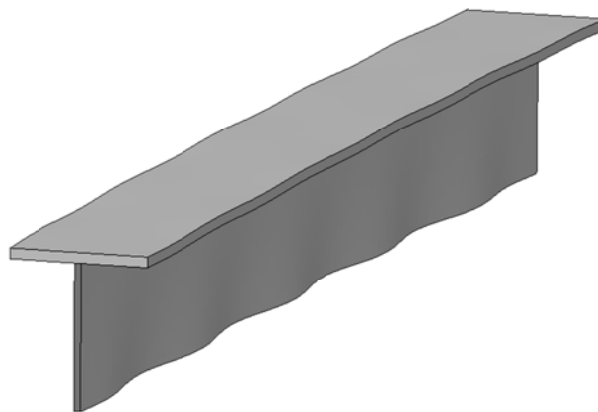


Figure 41: IPE 400, L=186 cm 100% local and 70% upward global imperfection (amplified by 300)

The second defining imperfection mode, when the global sideways imperfection was set to 100% and the local imperfections to 70%, was the defining imperfection mode for the longer lengths. The starting situation can be seen, amplified, in Figure 42.

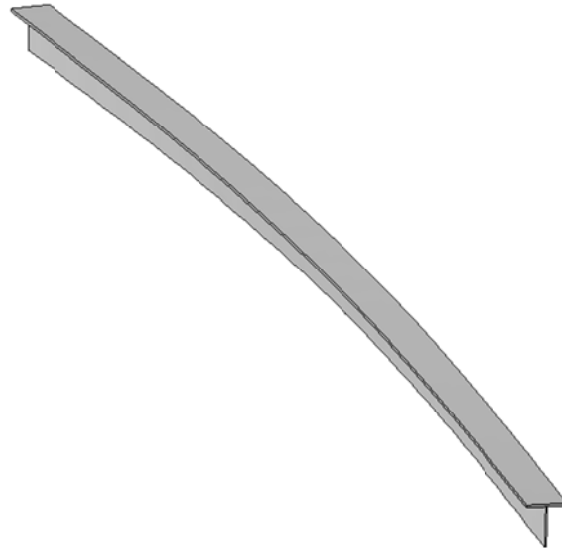


Figure 42: IPE 400, $L=705$ cm, 70% local and 100% sideways global imperfection (amplified by 300)

In Figure 43 and Figure 44 the stress distribution at the point of failure can be seen, the first one being 186cm long and the second 705cm long.

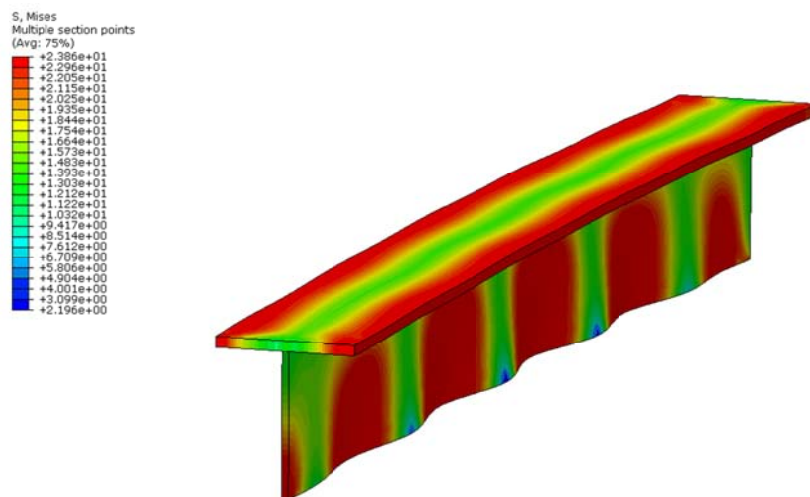


Figure 43 : Stress distribution at the point of failure IPE 400 length = 186cm

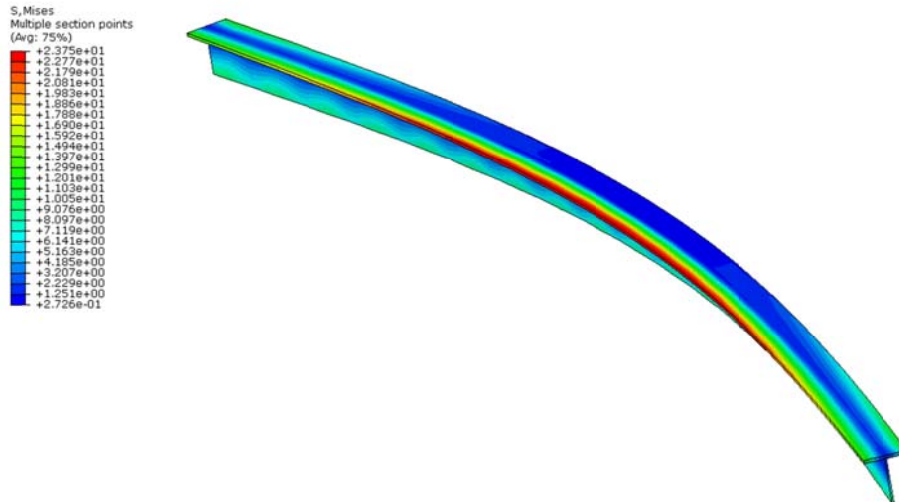


Figure 44: Stress distribution at the point of failure IPE 400 length = 705cm

These results (Figure 39) again show that the Eurocode is extremely conservative in the case of the IPE 400. The safety in Figure 39 reaches a maximum with the smallest slenderness at about 0.5. The finite element calculation returned a reduction factor value of over 0.97 whereas the Eurocode 3 returns a value under 0.5. This meant that when a T-section such as this was dimensioned using the Eurocode 3 under the influence of just an axial compression, it was more than 45% over dimensioned.

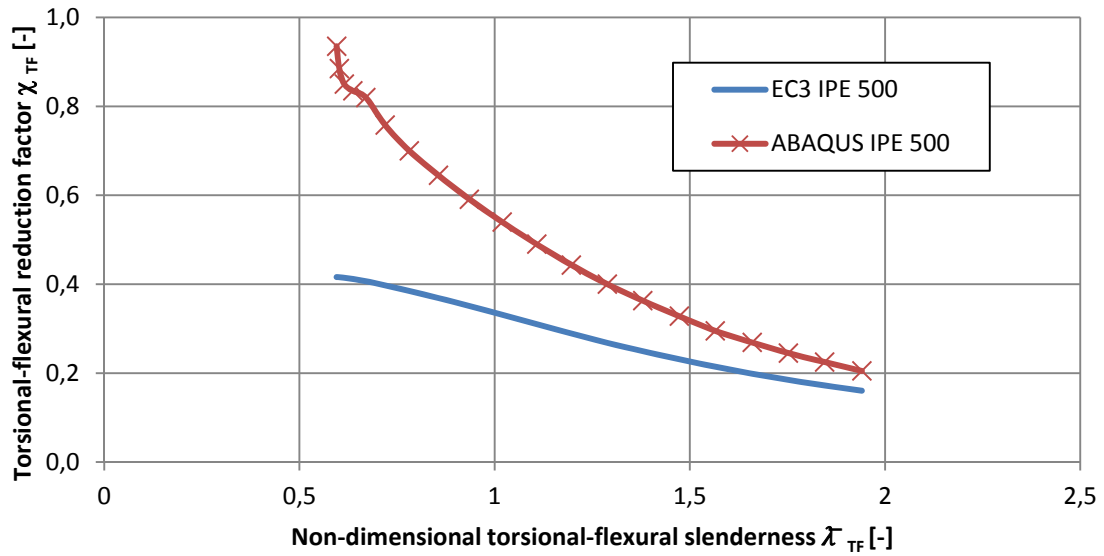
6.4.3 *Results for the IPE 500 section*

Figure 45: IPE 500 under compression - comparison between present Eurocode 3 and the ABAQUS calculations - plotted over the torsional-flexural slenderness

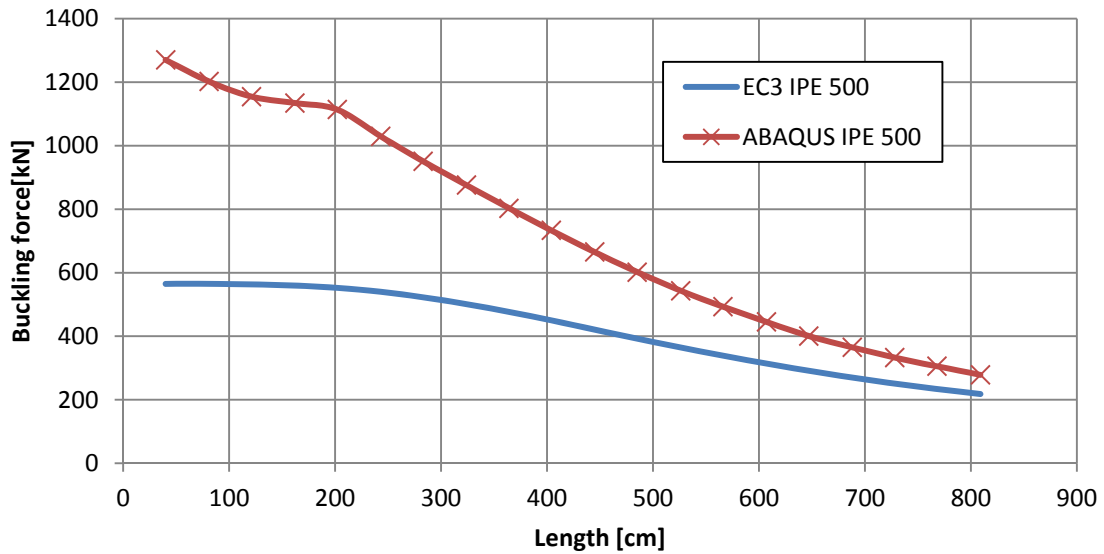


Figure 46: IPE 500 under compression - ABAQUS results and Eurocode 3 resistances - plotted over length

These results show again that the Eurocode is extremely conservative in the case of the IPE 500. The finite element calculation returned a reduction factor value of over 0.89 whereas

the Eurocode 3 returns a value just over 0.5. This meant that yet again Eurocode 3 allowed roughly half of the resistance from the section to be used for dimensioning.

6.4.4 Results for the IPE 600 section

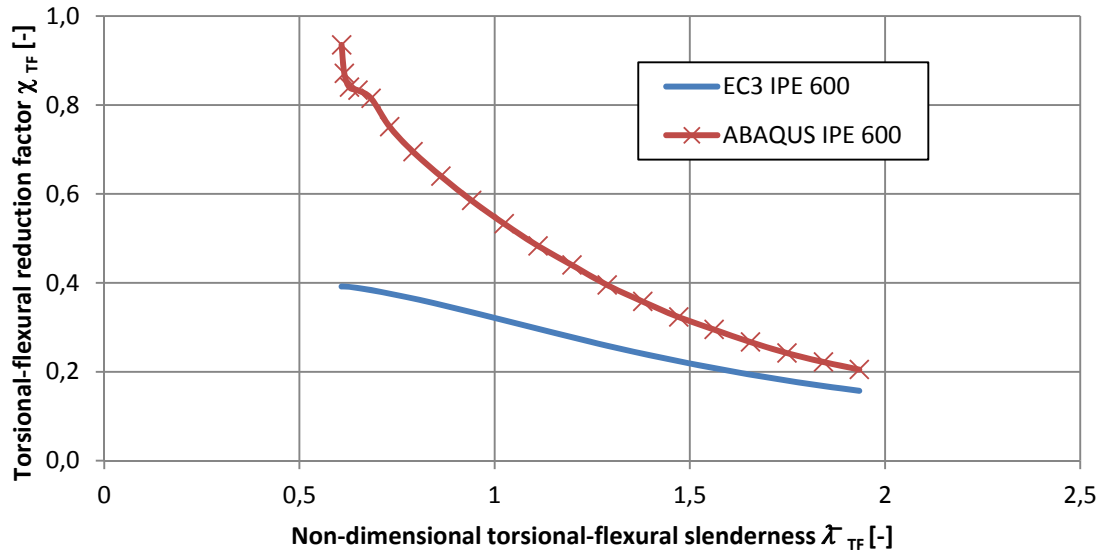


Figure 47: IPE 600 under compression - comparison between present Eurocode 3 and the ABAQUS calculations - plotted over the torsional-flexural slenderness

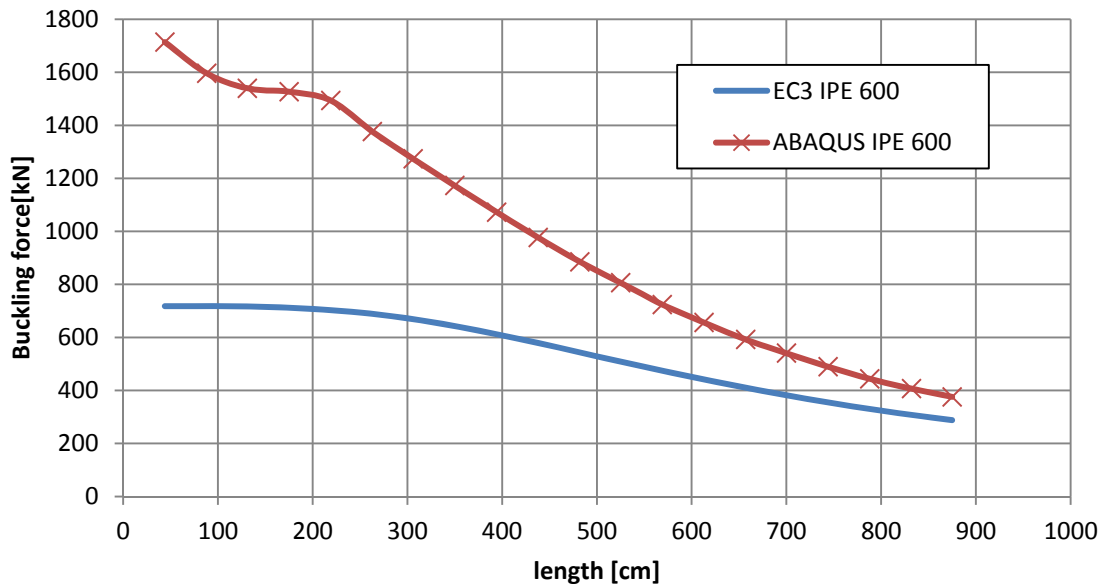


Figure 48: IPE 600 ABAQUS results and Eurocode 3 resistances - plotted over length

As expected the results followed a very similar pattern to the previous sections. What was interesting was the number of different failure modes, or rather, of relevant geometric imperfection patterns.

Cross Section	[cm]	Imperfection Mode
1/2 IPE 600	44	70% upwards global, 100% local
1/2 IPE 600	88	70% sideways global, 100% local
1/2 IPE 600	131	70% upwards global, 100% local
1/2 IPE 600	175	70% upwards global, 100% local
1/2 IPE 600	219	100% sideways global, 70% local
1/2 IPE 600	263	100% sideways global, 70% local
1/2 IPE 600	306	100% sideways global, 70% local
1/2 IPE 600	350	100% sideways global, 70% local
1/2 IPE 600	394	100% sideways global, 70% local
1/2 IPE 600	438	100% sideways global, 70% local
1/2 IPE 600	482	100% sideways global, 70% local
1/2 IPE 600	525	100% sideways global, 70% local
1/2 IPE 600	569	100% sideways global, 70% local
1/2 IPE 600	613	100% sideways global, 70% local
1/2 IPE 600	657	100% sideways global, 70% local
1/2 IPE 600	700	100% sideways global, 70% local
1/2 IPE 600	744	100% sideways global, 70% local
1/2 IPE 600	788	100% sideways global, 70% local
1/2 IPE 600	832	100% sideways global, 70% local
1/2 IPE 600	875	100% sideways global, 70% local

Table 27: Failure modes of the IPE 600

In Table 27 the imperfection modes are listed that all occur in the IPE 600 experiments. There were more imperfection modes present at failure in the IPE 600 than in the previous sections however the buckling curve looked remarkably similar.

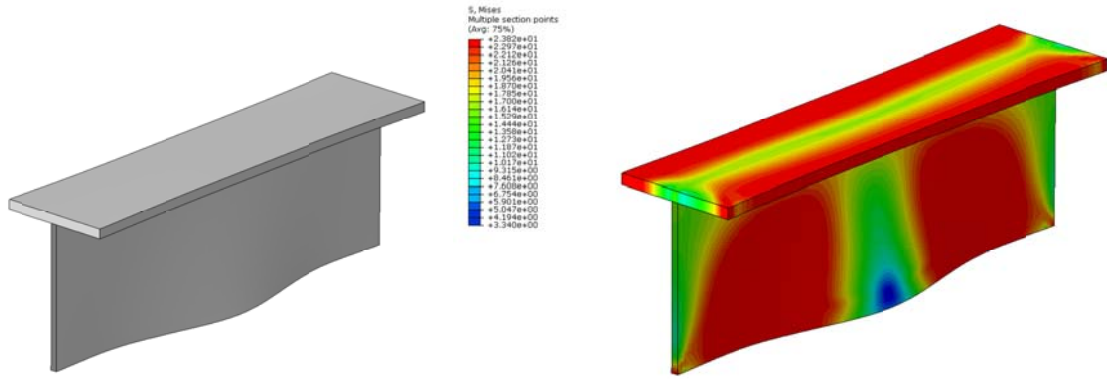


Figure 49: IPE 600 L=88cm - 70% sideways global, 100% local and stresses at failure

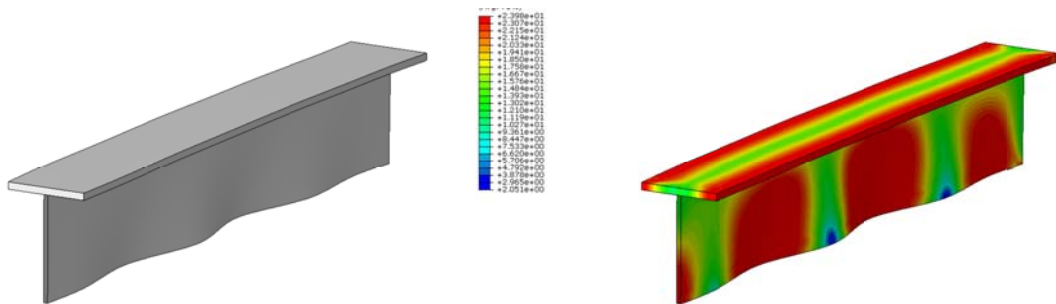


Figure 50: IPE 600 L=131cm - 70% upwards global, 100% local and stresses at failure

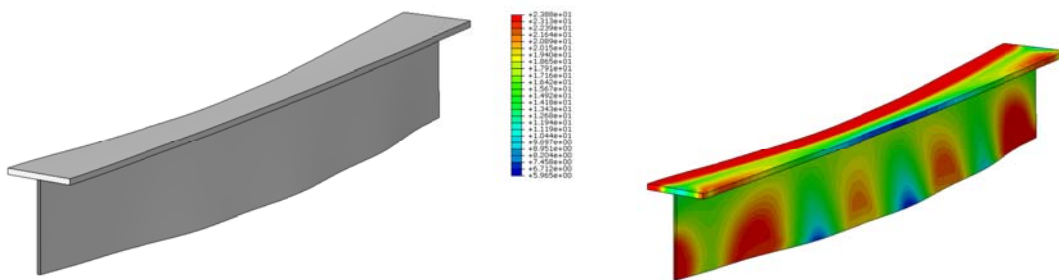


Figure 51 : IPE 600 L=175cm - 70% upwards global, 100% local and stresses at failure

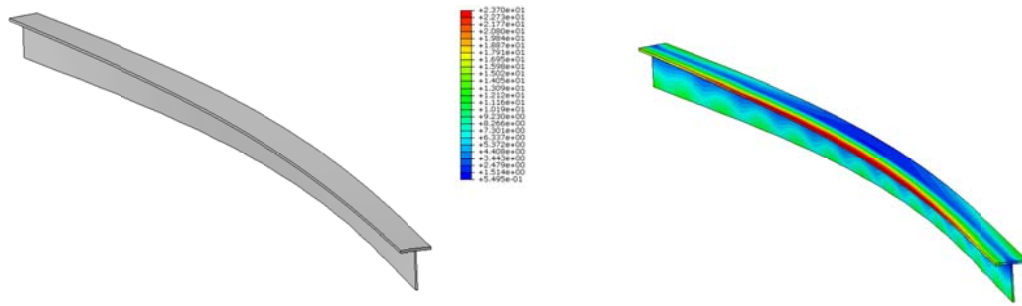


Figure 52 : IPE 600 L=700cm - 100% sideways global, 70% local and stresses at failure

These results show again that the Eurocode is extremely conservative in the case of the IPE 600. The safety in Figure 47 reaches a maximum with the smallest slenderness at about 0.6. The finite element calculation returned a reduction factor value of over 0.94 whereas the Eurocode 3 returns a value just under 0.4. This meant that yet again Eurocode 3 used less than half of the available resistance from the section to be used for dimensioning calculations.

6.4.5 Results for the HE-A 500 section

This section was a bit different to the IPE profiles that had been looked at previously. The main difference here was that the z-z axis was no longer the weaker of the two axes. Here it was the y-y axis. The methods did not change for the calculations of either the finite element model or the Eurocode 3 methods. It was only necessary to make sure that the Eurocode 3 equation representing in-plane buckling (with the term χ_y) was indeed used as the critical equation in determining the EC3 resistance.

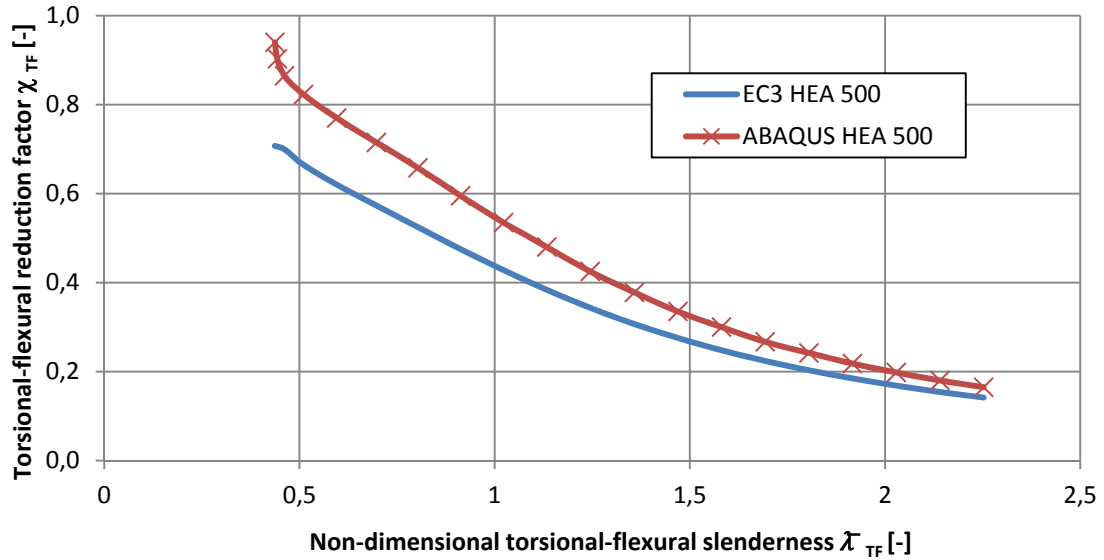


Figure 53: HE-A 500 under compression - comparison between present Eurocode 3 and the ABAQUS calculations - plotted over the torsional-flexural slenderness

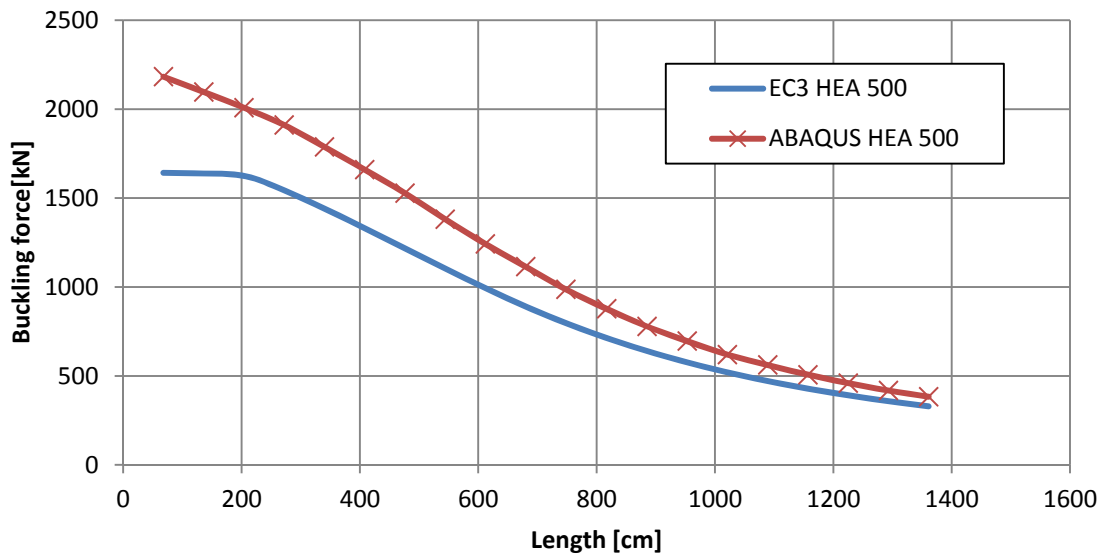


Figure 54: HE-A 500 under compression - ABAQUS results and Eurocode 3 resistances - plotted over length

It was clear to see here that the curve is smooth and that it was not divided into clear areas of different failure modes. The imperfection modes that lead to failure are all dependent on a global vertical imperfection in the upward direction. The failure of the shorter subjects was obviously more affected by the local imperfections and the longer members were more

susceptible to the global imperfections. In Figure 55 and Figure 56 the two similar modes can be seen.

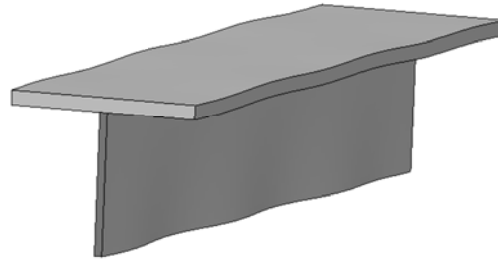


Figure 55: HE-A 500, $L=136\text{cm}$ - 70% upwards global, 100% clockwise local

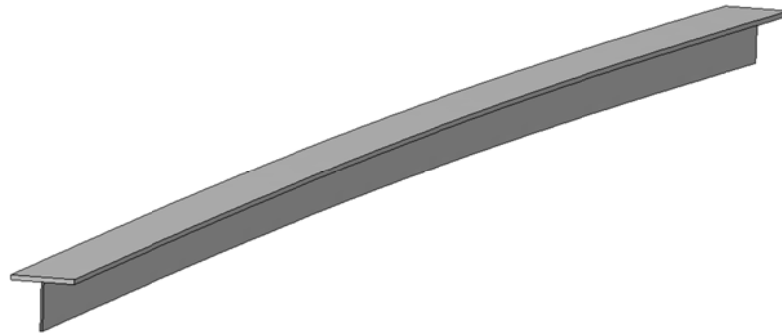


Figure 56: HE-A 500, $L=1021\text{cm}$ - 100% upwards global, 70% clockwise local

The stress distribution for these members at the point of failure can be seen in Figure 57 and Figure 58.

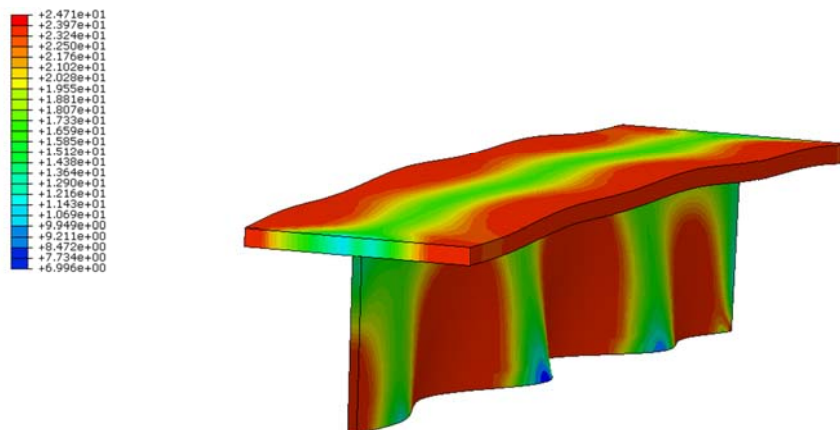


Figure 57: Stress distribution at the point of failure HE-A 500, $L=136\text{cm}$

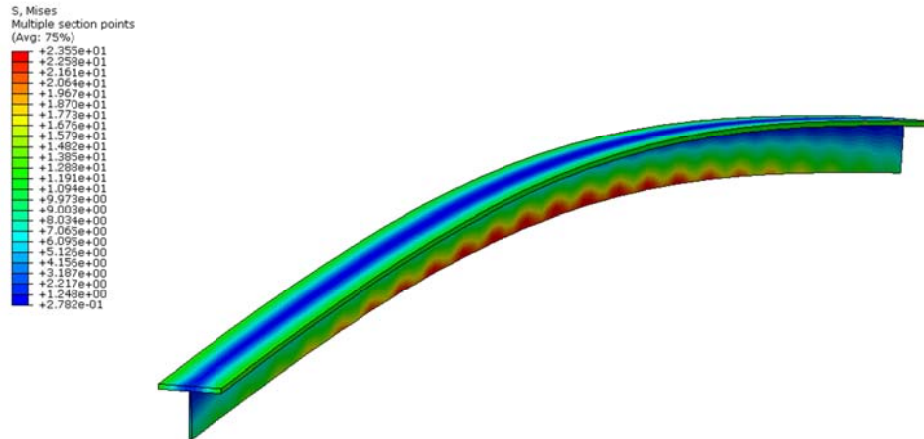


Figure 58: Stress distribution at the point of failure HE-A 500, $L=1021\text{cm}$

The results for the Eurocode implied that this member HEA 500 was more likely to fail due to lateral-torsional failure around the y-y axis (Equ.1). This was where the least resistance was achieved. Torsional-flexural failure was only the dominant equation up to slenderness of 0.3. This is the first section where it was possible to say that the Eurocode 3 dimensioning was almost acceptable as it was. Here the safety, although still very high in places, was closer to the ABAQUS calculations. The safety for the shorter subjects was only around 15%.

6.4.6 Results for the modified IPE 500 wide section

This was a very interesting section to investigate as both of the axes, y-y and z-z were seemingly equal in strength. This meant that it was unlike the sections investigated so far. In Figure 59 and Figure 60 the results for the buckling force, torsional-flexural reduction factor and the Eurocode 3 values are shown.

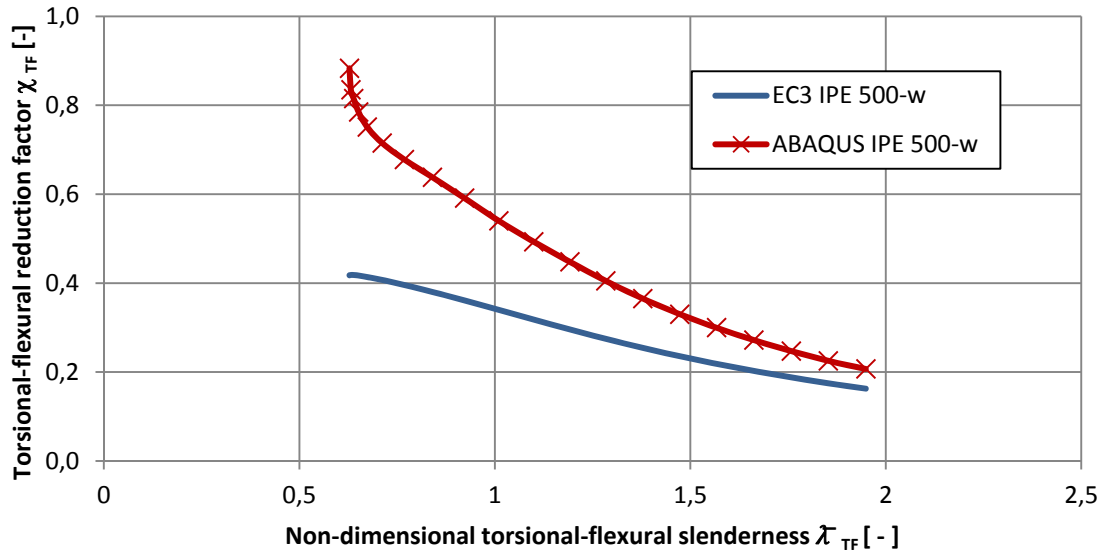


Figure 59: IPE 500 wide, under compression - comparison between Eurocode 3 and ABAQUS calculations - plotted over the torsional-flexural slenderness

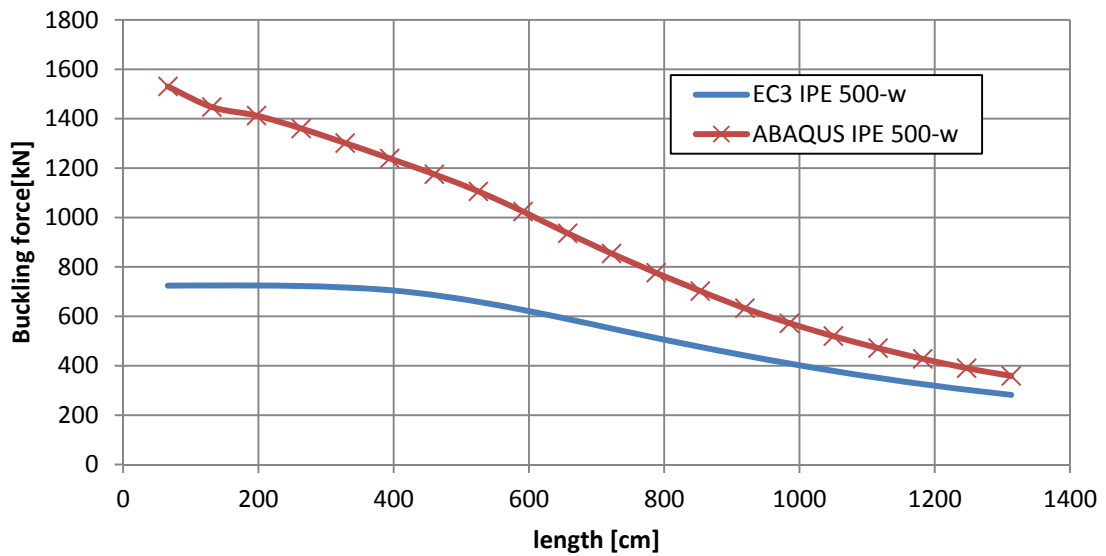


Figure 60: IPE 500 wide, under compression - ABAQUS results and Eurocode 3 resistances - plotted over length

Cross Section	[cm]	Imperfection Mode
1/2 IPE 500 - wide	66	70% upwards global, 100% local
1/2 IPE 500 - wide	131	70% upwards global, 100% local
1/2 IPE 500 - wide	197	70% upwards global, 100% local
1/2 IPE 500 - wide	263	70% upwards global, 100% local
1/2 IPE 500 - wide	328	70% upwards global, 100% local
1/2 IPE 500 - wide	394	70% upwards global, 100% local
1/2 IPE 500 - wide	460	70% upwards global, 100% local
1/2 IPE 500 - wide	525	70% upwards global, 100% local
1/2 IPE 500 - wide	591	100% upwards global, 70% local
1/2 IPE 500 - wide	657	100% upwards global, 70% local
1/2 IPE 500 - wide	722	100% upwards global, 70% local
1/2 IPE 500 - wide	788	100% upwards global, 70% local
1/2 IPE 500 - wide	853	100% upwards global, 70% local
1/2 IPE 500 - wide	919	100% upwards global, 70% local
1/2 IPE 500 - wide	985	100% upwards global, 70% local
1/2 IPE 500 - wide	1050	100% upwards global, 70% local
1/2 IPE 500 - wide	1116	100% upwards global, 70% local
1/2 IPE 500 - wide	1182	100% upwards global, 70% local
1/2 IPE 500 - wide	1247	100% upwards global, 70% local
1/2 IPE 500 - wide	1313	100% upwards global, 70% local

Table 28: Imperfection modes for the modified HE-A 500 wide

As with the normal IPE sections, this curve (Figure 60) also contained two parts. In the first part the local imperfections were decisive. In the second part the global imperfections were more decisive. With this section however the local imperfection was definitive for much longer members. The failure modes for this section can be seen in Table 28. The values for the Eurocode curve were mainly dominated by the equation for lateral-torsional failure around the y-y axis (Equ.1). Torsional-flexural failure (Equ.2) was, according to the Eurocode, dominant only up to a length of 197cm.

The ABAQUS calculation value for the reduction factor dropped far more rapidly under 0.7 as the other sections however, it was still above the value suggested by the Eurocode. The dimensioning for the Eurocode 3 was not only very conservative for members with a low slenderness but also for the longer members.

Similar to the other sections the Eurocode 3 and the ABAQUS calculations neared each other the more slender the members.

6.4.7 *Results for the modified IPE 500 thin section*

Finally the modified IPE 500 with a flange that was just 100mm wide was studied. Here there was no doubt about which axis was the weakest. The z-z was far weaker and therefore the section would be more sensitive to sideways imperfections. This was the first section where there was such a large difference between the strengths of the axes.

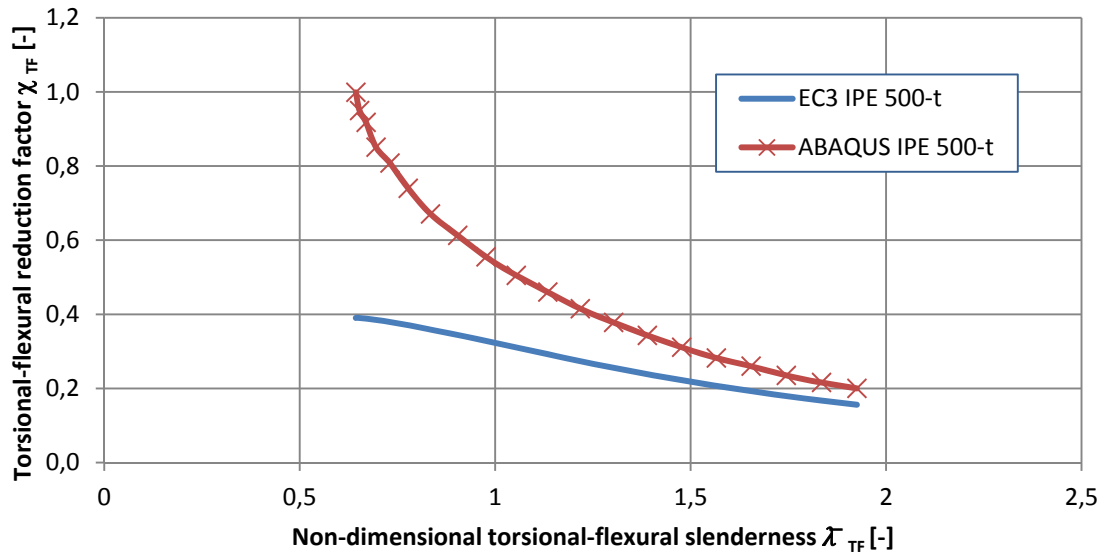


Figure 61: IPE 500 thin under compression - comparison between Eurocode 3 and ABAQUS calculations - plotted over the torsional-flexural slenderness

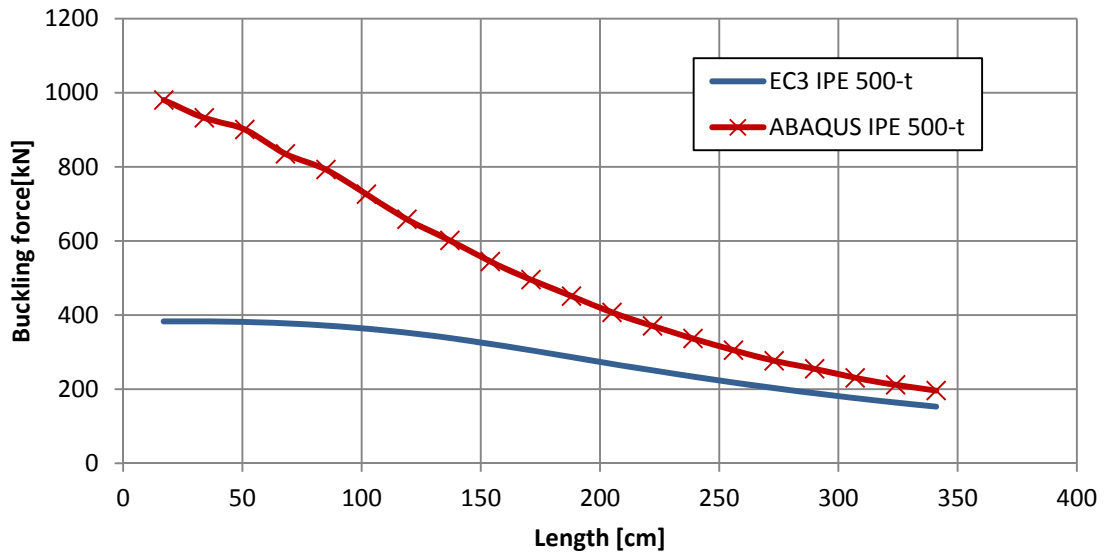


Figure 62 : IPE 500 thin under compression - ABAQUS results and Eurocode 3 resistances - plotted over length

A small inconsistency could be seen at a length of 50cm. At first it was assumed that this may be due to a change in the defining mode. The defining modes are shown in Table 29. As there was no change in the defining mode in this area of the plot, it must have had another explanation. It seems as if this inconsistency may be due to the way in which the local imperfections were implemented. It was assumed that the member length was equal to a length where the number of half sine waves was very favourable for the buckling resistance. Because of the size of this inconsistency, it can be ignored.

The results for this section also show that there is a large need for improvement to the Eurocode. How the large discrepancy could be countered will be looked at in chapter 7 “Development and verification of alternative design proposals for Class 4”.

Cross Section	[cm]	Imperfection Failure Mode
1/2 IPE 500 - thin	17	70% sideways global, 100% clockwise local
1/2 IPE 500 - thin	34	70% sideways global, 100% clockwise local
1/2 IPE 500 - thin	51	70% sideways global, 100% clockwise local
1/2 IPE 500 - thin	68	70% sideways global, 100% anti-clockwise local
1/2 IPE 500 - thin	85	100% sideways global, 70% clockwise local
1/2 IPE 500 - thin	102	100% sideways global, 70% clockwise local
1/2 IPE 500 - thin	119	100% sideways global, 70% anti-clockwise local
1/2 IPE 500 - thin	137	100% sideways global, 70% clockwise local
1/2 IPE 500 - thin	154	100% sideways global, 70% anti-clockwise local
1/2 IPE 500 - thin	171	100% sideways global, 70% anti-clockwise local
1/2 IPE 500 - thin	188	100% sideways global, 70% clockwise local
1/2 IPE 500 - thin	205	100% sideways global, 70% anti-clockwise local
1/2 IPE 500 - thin	222	100% sideways global, 70% anti-clockwise local
1/2 IPE 500 - thin	239	100% sideways global, 70% clockwise local
1/2 IPE 500 - thin	256	100% sideways global, 70% anti-clockwise local
1/2 IPE 500 - thin	273	100% sideways global, 70% clockwise local
1/2 IPE 500 - thin	290	100% sideways global, 70% clockwise local
1/2 IPE 500 - thin	307	100% sideways global, 70% anti-clockwise local
1/2 IPE 500 - thin	324	100% sideways global, 70% clockwise local
1/2 IPE 500 - thin	341	100% sideways global, 70% clockwise local

Table 29: Failure modes for the IPE 500 thin

7 Development and verification of alternative design proposals for Class 4 sections

As seen in chapter 6 there was room for improvement on the current Eurocode 3 method of dimensioning class 4 T-sections. The current method, even the method implemented in the Austrian national annex for mono-symmetric sections, is extremely conservative for class 4 T-sections in compression and would lead to over dimensioning of the T-sections. A large portion of the section's resistance is needed, in the Eurocode, to counteract the moment that is predicted to be relevant due to the shift of the centroid.

In the following pages, a number of alternative design proposals will be presented and verified against the available GMNIA results. In this chapter the results are displayed in graphs where $\frac{N_R}{A * f_y}$ is plotted against the length of the member. In Appendix A the results are shown again as $\frac{N_R}{A_{eff} * f_y}$ plotted against the effective torsional-flexural slenderness.

7.1 Proposal 1

The first suggestion was to ignore the aforementioned moment and see how unsafe the sections would be if the dimensioning was carried out just taking the axial force into account. It was expected that the load bearing capacity of the sections would be overestimated and that they would be unsafe, however it would give a good starting point for any other suggestions.

It meant that the equations from Eurocode 3, rewritten below for easier read, had to be adapted in a significant simpler form.

$$\frac{N_{Ed}}{\chi_y * A_{eff} * f_y} + k_y \frac{C_{my} * N_{Ed} * e_N}{\chi_{LT} * M_{y,Rk}} \leq 1 \quad Equ. (1)$$

$$\frac{N_{Ed}}{\chi_{TF} * A_{eff} * f_y} + k_{LT} \frac{N_{Ed} * e_N}{\chi_{LT(s)} * M_{y,Rk(s)}} \leq 1 \quad Equ. (2)$$

$$\frac{N_{Ed}}{\chi_z * A_{eff} * f_y} - k_{LT} \frac{N_{Ed} * e_N}{\chi_{LT(l)} * M_{y,Rk(l)}} \leq 1 \quad Equ. (3)$$

They were transformed to the following 3 very simple equations.

$$\frac{N_{Ed}}{\chi_y * A_{eff} * f_y} \leq 1 \quad Equ. (1) \text{ proposal 1}$$

$$\frac{N_{Ed}}{\chi_{TF} * A_{eff} * f_y} \leq 1 \quad Equ. (2) \text{ proposal 1}$$

$$\frac{N_{Ed}}{\chi_z * A_{eff} * f_y} \leq 1 \quad Equ. (3) \text{ proposal 1}$$

From here the new buckling force resistance could be calculated. ($N_{Rd} = N_{Ed}$ if all 3 equations are fulfilled)

All of the section properties for the gross section and effective section had already been calculated. The coefficients to help calculate the reduction factors were calculated using the *current* Eurocode 3 method and not the coefficient explained previously in chapter 5 as the “new proposal” according to Taras et al.

$$\Phi_{TF} = 0.5[1 + \alpha_z(\bar{\lambda}_{TF} - 0.2) + \bar{\lambda}_{TF}^2]$$

$$\Phi_z = 0.5[1 + \alpha_z(\bar{\lambda}_z - 0.2) + \bar{\lambda}_z^2]$$

$$\Phi_y = 0.5[1 + \alpha_y(\bar{\lambda}_y - 0.2) + \bar{\lambda}_y^2]$$

$$\chi_{LT} = \frac{1}{\Phi_{LT} + \sqrt{\Phi_{LT}^2 - \bar{\lambda}_{LT}^2}} \leq 1.0$$

$$\chi_z = \frac{1}{\Phi_z + \sqrt{\Phi_z^2 - \bar{\lambda}_z^2}} \leq 1.0$$

$$\chi_y = \frac{1}{\Phi_y + \sqrt{\Phi_y^2 - \bar{\lambda}_y^2}} \leq 1.0$$

So these have also previously been calculated. The criteria were then simply transformed so that a buckling force resistance was found to be the smallest result returned.

$$N_{R,y} = \chi_y * A_{eff} * f_y$$

$$N_{R,TF} = \chi_{TF} * A_{eff} * f_y$$

$$N_{R,z} = \chi_z * A_{eff} * f_y$$

These criteria were then evaluated for all of the lengths that we had used for the finite element calculations. The results could then be plotted into a buckling curve. Using a 364cm long IPE 500 member the method is explained here. The properties that were calculated previously are also listed.

$$G = 8076 \text{ kN/cm}^2; E = 21000 \text{ kN/cm}^2; A = 57.8 \text{ cm}^2; A_{eff} = 52.85 \text{ cm}^2;$$

$$I_y = 3260 \text{ cm}^4; I_z = 1070 \text{ cm}^4; I_T = 44.6 \text{ cm}^4; i_z = 4.3026 \text{ cm}; i_y = 7.5101 \text{ cm}$$

$$z_0 = z_s - \frac{t_f}{2} = 6.01 - \frac{1.6}{2} = 5.2 \text{ cm}$$

$$i_0^2 = i_y^2 + i_z^2 + z_0^2 = 102.06 \text{ cm}^2$$

$$N_{cr,y} = \frac{\pi^2 * E * I_y}{l^2} = \frac{\pi^2 * 21000 * 3260}{364^2} = 5104.4 \text{ kN}$$

$$N_{cr,z} = \frac{\pi^2 * E * I_z}{l^2} = \frac{\pi^2 * 21000 * 1070}{364^2} = 1673.8 \text{ kN}$$

$$N_{cr,T} = \frac{1}{i_0^2} G I_T = \frac{1}{102.06} * 8076 * 44.6 = 3529.3 \text{ kN}$$

$$N_{cr,TF} = \frac{N_{cr,z}}{2 * \left(1 - \frac{z_0^2}{i_0^2}\right)} \left[1 + \frac{N_{cr,T}}{N_{cr,z}} - \sqrt{\left(1 - \frac{N_{cr,T}}{N_{cr,z}}\right)^2 + 4 * \left(\frac{z_0^2}{i_0^2}\right) * \frac{N_{cr,T}}{N_{cr,z}}} \right]$$

$$N_{cr,TF} = \frac{1673.8}{2 * \left(1 - \frac{5.21^2}{102.06}\right)} \left[1 + \frac{3529}{1673.8} - \sqrt{\left(1 - \frac{3529}{1673.8}\right)^2 + 4 * \left(\frac{5.21^2}{102.06}\right) * \frac{3529}{1673.8}} \right]$$

$$N_{cr,TF} = 1419.7 \text{ kN}$$

a) Torsional-flexural buckling

$$\bar{\lambda}_{TF} = \sqrt{\frac{A_{eff} * f_y}{N_{cr,TF}}} = \sqrt{\frac{52,85 * 23.5}{1419.7}} = 0.93532$$

$$\Phi_{TF} = 0.5[1 + \alpha_z(\bar{\lambda}_{TF} - 0.2) + \bar{\lambda}_{TF}^2] = 0.5[1 + 0.49(0.93532 - 0.2) + 0.93532^2]$$

$$\Phi_{TF} = 1.1176$$

$$\chi_{TF} = \frac{1}{\Phi_{TF} + \sqrt{\Phi_{TF}^2 - \bar{\lambda}_{TF}^2}} \leq 1.0$$

$$\chi_{TF} = \frac{1}{1.1176 + \sqrt{1.1176^2 - 0.93532^2}} = 0.57829 \leq 1.0$$

The buckling force resistance in respect to the torsional-flexural buckling was calculated.

$$N_{R,TF} = 0.57829 * 52.85 * 23.5 = 718.65 \text{ kN} \quad \text{Equ. (2) proposal 1}$$

b) Flexural buckling about the z-z axis

$$N_{cr,z} < N_{cr,TF} \quad - \quad \chi_z > \chi_{TF}$$

This means that this equation is never relevant

c) Flexural buckling about the y-y axis

$$\bar{\lambda}_y = \sqrt{\frac{A_{eff} * f_y}{N_{cr,y}}} = \sqrt{\frac{52.85 * 23.5}{5104.4}} = 0.4933$$

$$\Phi_y = 0.5[1 + \alpha_y(\bar{\lambda}_y - 0.2) + \bar{\lambda}_y^2] = 0.5[1 + 0.49(0.4933 - 0.2) + 0.4933^2]$$

$$\Phi_y = 0.6935$$

$$\chi_y = \frac{1}{\Phi_y + \sqrt{\Phi_y^2 - \bar{\lambda}_y^2}} = \frac{1}{0.6935 + \sqrt{0.6935^2 - 0.4933^2}} = 0.8468 \leq 1.0$$

The buckling resistance for the y-y axis buckling was then calculated.

$$N_{R,y} = 0.8468 * 52.85 * 23.5 = 1051.7 \text{ kN} \quad \text{Equ. (1) proposal 1}$$

So the smallest of the values was the result. This was the torsional-flexural resistance. A buckling resistance of $N_{R,TF} = 718.65 \text{ kN}$ was obtained. This value was divided by the gross section resistance.

$$\frac{N_{R,TF}}{A * f_y} = \frac{718.65}{57.8 * 23.5} = 0.529$$

A is the gross area of the section. This value can be seen in Figure 65.

The IPE 300 was the first section on which this theory was tested. The results for every length were calculated and plotted over the length of the members (see Figure 63).

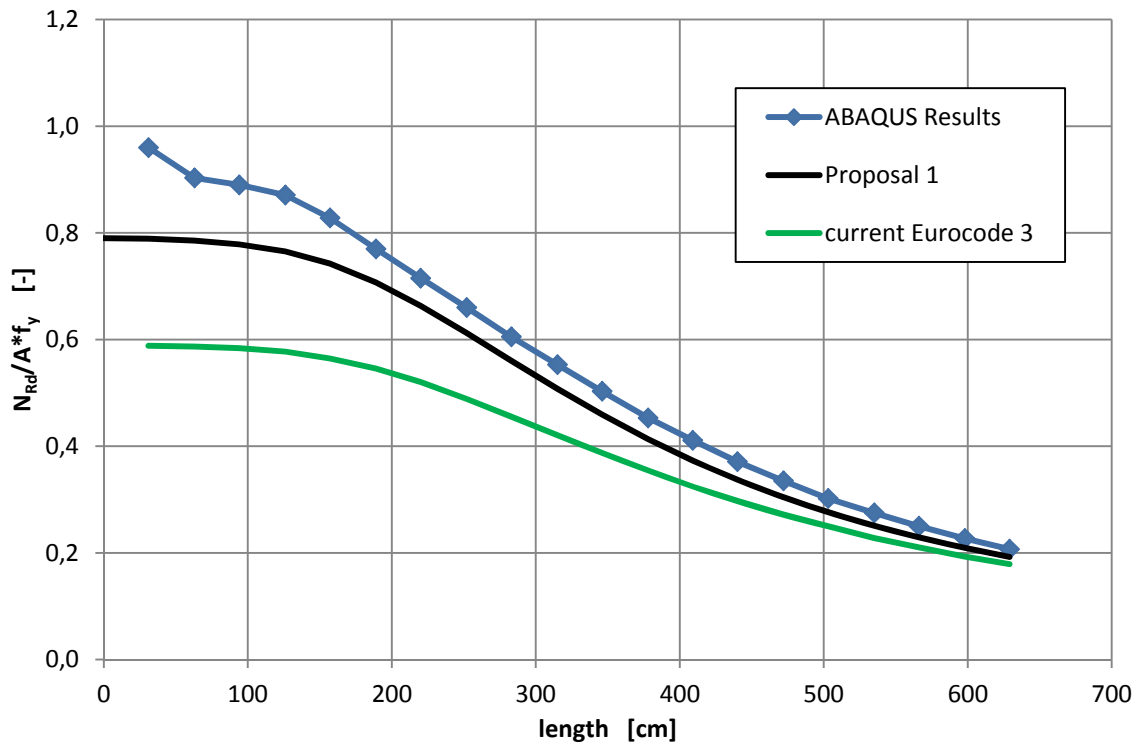


Figure 63: IPE 300 - proposal 1

The results in Figure 63 for an IPE 300, were surprising because they are conservative for every different length member. If this were true for all of the sections this would be a good suggestion for dimensioning T-sections under an axial force (see Figure 64 - Figure 69).

7 Development and verification of alternative design proposals for Class 4 sections

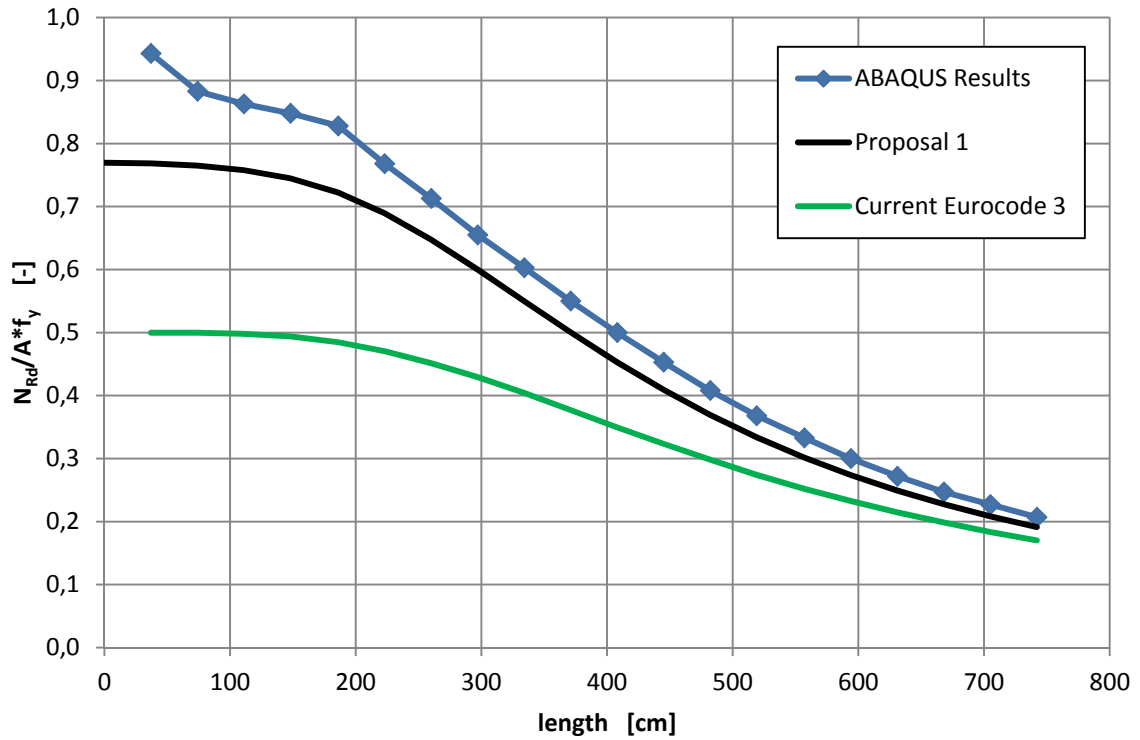


Figure 64 : IPE 400 - proposal 1

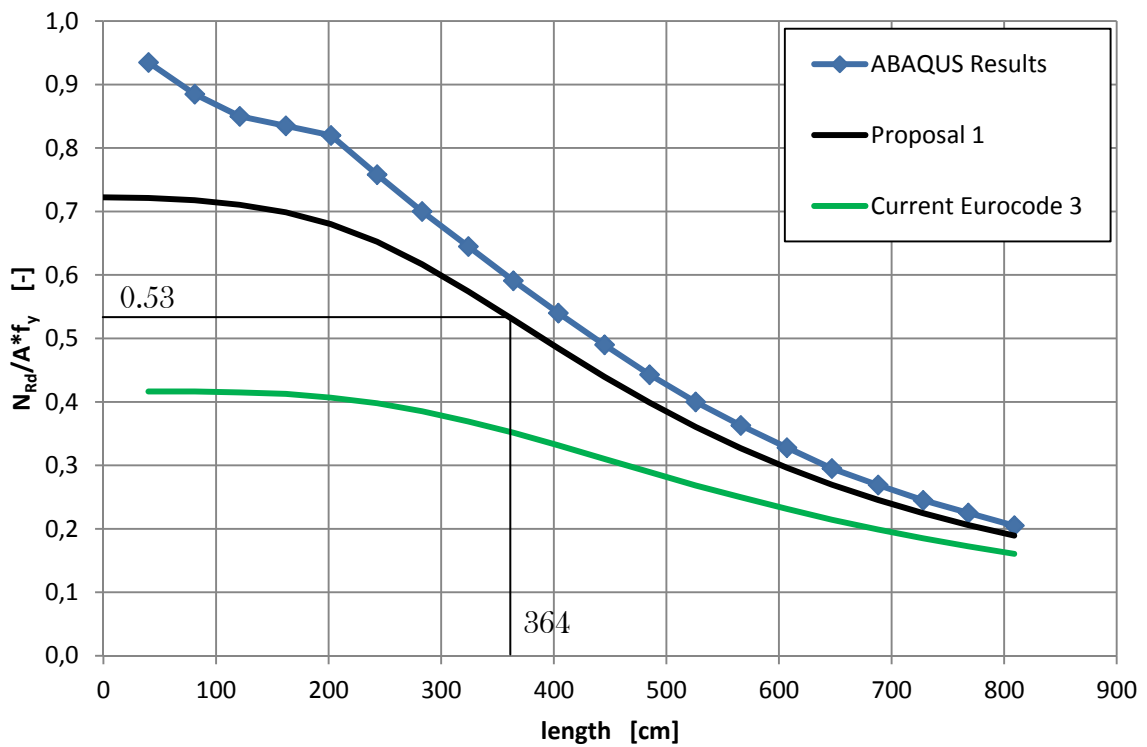


Figure 65: IPE 500 - proposal 1

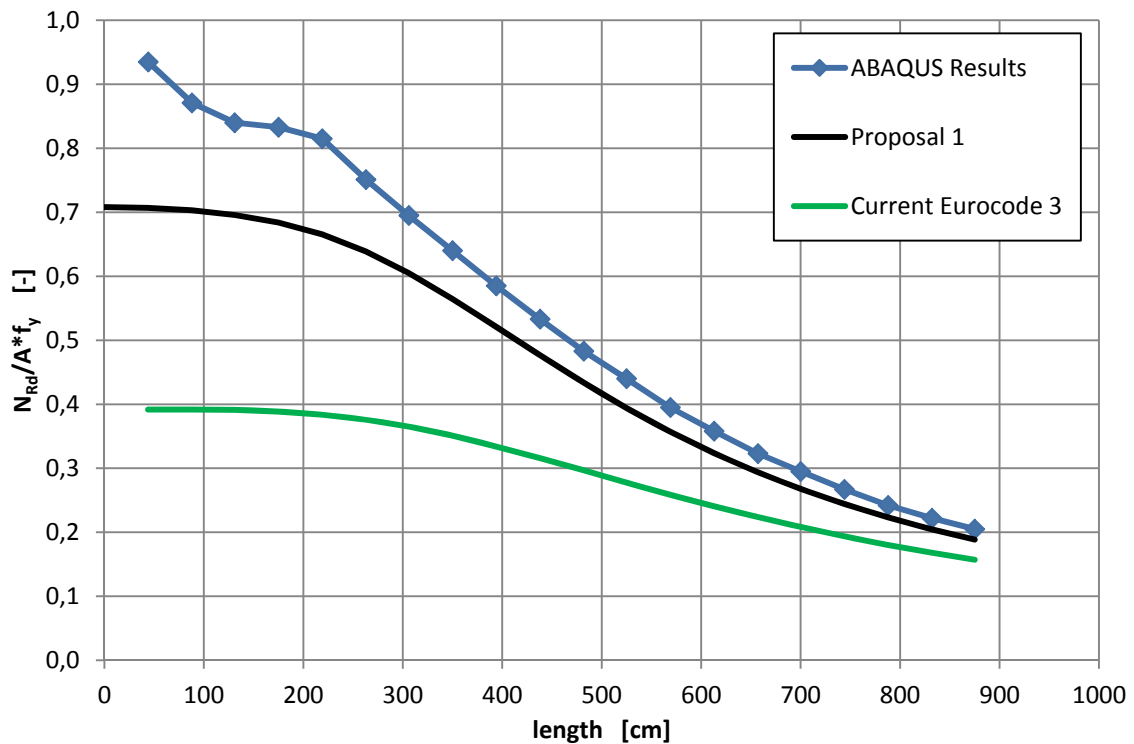


Figure 66: IPE 600 - proposal 1

The results for all of the standard IPE sections, shown in Figure 63, Figure 64, Figure 65 and Figure 66 returned positive to this proposal. The results were all on the safe side. This means that for these sections the moment that would be induced by the reduced section could actually be totally ignored!

The results for the other sections were also then obtained. Figure 67 shows the results obtained for the IPE 500-t which had a flange width of only 10cm. Again the proposal looks to fit very well to the finite element results. The results were almost too conservative.

The results for the IPE 500-w are shown in Figure 68. Here we can see that the values follow the results almost perfectly and are always on the side of caution, providing an acceptable margin of safety.

7 Development and verification of alternative design proposals for Class 4 sections

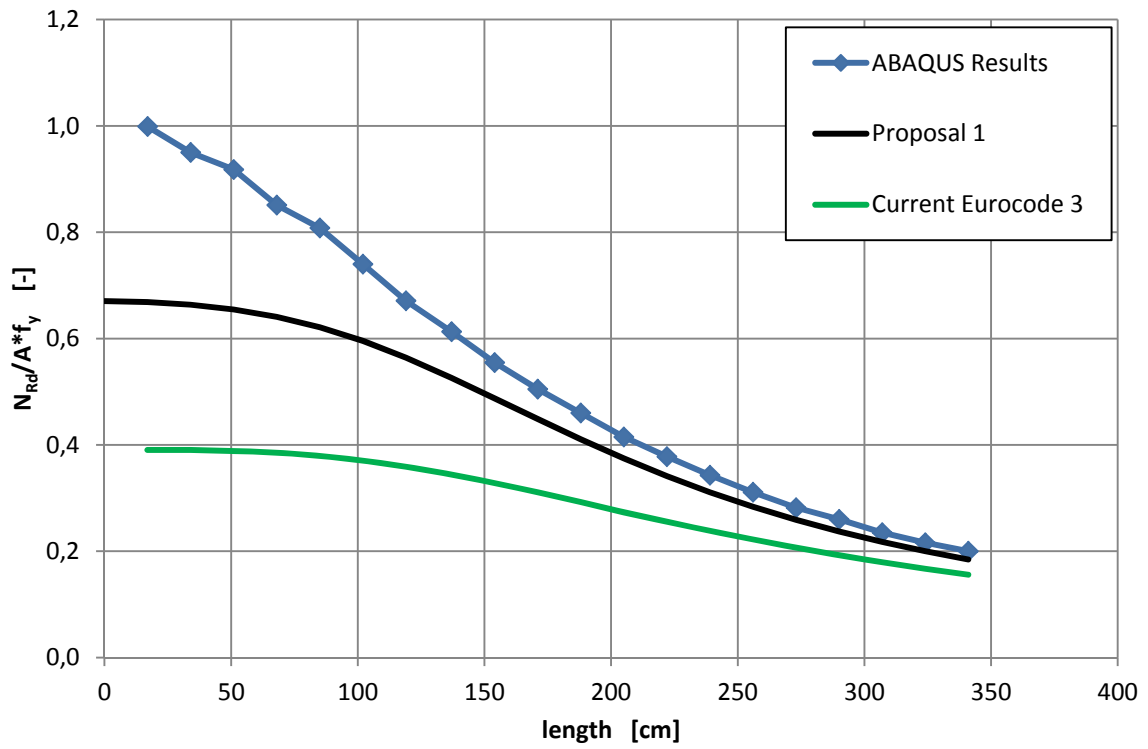


Figure 67: IPE 500-t - proposal 1

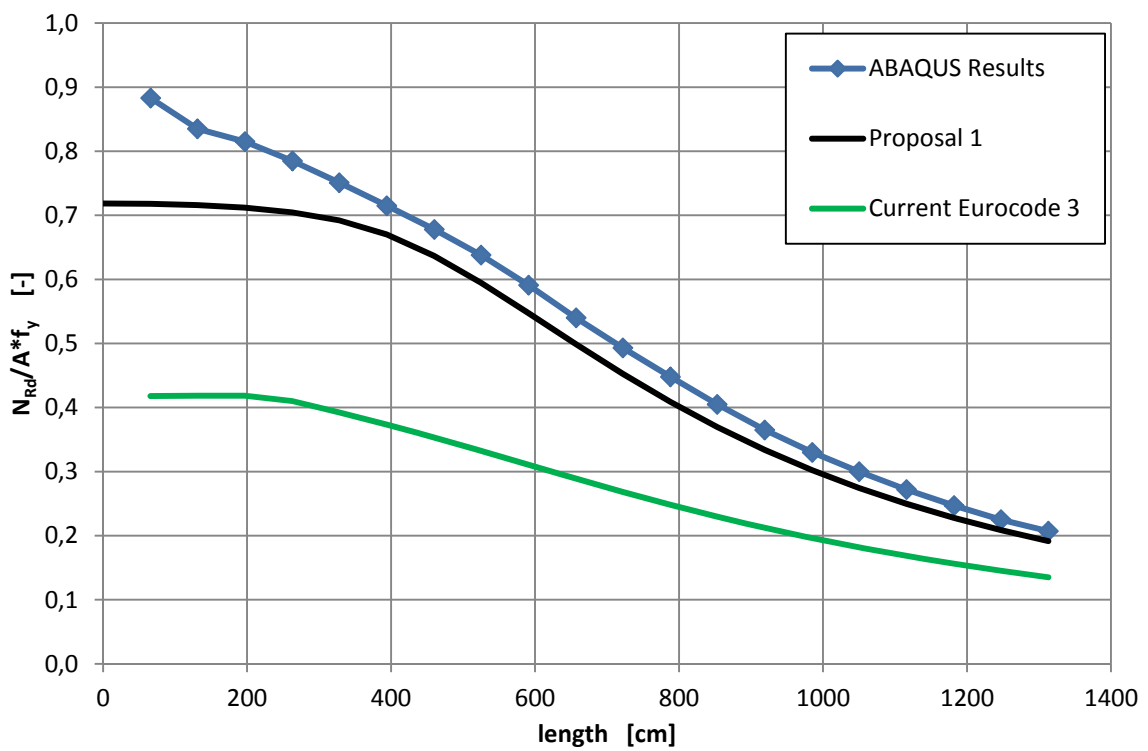


Figure 68: IPE 500-w - proposal 1

Finally the HE-A 500 was investigated. This was different to all the other sections as the y-y axis was the weaker one. The results can be seen in Figure 69. This was the first section where “Proposal 1” did not consistently stay on the safe side. It did lean minimally to being unsafe; however such a small difference could be seen as acceptable and may then be covered once the residual stress distribution for such sections are more accurately known.

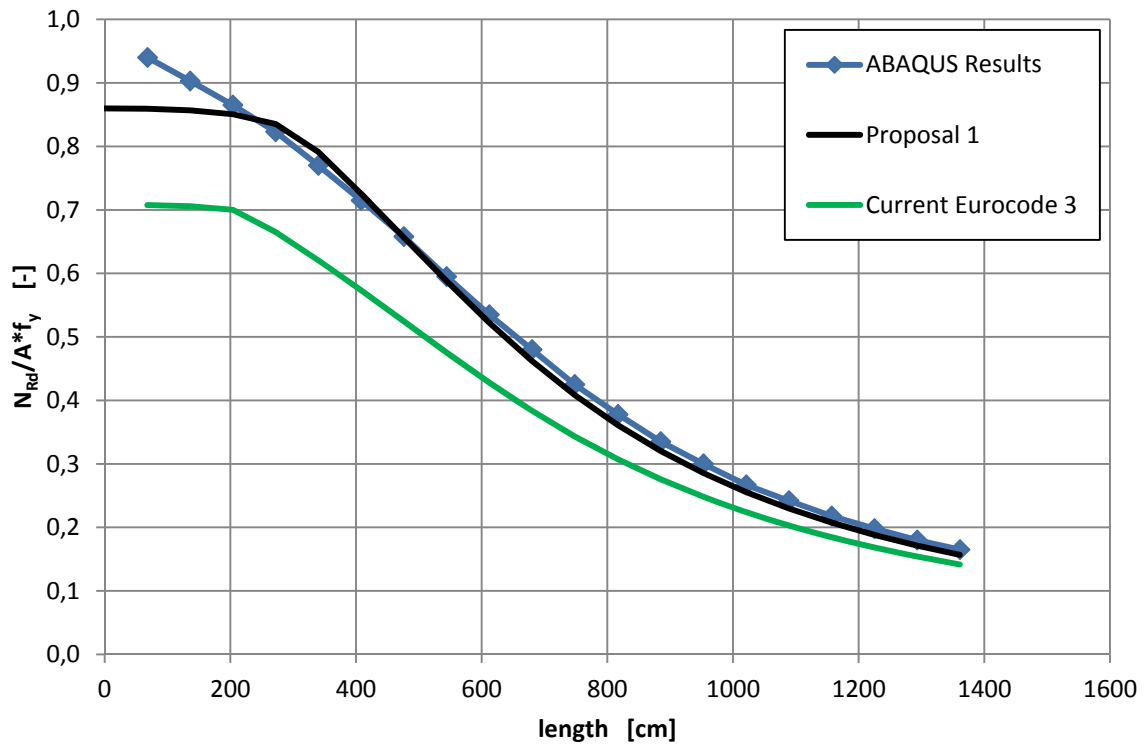


Figure 69: HE-A 500 - proposal 1

After nearly all of the results for proposal 1 were better than expected, a second proposal was tested.

7.2 Proposal 2

The second proposal involved removing the effective cross section properties and seeing if, in the case of the structural T-sections, the gross section values could be used for the calculations.

As an example the IPE 500 with a length of 364cm was calculated.

a) Calculation of slenderness

$$\bar{\lambda}_y = \sqrt{\frac{A * f_y}{N_{cr,y}}} = \sqrt{\frac{57.8 * 23.5}{5104.4}} = 0.5157$$

$$\bar{\lambda}_z = \sqrt{\frac{A * f_y}{N_{cr,z}}} = \sqrt{\frac{57.8 * 23.5}{1673.8}} = 0.900$$

$$\bar{\lambda}_{TF} = \sqrt{\frac{A * f_y}{N_{cr,TF}}} = \sqrt{\frac{57.8 * 23.5}{1419.7}} = 0.9772$$

b) Calculation of buckling factors

$$\Phi_y = 0.5[1 + \alpha_y(\bar{\lambda}_y - 0.2) + \bar{\lambda}_y^2] = 0.5[1 + 0.49(0.5157 - 0.2) + 0.5157^2]$$

$$\Phi_y = 0.71$$

$$\Phi_{TF} = 0.5[1 + \alpha_z(\bar{\lambda}_{TF} - 0.2) + \bar{\lambda}_{TF}^2] = 0.5[1 + 0.49(0.9772 - 0.2) + 0.9772^2]$$

$$\Phi_{TF} = 1.1679$$

$$\chi_y = \frac{1}{\Phi_y + \sqrt{\Phi_y^2 - \bar{\lambda}_y^2}} = \frac{1}{0.71 + \sqrt{0.71^2 - 0.5157^2}} = 0.8347 \leq 1.0$$

$$\chi_{TF} = \frac{1}{\Phi_{TF} + \sqrt{\Phi_{TF}^2 - \bar{\lambda}_{TF}^2}} = \frac{1}{1.1679 + \sqrt{1.1679^2 - 0.9772^2}} = 0.5533 \leq 1.0$$

The smallest of the reduction factor values was then the result. Here the value was 0.5533. This value can be plotted directly in Figure 72. For the final compression capacity we get:

$$N_{R,TF} = \chi_{TF} * A * f_y$$

In this case

$$0.5533 * 57.8 * 23.5 = 751.5 \text{ kN}$$

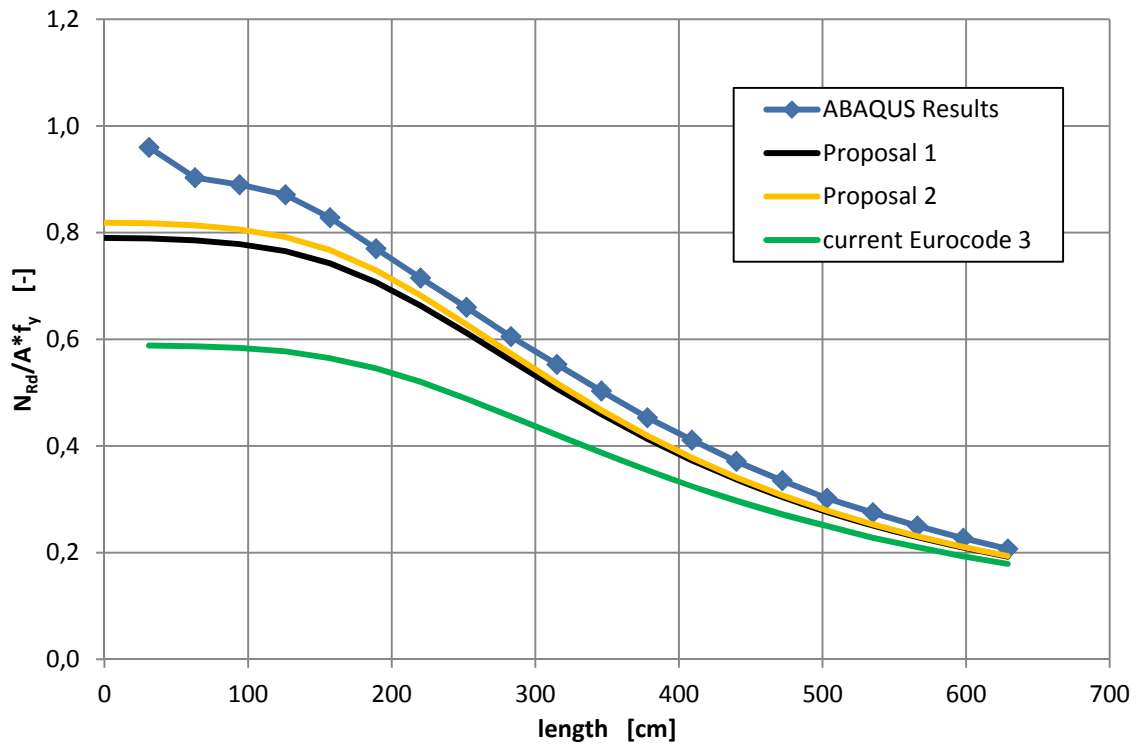


Figure 70: IPE 300 - proposal 2 compared to proposal 1

The IPE 300 was the first section on which this proposal was tested (see Figure 70). The results showed that this curve coincided with the finite element results better than the “Proposal 1”. Here there was a marginal improvement in the results. “Proposal 2” was then compared to the results for the other sections.

7 Development and verification of alternative design proposals for Class 4 sections

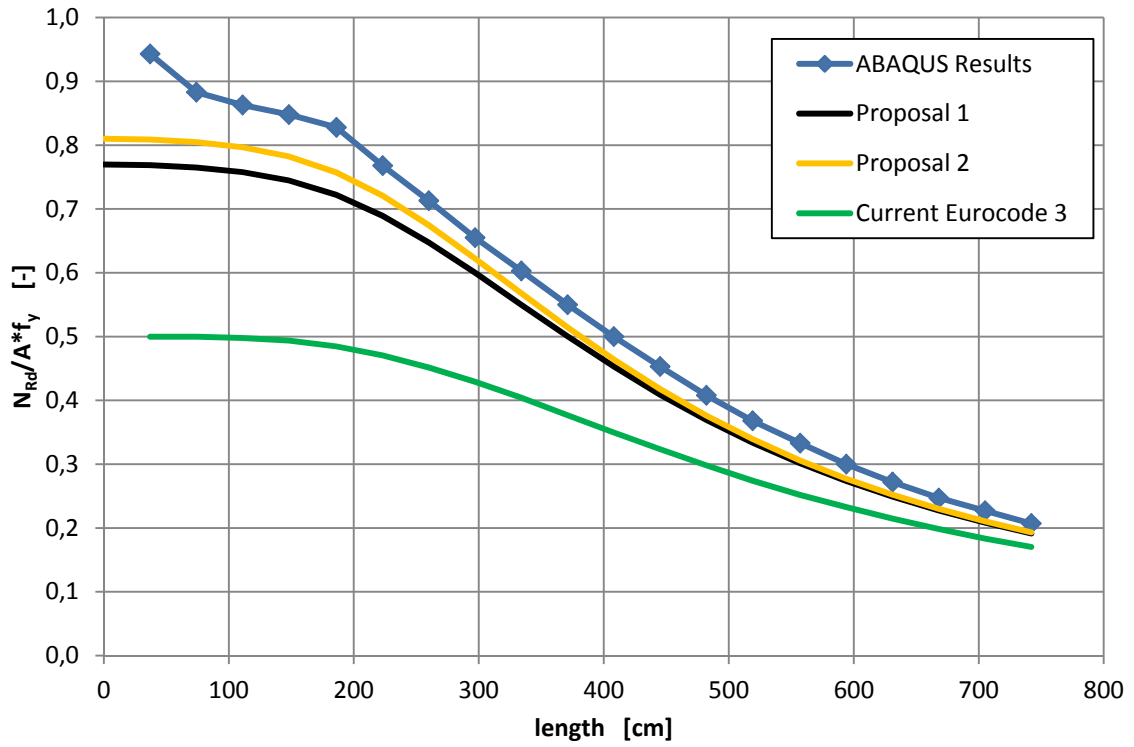


Figure 71: IPE 400 - proposal 2 compared to proposal 1

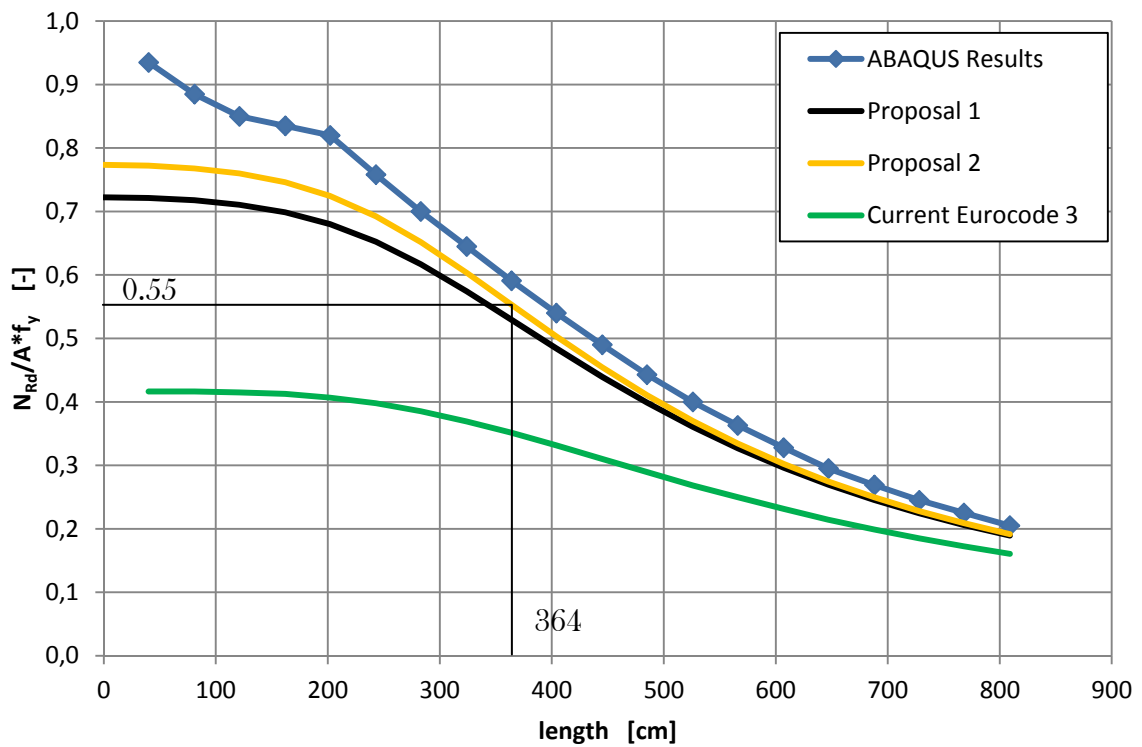


Figure 72: IPE 500 - proposal 2 compared to proposal 1

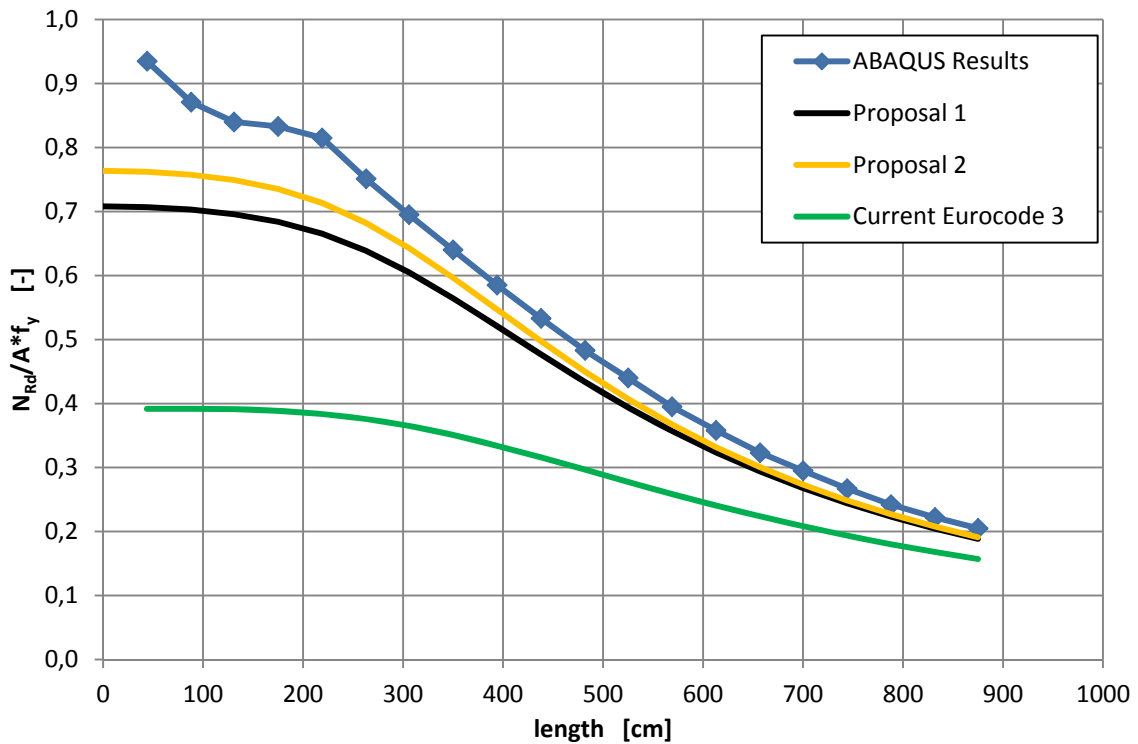


Figure 73: IPE 600 - proposal 2 compared to proposal 1

The results showed (Figure 71 to Figure 73) that the proposal was very fitting for all of the standard IPE sections which had been calculated. This was a considerable improvement on the shortest length members over “Proposal 1”. This left the question how it looked compared to the modified sections. The results for the IPE 500-t still seemed to be conservative for the shorter length members. The section would still be over dimensioned if this curve is used, however still an improvement on “Proposal 1”.

The behaviour of the IPE 500-w (Figure 75) is described very well with “Proposal 2”. It is still a slightly conservative for the shorter lengths however at lengths of 400cm and longer it always had an appropriate margin of safety. It was an improvement on “Proposal 1”.

Finally the HE-A 500, which was already slightly on the unsafe side using the curve from “Proposal 1”, was looked at. The results can be seen in Figure 76. The second proposal did not create any advantages for this section! It just amplified the problems from the first proposal.

These errors, however, could be in an acceptable range that may be covered once the residual stresses for T-sections have been investigated more thoroughly.

7 Development and verification of alternative design proposals for Class 4 sections

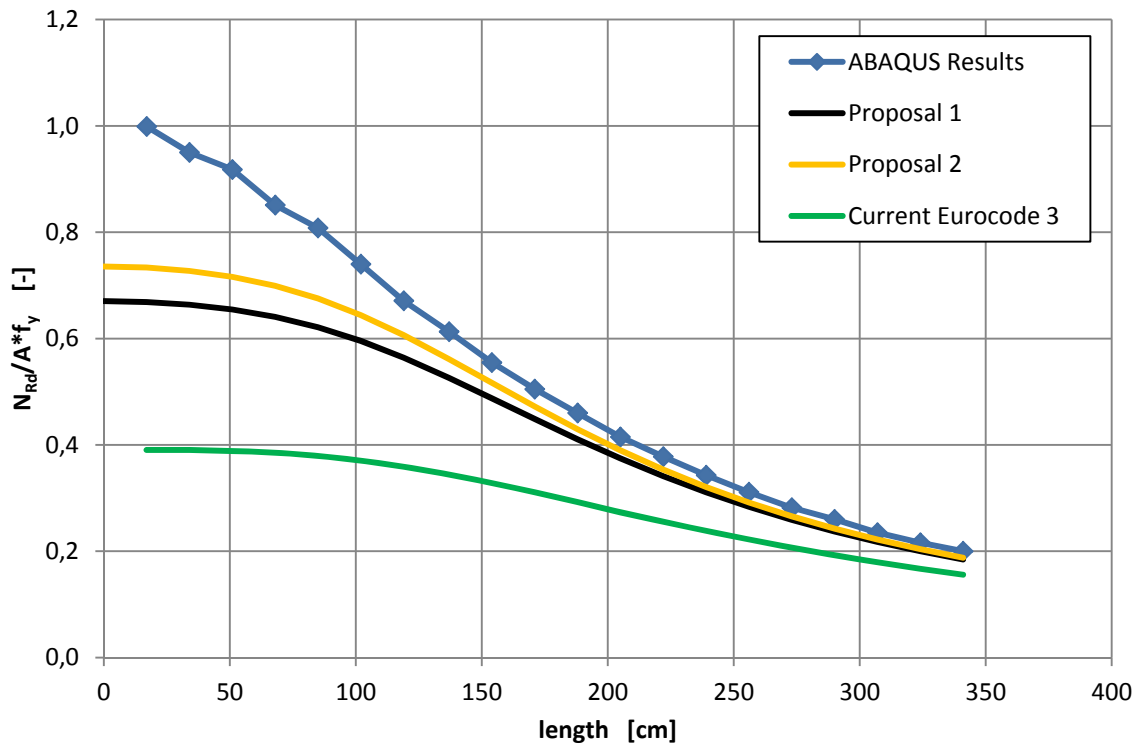


Figure 74: IPE 500-t - proposal 2 compared to proposal 1

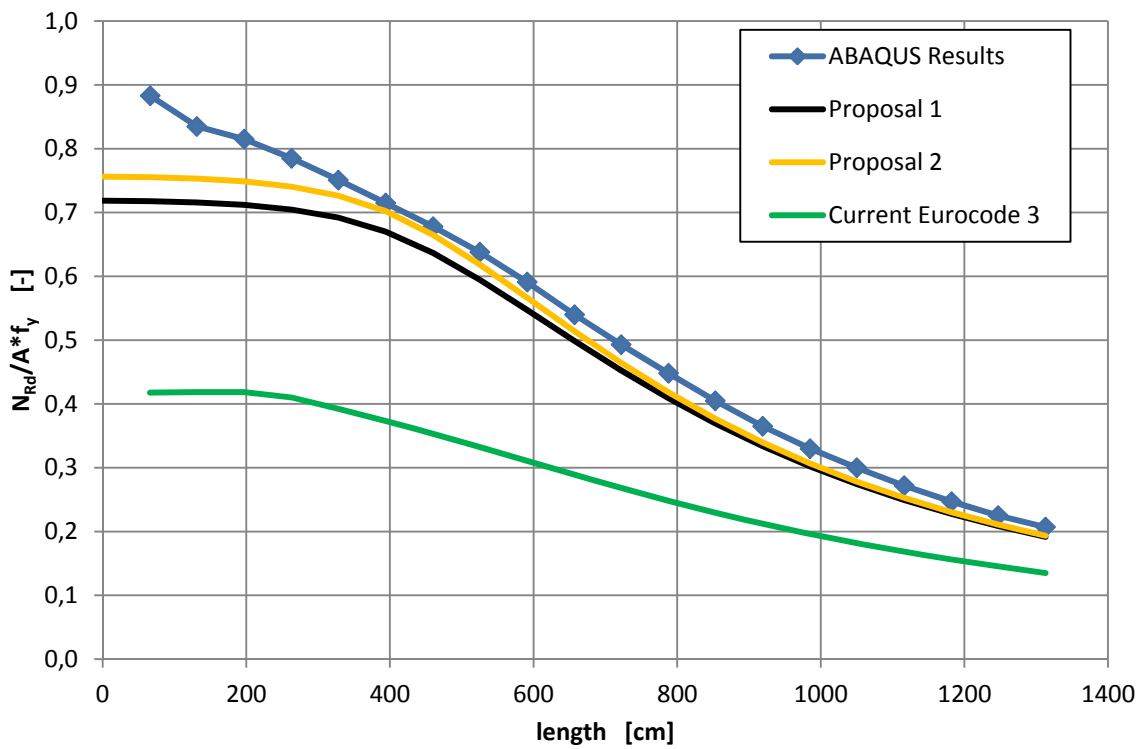


Figure 75: IPE 500-w - proposal 2 compared to proposal 1

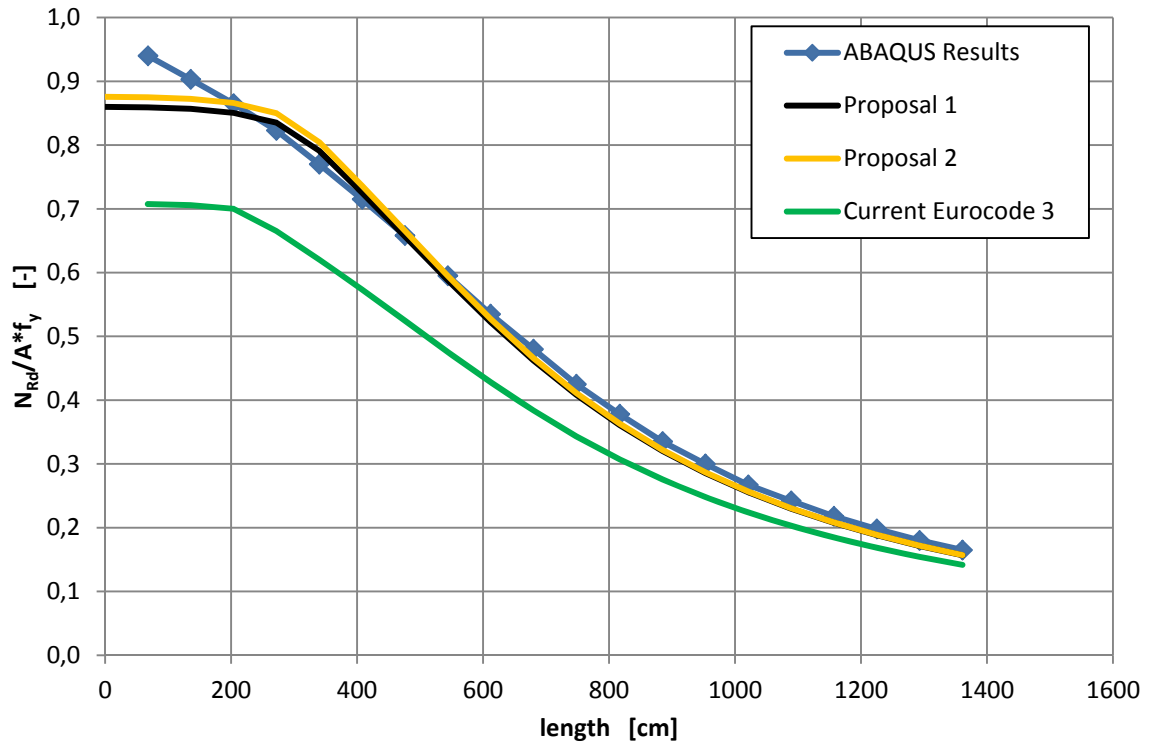


Figure 76: HE-A 500 - proposal 2 compared to proposal 1

7.3 Proposal 3

When looking at the previous results for the standard IPE sections for “Proposal 2”, it was clear that for the shorter members of each section, the margin of safety was still very high. This looked very similar to the problem investigated in chapter 5 “Buckling Strength of Class 2 Sections”. It was decided that, as the problems looked very similar, the improvements found for class 2 sections could possibly be implemented in class 4 sections.

N.B. only $N_{R,TF}$ and χ_{TF} are modified the rest is the same as proposal 1.

This meant going back to the effective sectional properties and using the equation from chapter 5 “Buckling Strength of Class 2 Sections”.

$$\Phi_{TF} = 0.5[1 + 0.49(\bar{\lambda}_z - 0.2) + \bar{\lambda}_{TF}^2]$$

$$\chi_{TF} = \frac{1}{\Phi_{TF} + \sqrt{\Phi_{TF}^2 - \bar{\lambda}_{TF}^2}}$$

N.B. $\bar{\lambda}_z$ is used instead of $\bar{\lambda}_{TF}$

As an example the IPE 500 with a length of 364cm was calculated.

$$\bar{\lambda}_y = \sqrt{\frac{A_{\text{eff}} * f_y}{N_{\text{cr},y}}} = \sqrt{\frac{52.85 * 23.5}{5104.4}} = 0.4933$$

$$\Phi_y = 0.5[1 + \alpha_y(\bar{\lambda}_y - 0.2) + \bar{\lambda}_y^2] = 0.5[1 + 0.49(0.4933 - 0.2) + 0.4933^2]$$

$$\Phi_y = 0.6935$$

$$\chi_y = \frac{1}{\Phi_y + \sqrt{\Phi_y^2 - \bar{\lambda}_y^2}} = \frac{1}{0.6935 + \sqrt{0.6935^2 - 0.4933^2}} = 0.8468 \leq 1.0 \quad (= \text{prop. 1})$$

$$\bar{\lambda}_z = \sqrt{\frac{A_{\text{eff}} * f_y}{N_{\text{cr},z}}} = \sqrt{\frac{52.85 * 23.5}{1673.8}} = 0.8614$$

$$\bar{\lambda}_{TF} = \sqrt{\frac{A_{\text{eff}} * f_y}{N_{\text{cr},TF}}} = \sqrt{\frac{52,85 * 23.5}{1419.7}} = 0.93532$$

$$\Phi_{TF} = 0.5[1 + \alpha_z(\bar{\lambda}_z - 0.2) + \bar{\lambda}_{TF}^2] = 0.5[1 + 0.49(0.8614 - 0.2) + 0.93532^2]$$

$$\Phi_{TF} = 1.0994$$

$$\chi_{TF} = \frac{1}{\Phi_{TF} + \sqrt{\Phi_{TF}^2 - \bar{\lambda}_{TF}^2}} \leq 1.0$$

$$\chi_{TF} = \frac{1}{1.0994 + \sqrt{1.0994^2 - 0.93532^2}} = 0.59617 \leq 1.0$$

The buckling resistances for the y-y axis were then calculated. Here the effective area was used to obtain the resistance.

$$N_{Ed} = \chi * A_{\text{eff}} * f_y$$

$$N_{R,y} = 0.8468 * 52.85 * 23.5 = 1051.7 \text{ kN}$$

$$N_{R,TF} = 0.59617 * 52.85 * 23.5 = 740,50 \text{ kN}$$

Here again, the torsional-flexural failure was the definitive value with 740.50 kN. This value was divided by the gross section resistance.

$$\frac{N_{R,TF}}{A * f_y} = \frac{740.50}{57.8 * 23.5} = 0.5452$$

Where A was the gross area of the section.

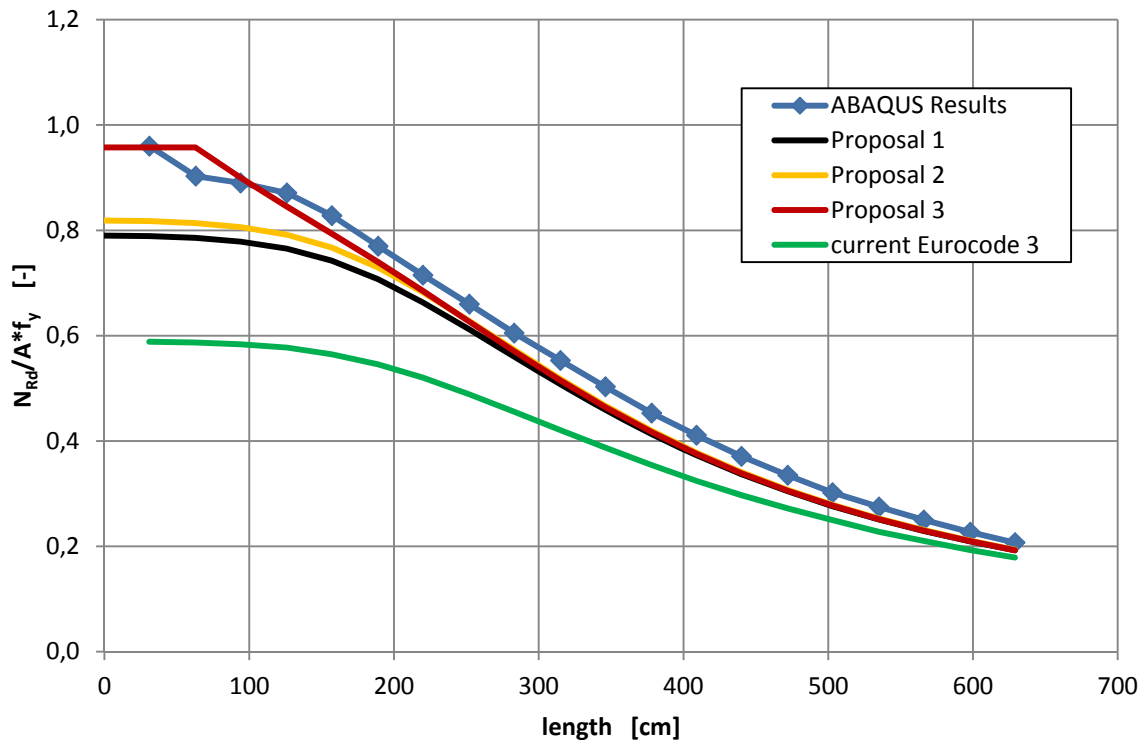


Figure 77: IPE 300 - proposal 3 and comparison

The results from “Proposal 2” were plotted alongside the new results for “Proposal 3”.

The effect that was wanted was also achieved for the IPE 300. Figure 77 shows the gap between the finite element calculations and the suggested resistance function narrowed for the less slender members. This was the first proposal where the results for an IPE section were on the unsafe side. This phenomenon needed to be checked on the other sections.

7 Development and verification of alternative design proposals for Class 4 sections

As assumed, this was the case for all of the standard IPE sections (Figure 78 to Figure 80). The earlier values are much better than those predicted by “Proposal 2” however they do go onto the unsafe side.

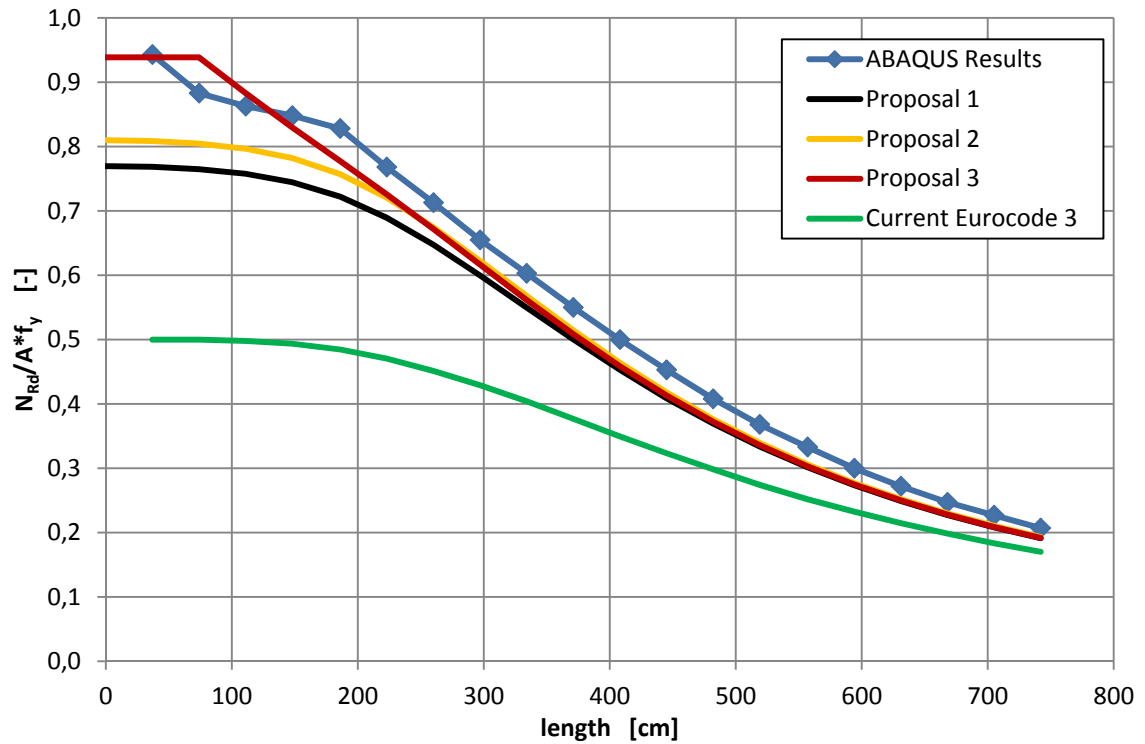


Figure 78: IPE 400 - proposal 3 and comparison

7 Development and verification of alternative design proposals for Class 4 sections

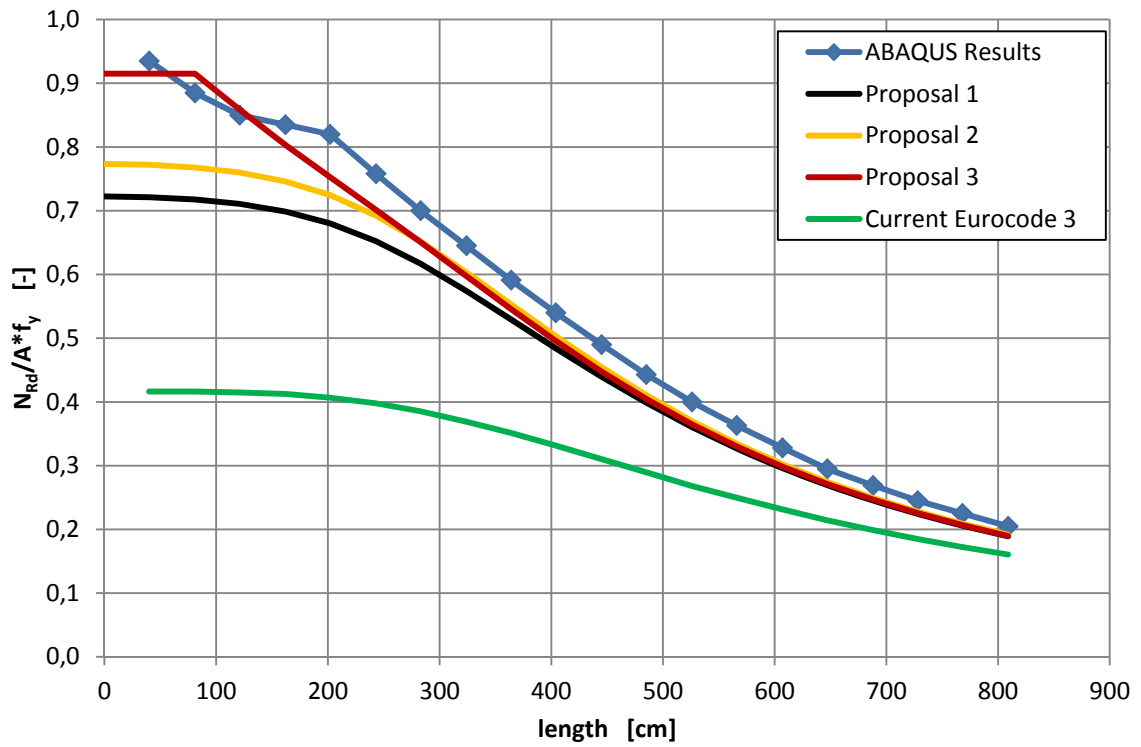


Figure 79: IPE 500 - proposal 3 and comparison

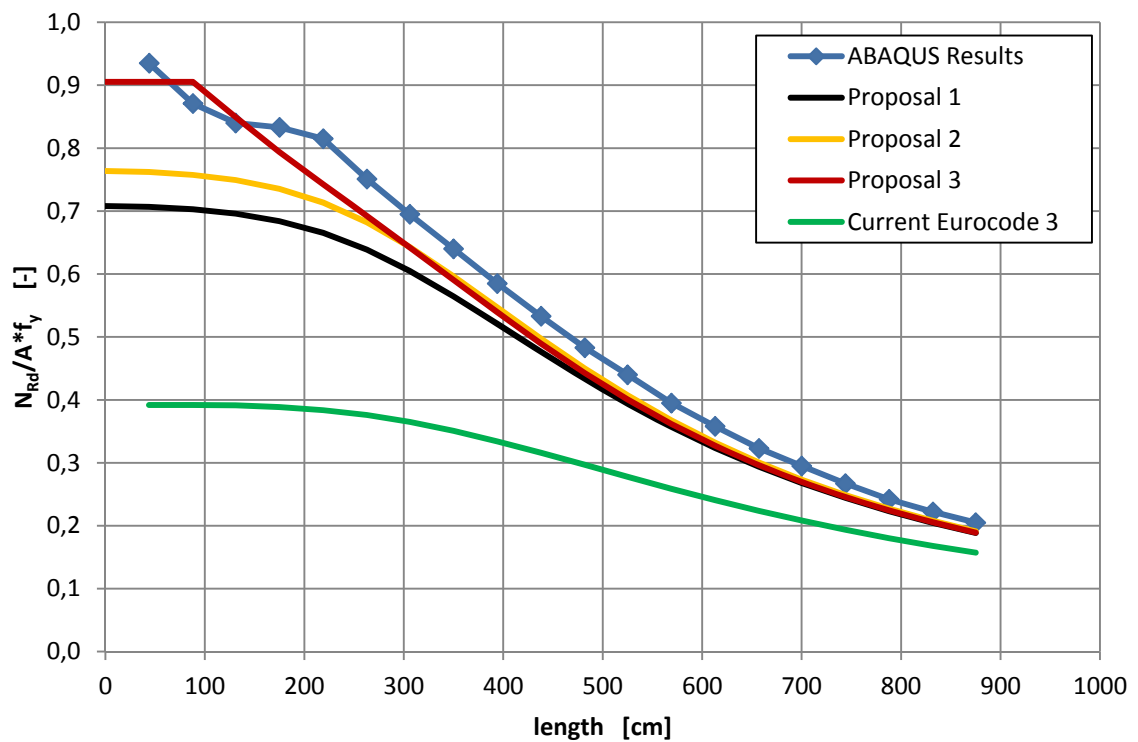


Figure 80: IPE 600 - proposal 3 and comparison

It can also be seen in Figure 81, that the new proposal brought advantages for the dimensioning of IPE 500-t. The difference between the resistance curve and the finite element results was more than halved for the shorter members using the third proposal instead of the second.

For the IPE 500-w the results were slightly “un-conservative” for the shorter members (Figure 82). This discrepancy may well be covered after further investigations into the residual stress. It looks, however as if this may be a discrepancy in the way the effective section is defined in EC 1993-1-1(see proposal 4).

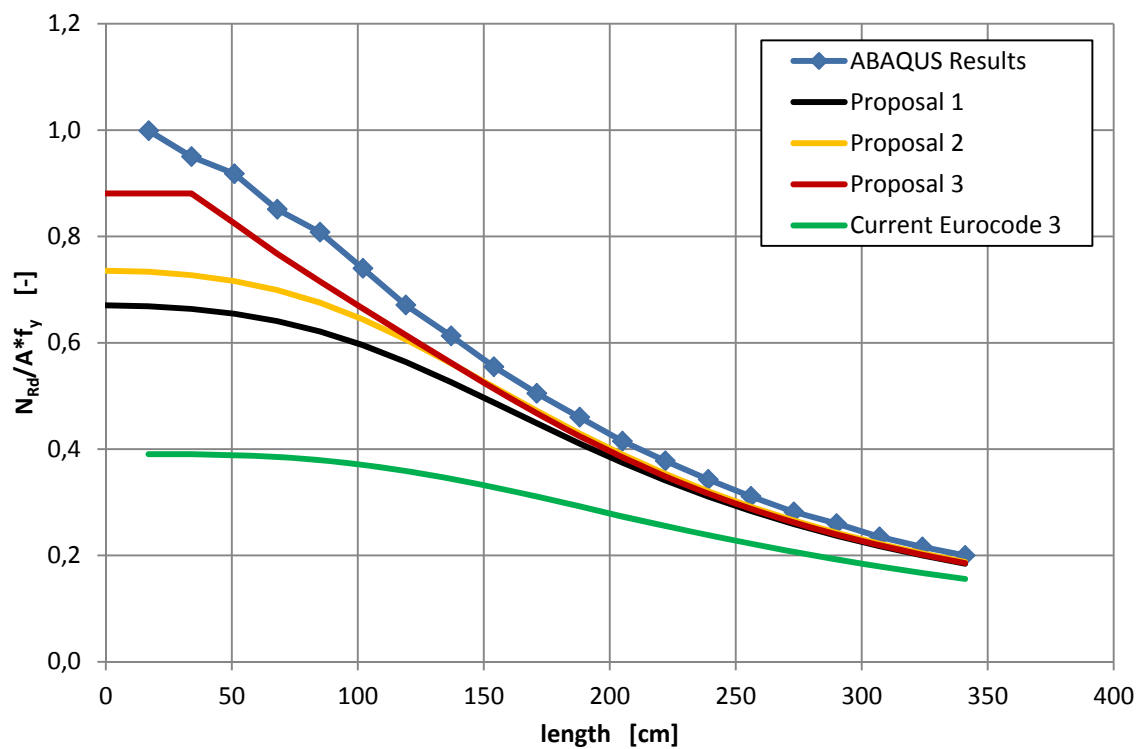


Figure 81: IPE 500-t - proposal 3 and comparison

7 Development and verification of alternative design proposals for Class 4 sections

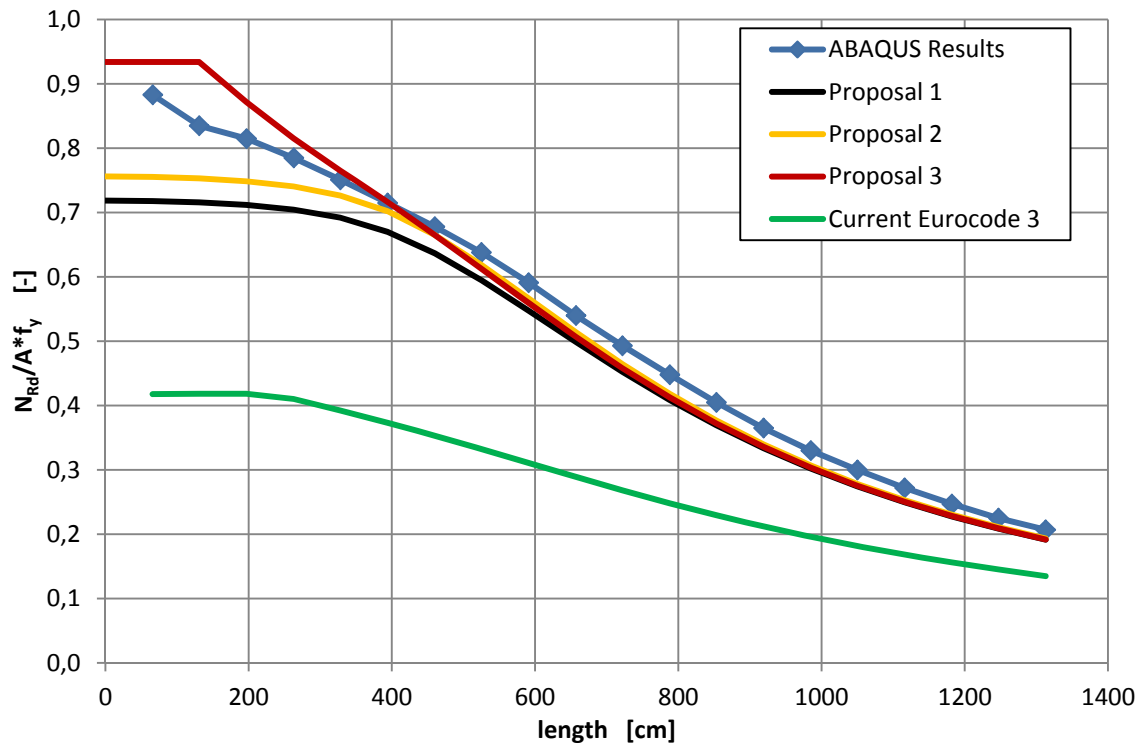


Figure 82: IPE 500-w - proposal 3 and comparison

This just left the HE-A 500. The new proposal had achieved more accurate results for the very short members however these values were not on the safe side. They were not conservative.

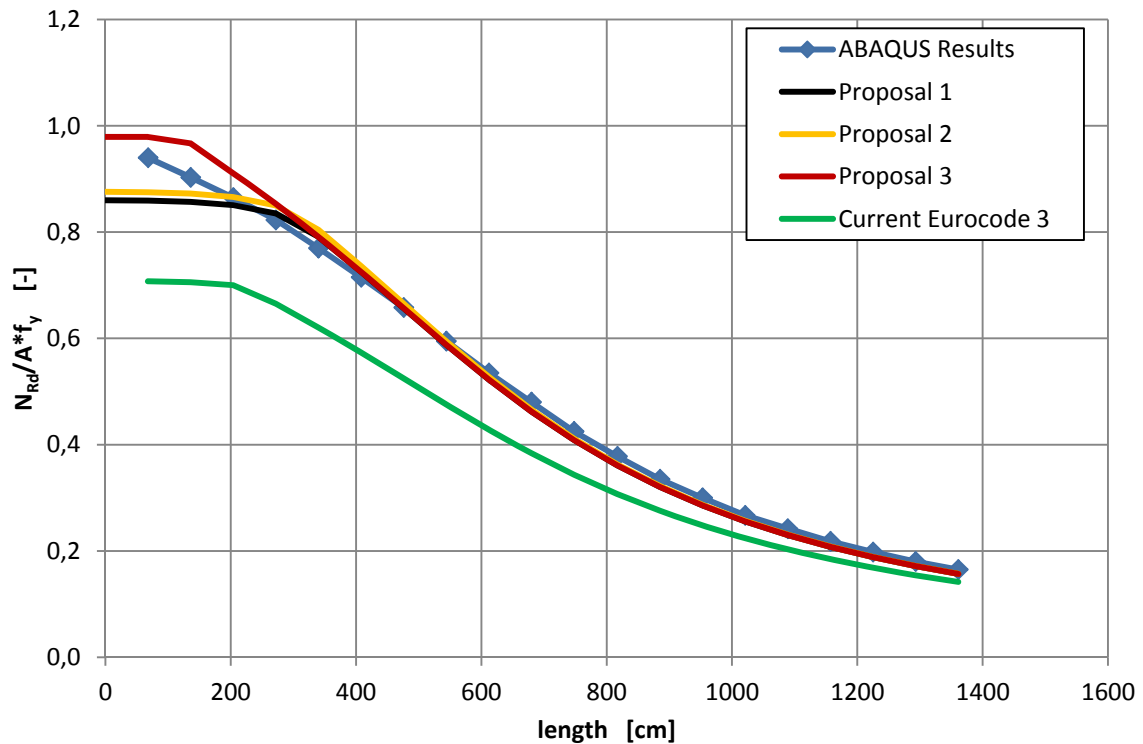


Figure 83: HE-A 500 - proposal 3 and comparison

“Proposal 3” describes the real results for the longer members very accurately and safely. The one down side to this proposal is that for the short lengths it does go onto the unsafe side.

The difference between the Eurocode 3 dimensioning and that of “proposal 3” is huge. If the T-sections were to be dimensioned using the proposed rule instead of the current rule it would mean that an IPE 500 with a length of 400 cm could resist a force up to 40% larger than that the results calculated using Eurocode 3.

As the starting resistance was sometimes over the ABAQUS values, it implied that the effective area used to calculate the results was over estimated. Therefore another proposal was made with a reduced value for the effective area.

7.4 Proposal 4

It was considered that the eccentricity of the axial force may well have some noticeable effects, however not in the form stated in the Eurocode Austrian annex[10], that was previously investigated.

$$\frac{N_{Ed}}{\chi_{TF} * A_{eff} * f_y} + k_{LT} \frac{N_{Ed} * e_N}{\chi_{LT(s)} * M_{y,Rk(s)}} \leq 1$$

If the effects of buckling are ignored ($\lambda \ll$) one gets the ultimate capacity. The following formula adapted from Eurocode 3 to find the capacity was considered:

$$\frac{N_{Ed}}{A_{eff} * f_y} + \frac{N_{Ed} * e_N}{W_{y,eff} * f_y} = 1$$

$$\frac{1}{N_{Ed}} = \frac{1}{A_{eff} * f_y} + \frac{e_N}{W_{y,eff} * f_y}$$

$$\frac{1}{N_{Ed}} = \frac{W_{y,eff} * f_y + A_{eff} * f_y * e_N}{A_{eff} * f_y * W_{y,eff} * f_y}$$

$$\frac{1}{N_{Ed}} = \frac{W_{y,eff} + A_{eff} * e_N}{A_{eff} * W_{y,eff} * f_y}$$

$$N_{Ed} = N_{Rd} = \frac{A_{eff} * W_{y,eff} * f_y}{W_{y,eff} + A_{eff} * e_N} = A_{eff}^* * f_y$$

N_{Rd} was then considered as $N_{Rd} = A_{eff}^* * f_y$, where A_{eff}^* was a new effective area, that would be used to calculate the new proposed values. This new effective area was calculated like this:

$$A_{eff}^* = \frac{A_{eff} * W_{y,eff}}{W_{y,eff} + A_{eff} * e_N}$$

The reduction factor was then calculated in exactly the same way as in “proposal 3” however A_{eff}^* replaced A_{eff} .

N.B. In this thesis the effective values for A_{eff} and $W_{y,eff}$ are obtained using the more exact effective width method from EC 3, part 1.5 described in chapter 3.5 “Defining the effective sections used in this thesis”.

As an example the IPE 500 with a length of 364cm was calculated.

$A_{eff} = 52.9$, $W_{eff} = 113.1$, $e_N = 1.54$ all the other values are the same as in proposal 3

$$A_{eff}^* = \frac{A_{eff} * W_{eff}}{W_{eff} + A_{eff} * e_N} = \frac{52.9 * 113.1}{113.1 + 52.9 * 1.54} = 30.75 \text{ cm}^2$$

$$\bar{\lambda}_y = \sqrt{\frac{A_{eff}^* * f_y}{N_{cr,y}}} = \sqrt{\frac{30.75 * 23.5}{5104.4}} = 0.3763$$

$$\Phi_y = 0.5[1 + \alpha_y(\bar{\lambda}_y - 0.2) + \bar{\lambda}_y^2] = 0.5[1 + 0.49(0.3763 - 0.2) + 0.3763^2]$$

$$\Phi_y = 0.6140$$

$$\chi_y = \frac{1}{\Phi_y + \sqrt{\Phi_y^2 - \bar{\lambda}_y^2}} = \frac{1}{0.6140 + \sqrt{0.6140^2 - 0.3763^2}} = 0.9098 \leq 1.0 \quad (= \text{prop. 1})$$

$$\bar{\lambda}_z = \sqrt{\frac{A_{eff}^* * f_y}{N_{cr,z}}} = \sqrt{\frac{30.75 * 23.5}{1673.8}} = 0.6571$$

$$\bar{\lambda}_{TF} = \sqrt{\frac{A_{eff}^* * f_y}{N_{cr,TF}}} = \sqrt{\frac{30.75 * 23.5}{1419.7}} = 0.7134$$

$$\Phi_{TF} = 0.5[1 + \alpha_z(\bar{\lambda}_z - 0.2) + \bar{\lambda}_{TF}^2] = 0.5[1 + 0.49(0.6571 - 0.2) + 0.7134^2]$$

$$\Phi_{TF} = 0.8665$$

$$\chi_{TF} = \frac{1}{\Phi_{TF} + \sqrt{\Phi_{TF}^2 - \bar{\lambda}_{TF}^2}} \leq 1.0$$

$$\chi_{TF} = \frac{1}{0.8665 + \sqrt{0.8665^2 - 0.7134^2}} = 0.7363 \leq 1.0$$

The buckling resistances for the y-y axis were then calculated. Here the effective area was used to obtain the resistance.

$$N_{Ed} = \chi * A_{eff}^* * f_y$$

$$N_{R,y} = 0.9098 * 30.75 * 23.5 = 657.4 \text{ kN}$$

$$N_{R,TF} = 0.7363 * 30.75 * 23.5 = 532.03 \text{ kN}$$

Here again, the torsional-flexural failure was the definitive value with 532.03 kN. This value was divided by the gross section resistance.

$$\frac{N_{R,TF}}{A * f_y} = \frac{532.03}{57.8 * 23.5} = 0.392$$

Where A was the gross area of the section.

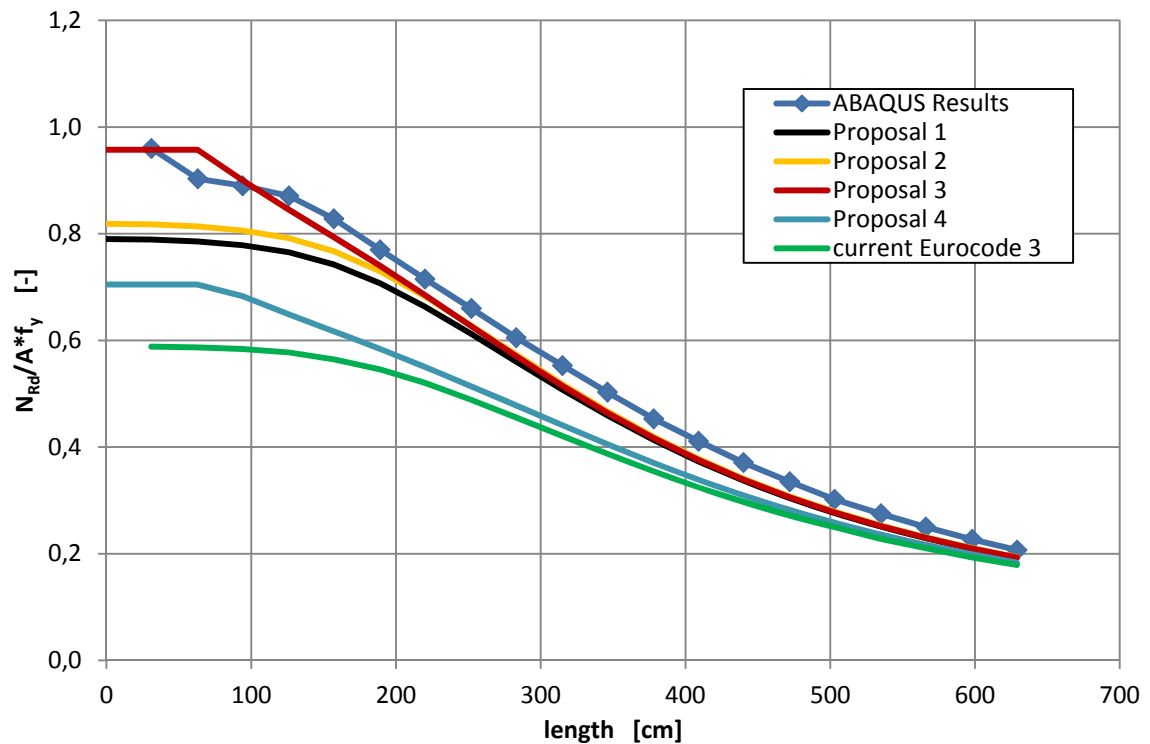


Figure 84: IPE 300 - proposal 4

7 Development and verification of alternative design proposals for Class 4 sections

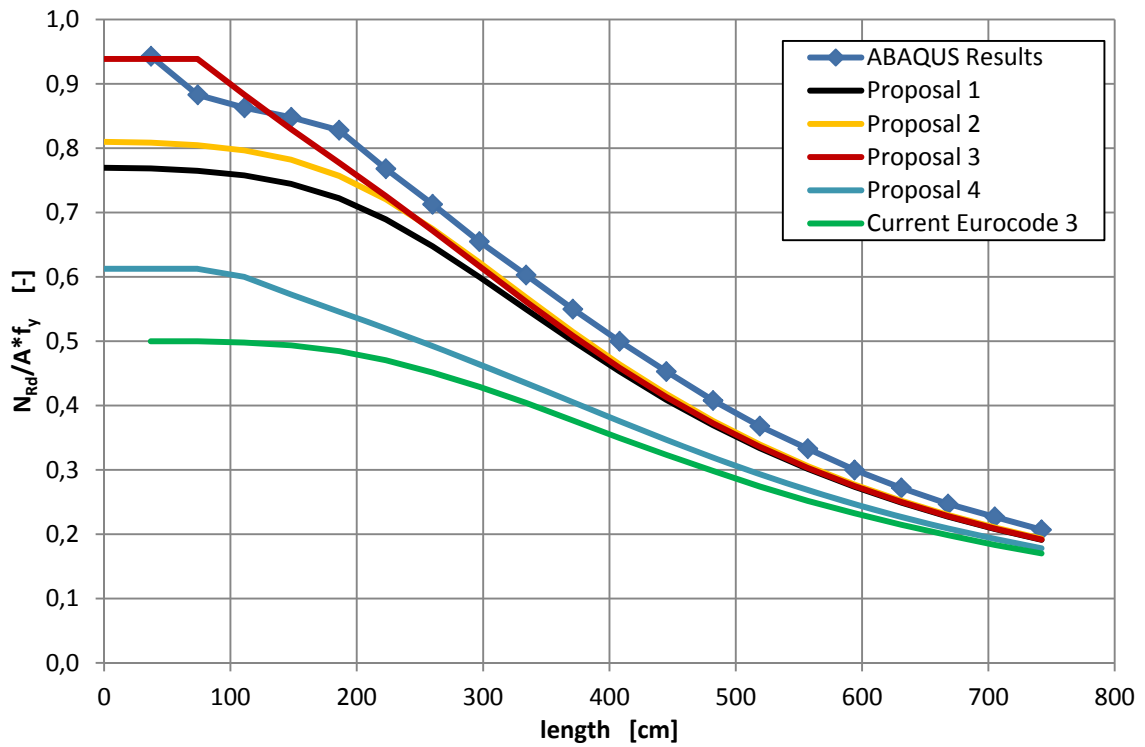


Figure 85: IPE 400 - proposal 4

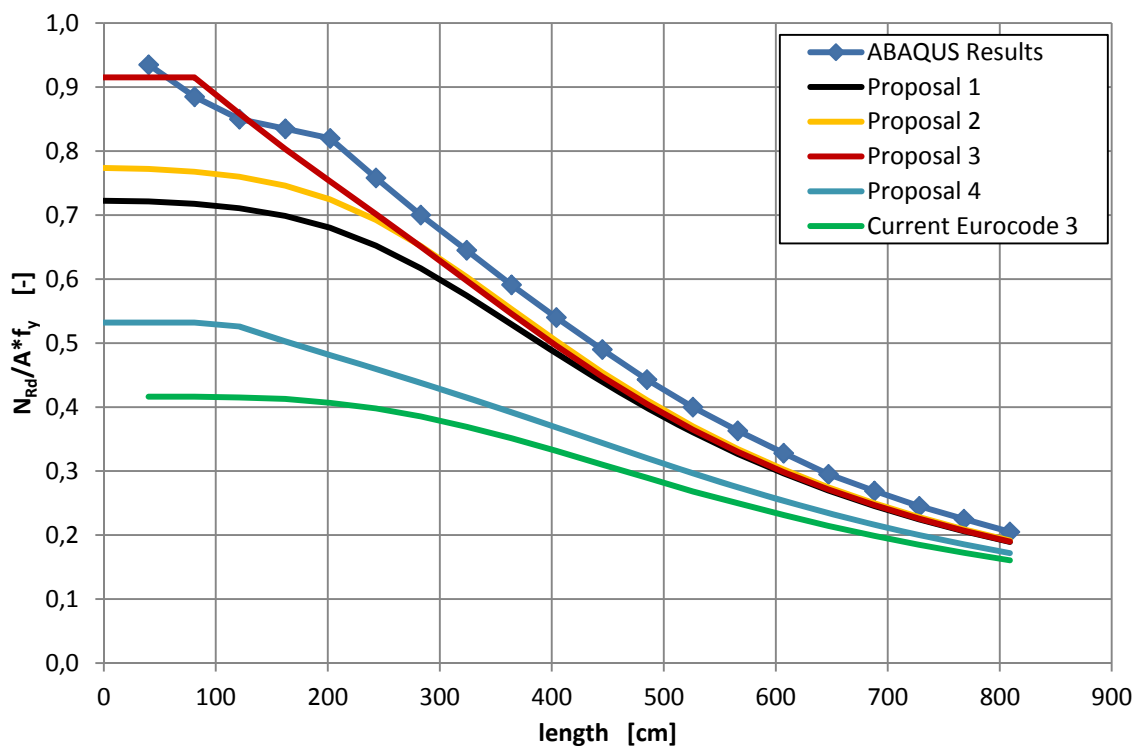


Figure 86: IPE 500 - proposal 4

7 Development and verification of alternative design proposals for Class 4 sections

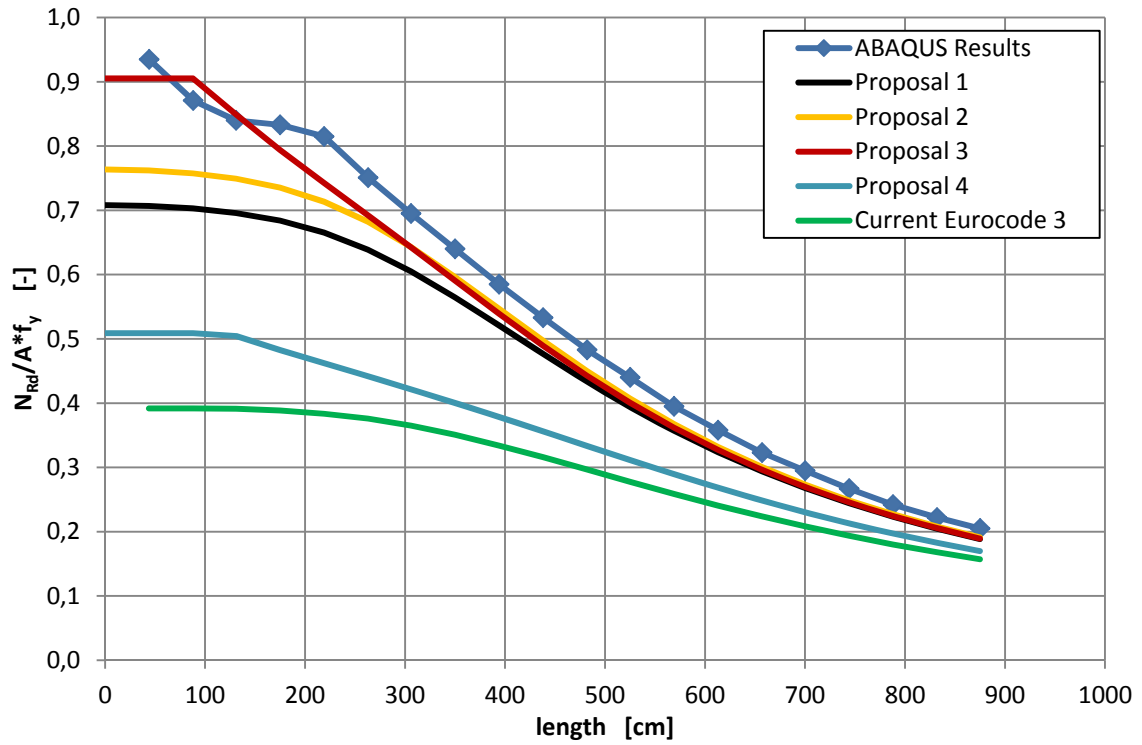


Figure 87: IPE 600 - proposal 4

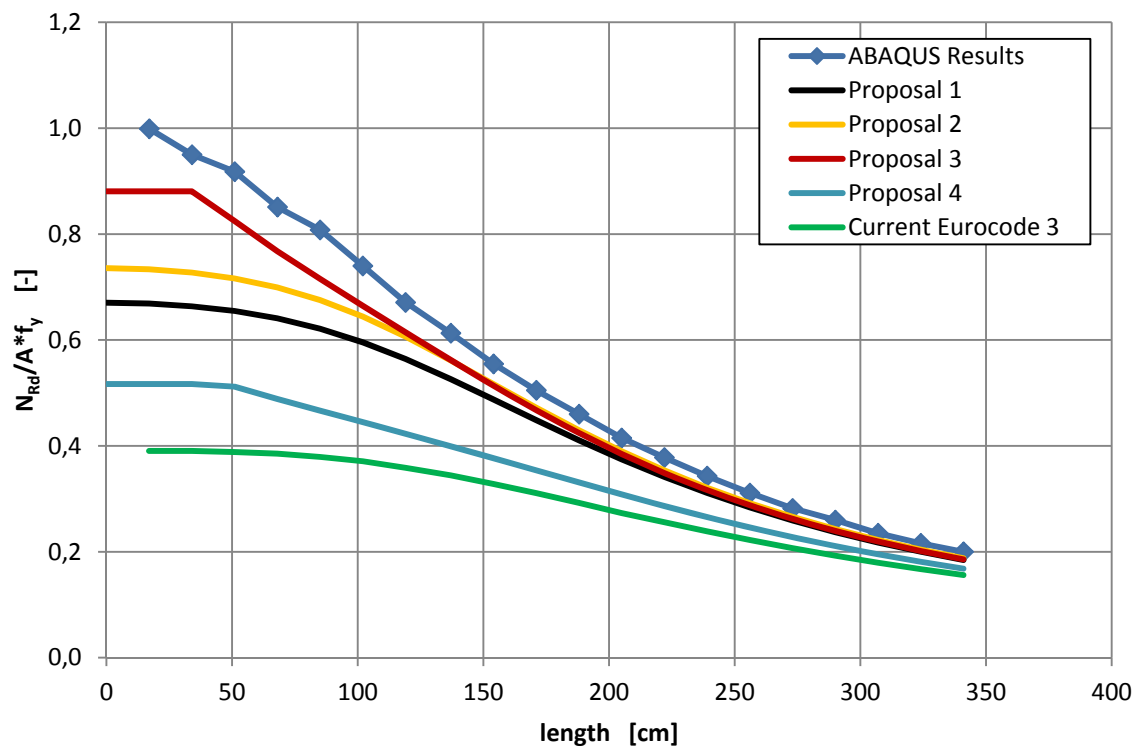


Figure 88: IPE 500-t - proposal 4

7 Development and verification of alternative design proposals for Class 4 sections

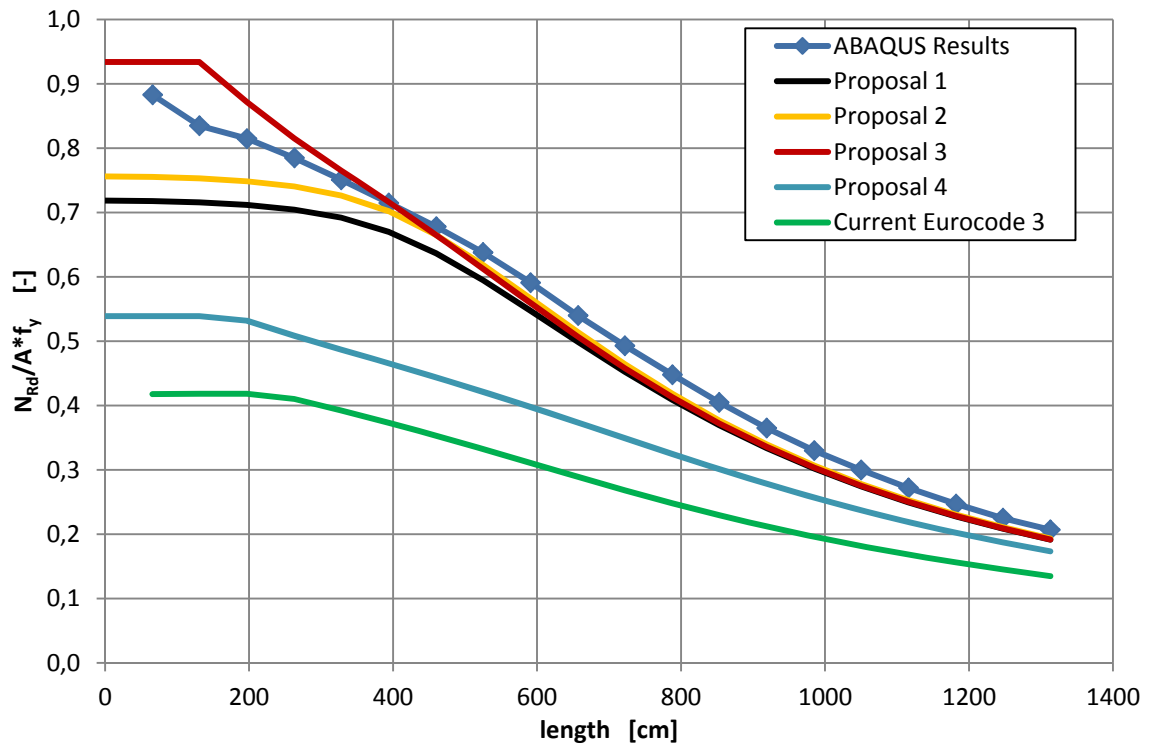


Figure 89: IPE 500-w - proposal 4

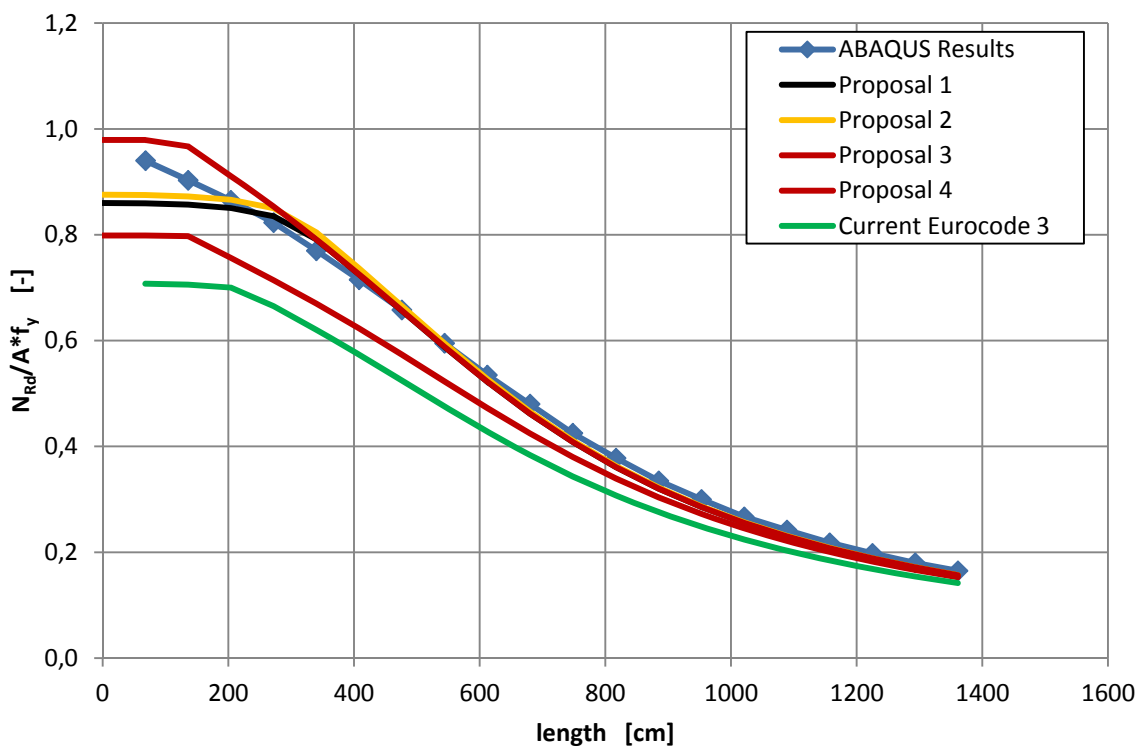


Figure 90: HE-A 500 - proposal 4

7 Development and verification of alternative design proposals for Class 4 sections

As we can see in these results, proposal 4 is very conservative. It makes more use of the available section compared to the present Eurocode calculations however in comparison to proposal 3 it is extremely conservative.

8 Conclusion

This thesis has looked at the stability behaviour of slender T-sections - affected by local buckling - under an axial force. It looked at different methods provided by Eurocode 3 in order to define the effective section's properties. The methods were “effective widths” method described in part 1-5 of Eurocode 3 as well as “effective thicknesses” method described in part 1-3 of Eurocode 3.

Firstly it was confirmed that when considering an “outstand flange” (i.e. the web of the T-section) the stress maximum (yield strength) needed to be applied to the furthest point of the effective cross section and not to the gross section. This was not clearly specified in Eurocode 3, and so it was proved using a comparison between the two methods mentioned above.

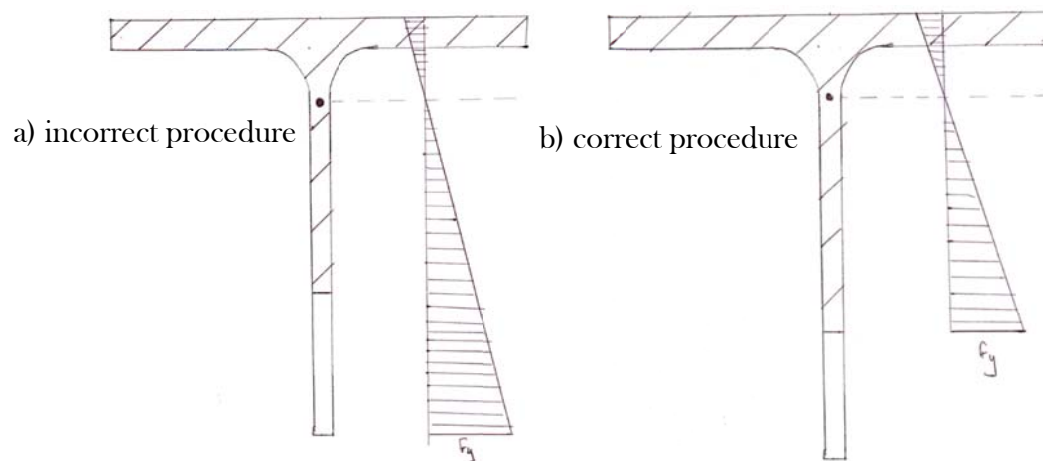


Figure 91 : Investigated distribution possibilities from Eurocode 3 part 1-5

A finite element model was produced that corresponded to reality taking into account the estimated residual stresses, both global and local imperfections as well as modelling the fillets as an appropriate beam element.

Class two sections were investigated to see the effects of torsional-flexural buckling and to see if any improvements were possible in this area. It was found that improvements could be made. It was then shown that the new proposals made by Taras et al corresponded to reality far better than the current Eurocode. Here, the slenderness of the member around the z-z axis is used to calculate the “generalized slenderness” component of the coefficient Φ_{TF} used to calculate the reduction factor χ_{TF} instead of the torsional-flexural slenderness.

$$\Phi_{TF} = 0.5[1 + \alpha_z(\bar{\lambda}_z - 0.2) + \bar{\lambda}_{TF}^2]$$

Thereby, $\alpha_z = 0.49$ for buckling curve c was found to be most appropriate to describe the buckling strength of T-sections with the residual stress patterns implied in the GMNIA calculations; however, if future experimental or numerical studies were to show more convenient residual stress distributions in actual T-sections, this coefficient and the resulting buckling curve could easily be adapted accordingly.

The main part of the thesis dealt with are slender class 4 sections. The Eurocode 3 buckling force resistances were then compared to the finite element results for class 4 sections. This showed indisputably, that the Eurocode is extremely conservative when calculating axially loaded T-sections because of the additional moment $\Delta M = N * e_N$ which must be considered, due to the shift of the centroids.

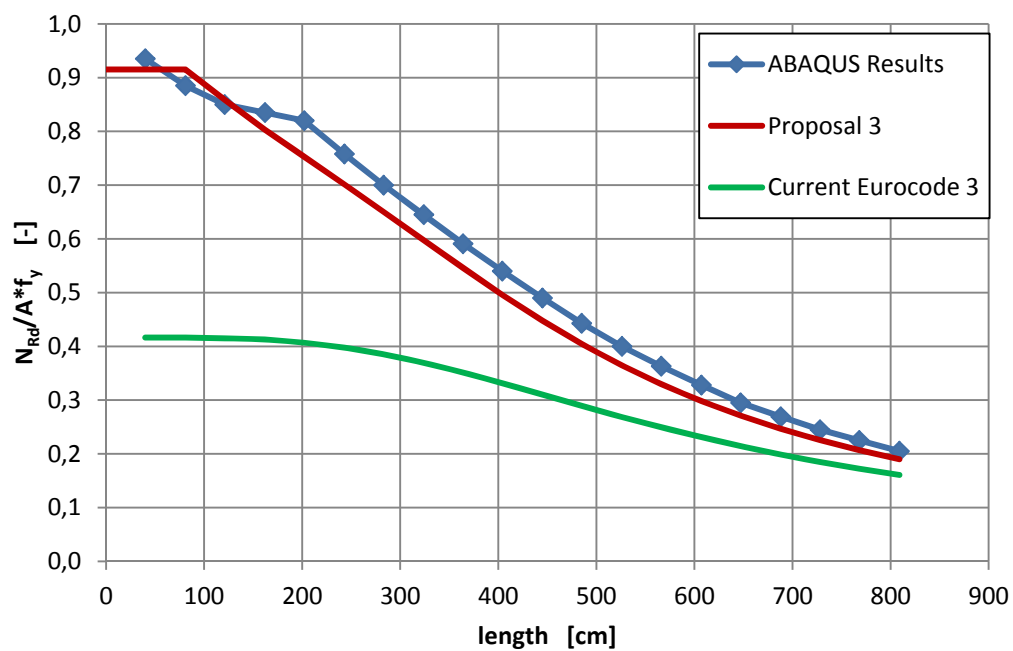


Figure 92: Comparison of the present Eurocode 3 and proposal for IPE 500 section

Proposals were then calculated ignoring the additional moment and compared to the finite element results. These comparisons were then evaluated and “proposal 3” was then seen as the most appropriate method. This involved using the slenderness of the member around the z-z axis to calculate the “generalized slenderness” component of the coefficient Φ_{TF} used to calculate the reduction factor χ_{TF} instead of the torsional-flexural slenderness. The wrongly predicted effects of the shift of centroid and lateral-torsional buckling were also removed.

$$\Phi_{TF} = 0.5[1 + \alpha_z(\bar{\lambda}_z - 0.2) + \bar{\lambda}_{TF}^2]$$

The criteria that should then be used for dimensioning class 4 T-sections are shown here.

$$\frac{N_{Ed}}{\chi_y * A_{eff} * f_y} \leq 1$$

$$\frac{N_{Ed}}{\chi_{TF} * A_{eff} * f_y} \leq 1$$

Although many questions have been answered in this thesis there are more questions that still need to be answered. These include:

- What is the exact residual stress distribution in a T-section?
- How do class 4 T-section sections behave when under the influence of a bending force?
- What is the behaviour when being bent and axially loaded?
- How do other mono-symmetrical class 4 sections behave, such as C shaped beams?
- How should the effective cross section be defined?

End

Appendix A. Results - reduction factor against torsional-flexural slenderness

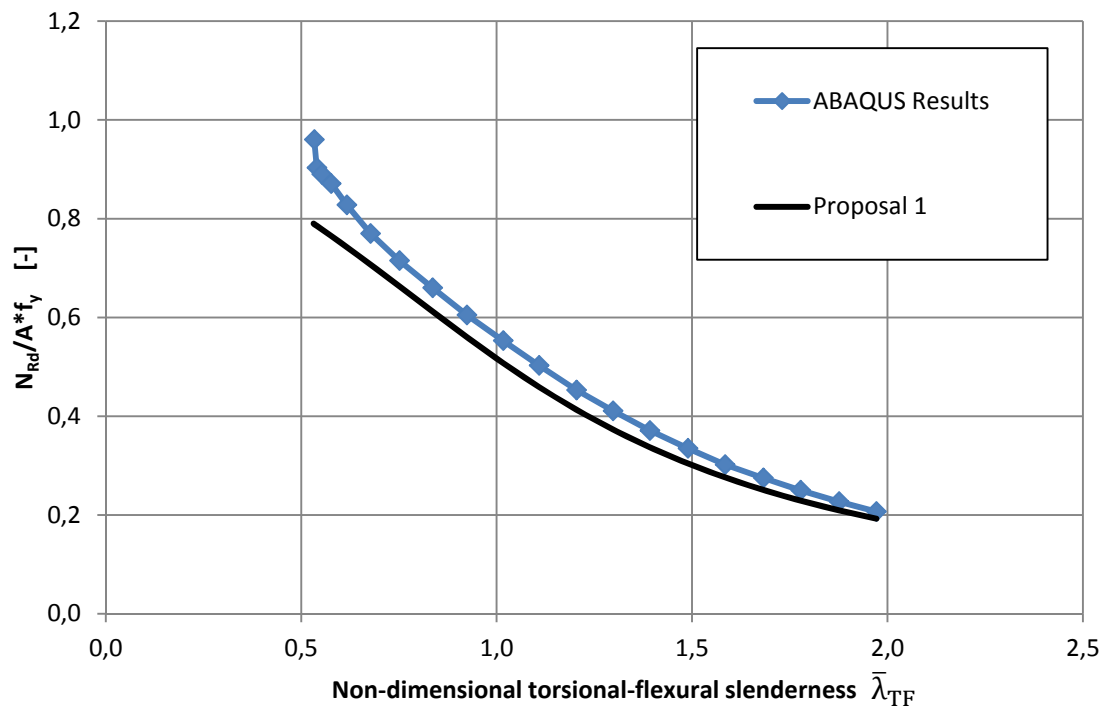


Figure 93: IPE 300 proposal 1

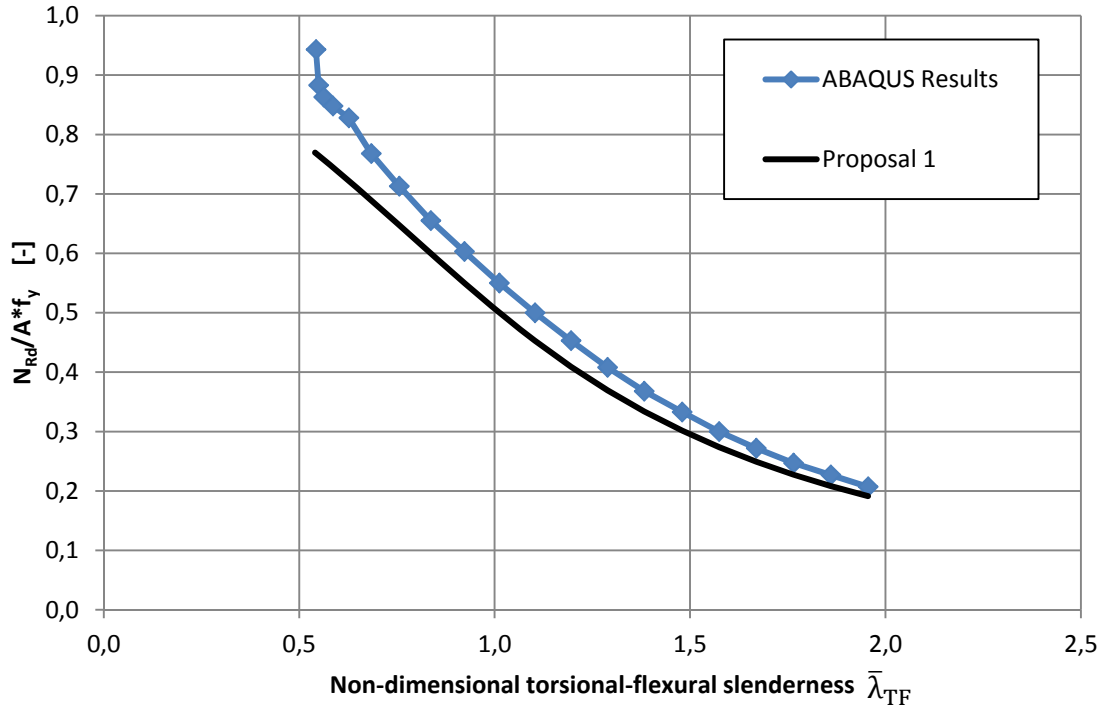


Figure 94: IPE 400 proposal 1

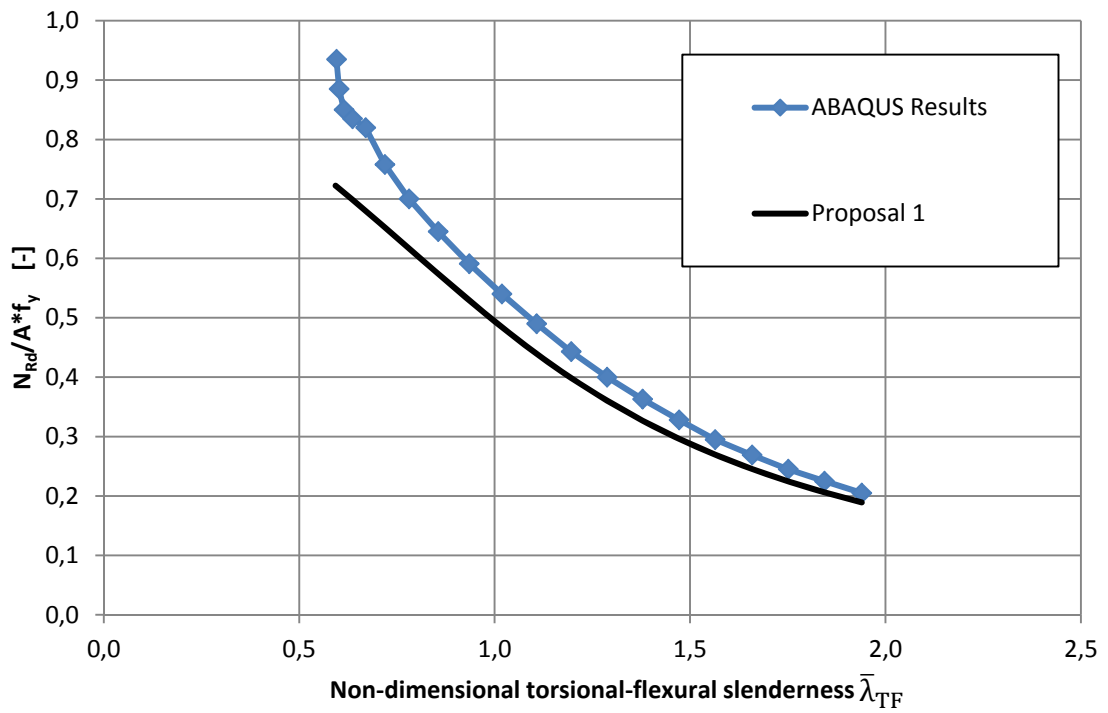


Figure 95: IPE 500 proposal 1

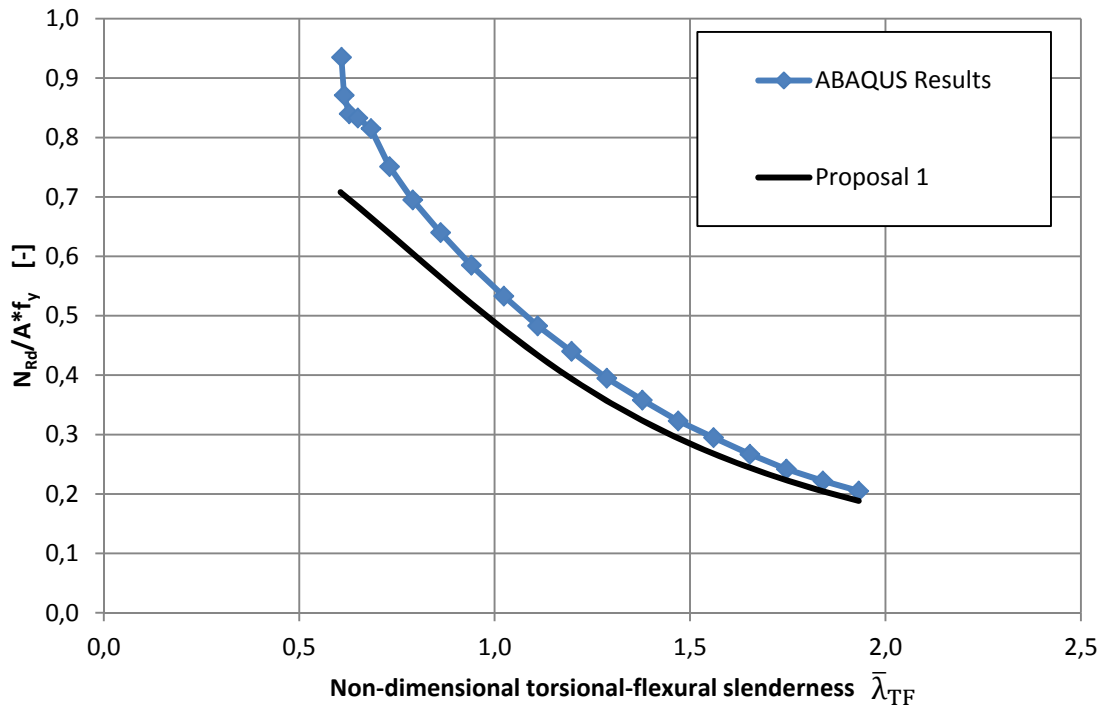


Figure 96: IPE 600 proposal 1

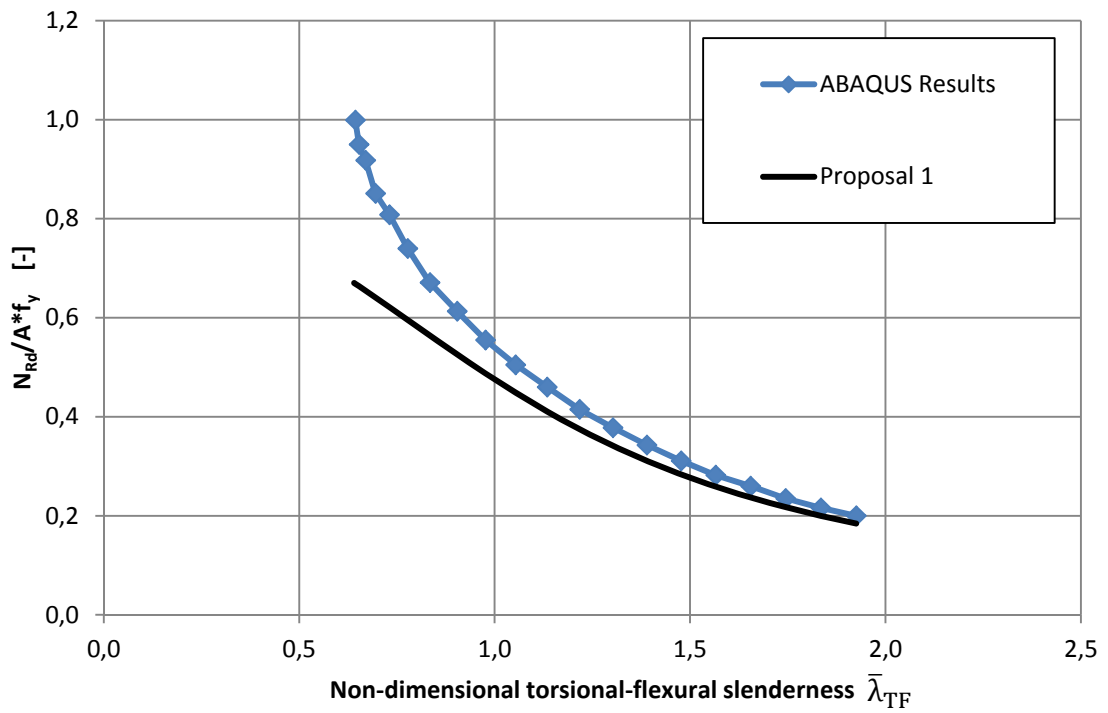


Figure 97: IPE 500-t proposal 1

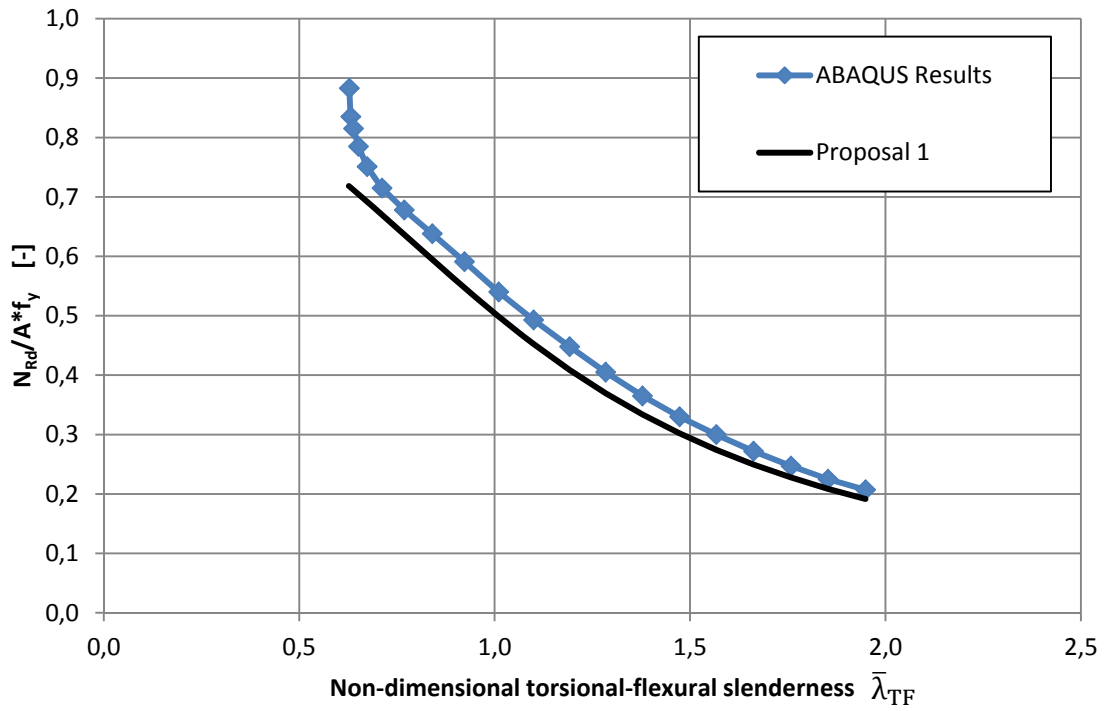


Figure 98: IPE 500-w proposal 1

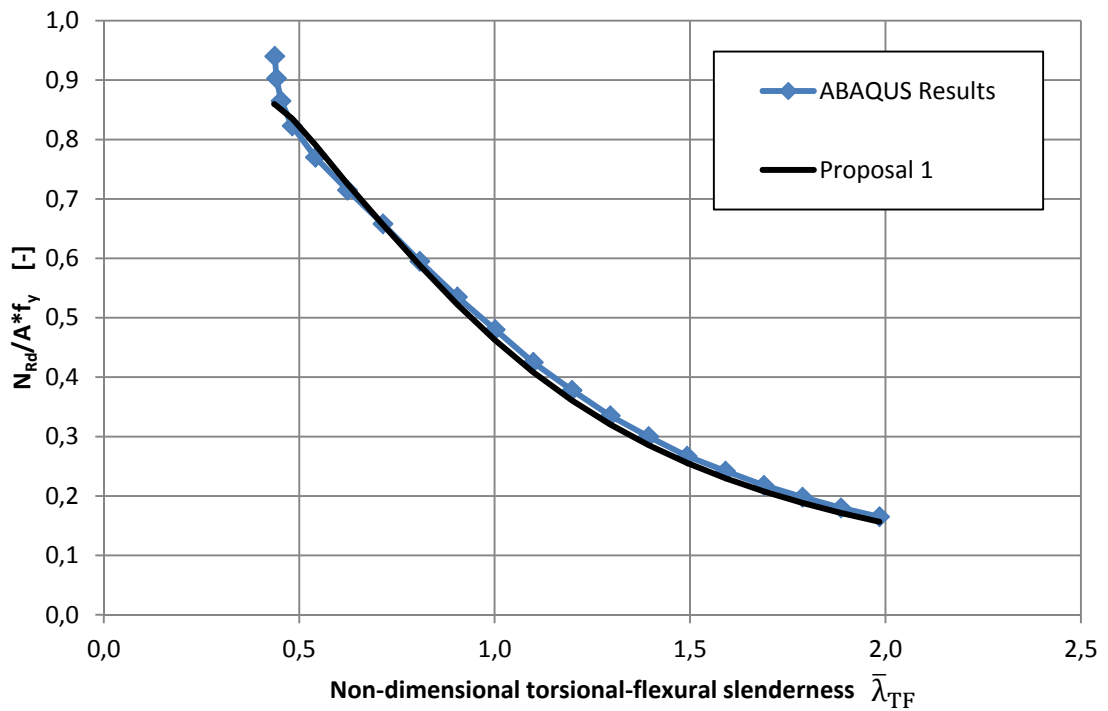


Figure 99: HE-A 500 proposal 1

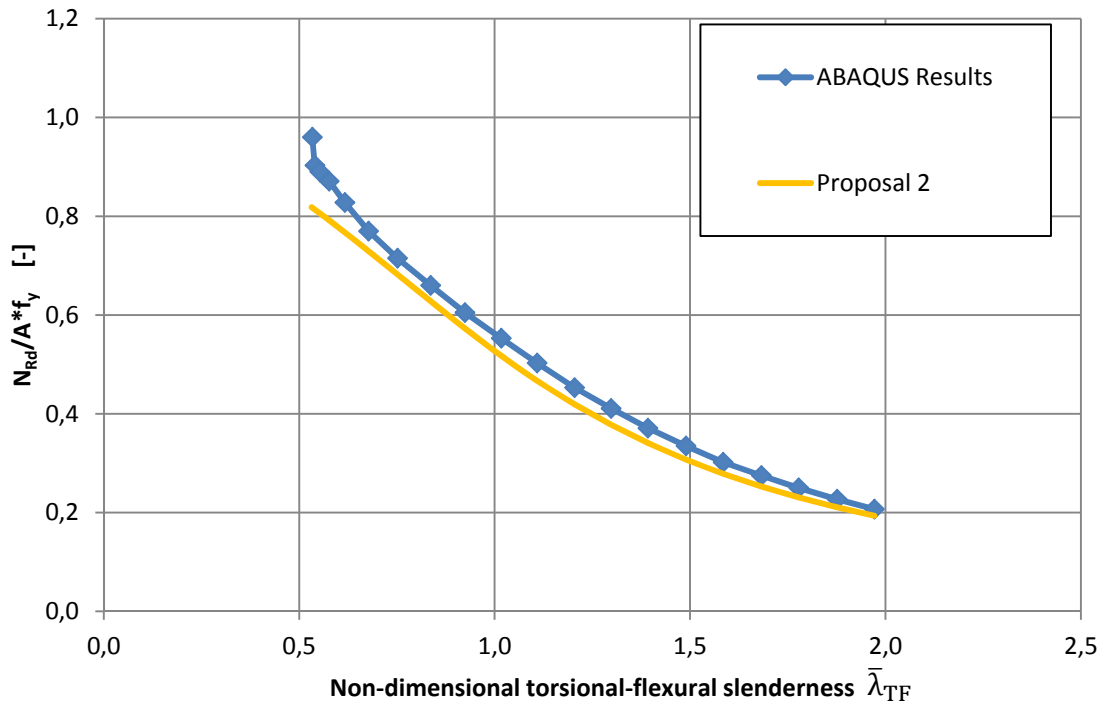


Figure 100: IPE 300 proposal 2

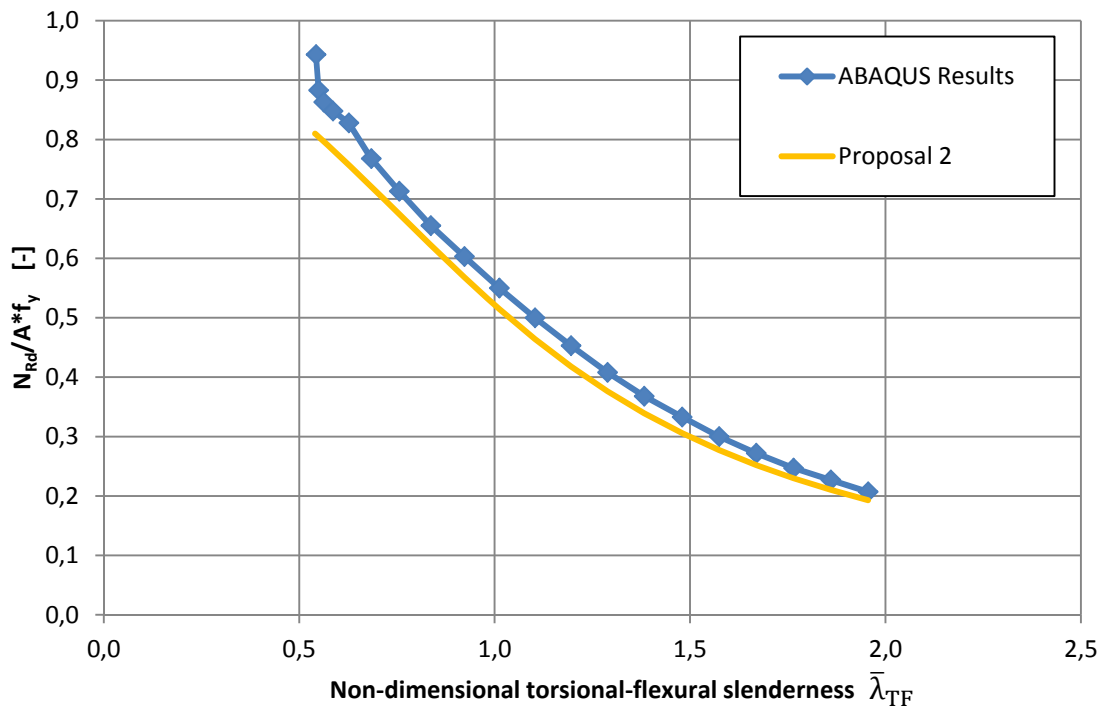


Figure 101: IPE 400 proposal 2

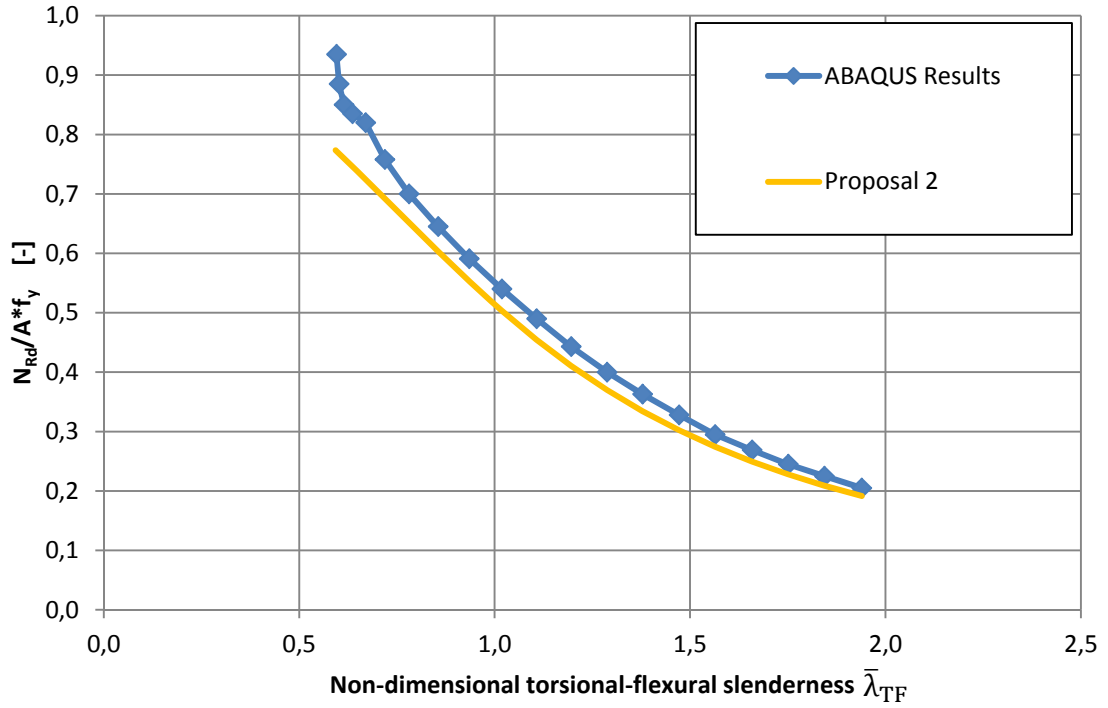


Figure 102: IPE 500 proposal 2

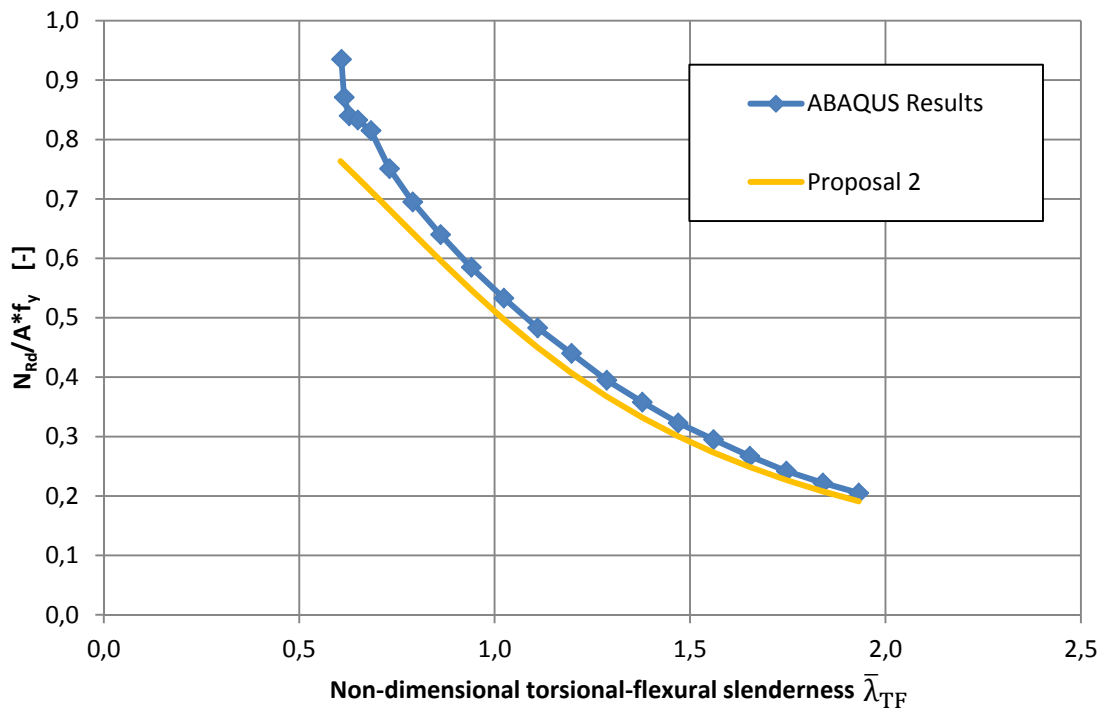


Figure 103: IPE 600 proposal 2

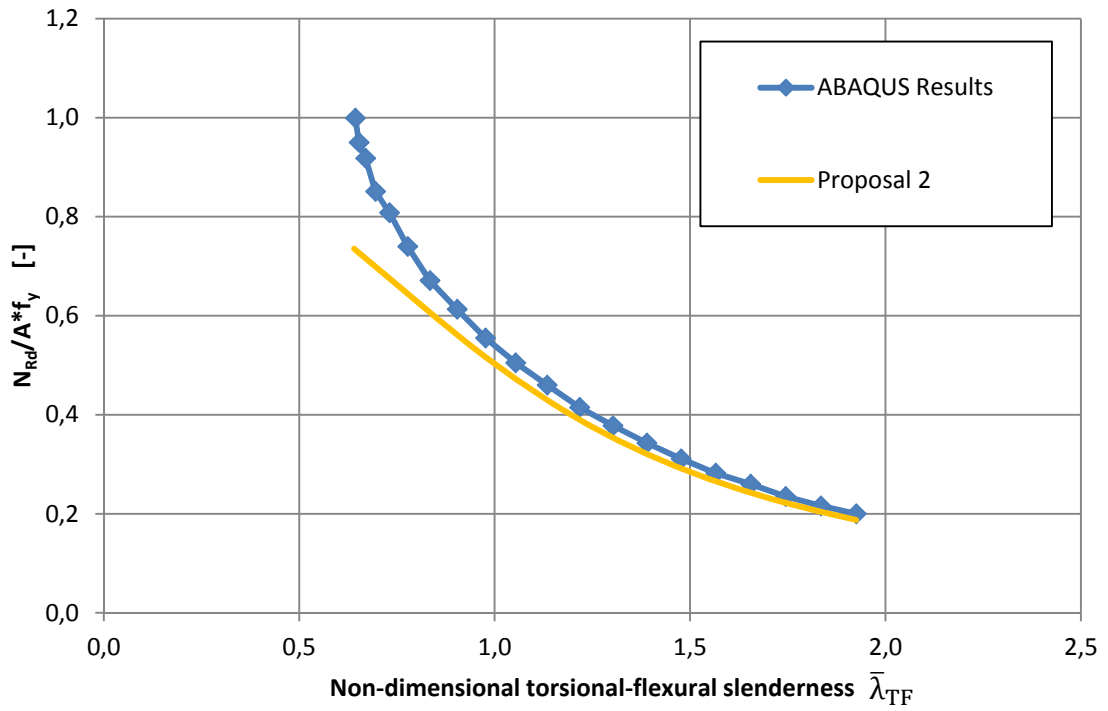


Figure 104: IPE 500-t proposal 2

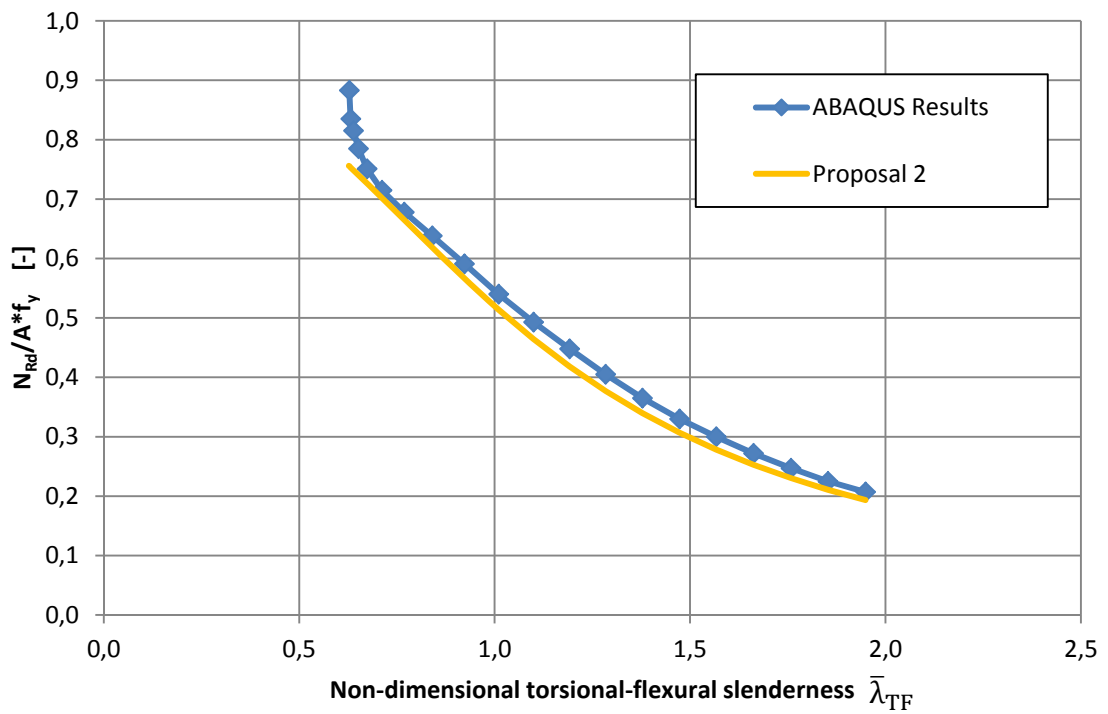


Figure 105: IPE 500-w proposal 2

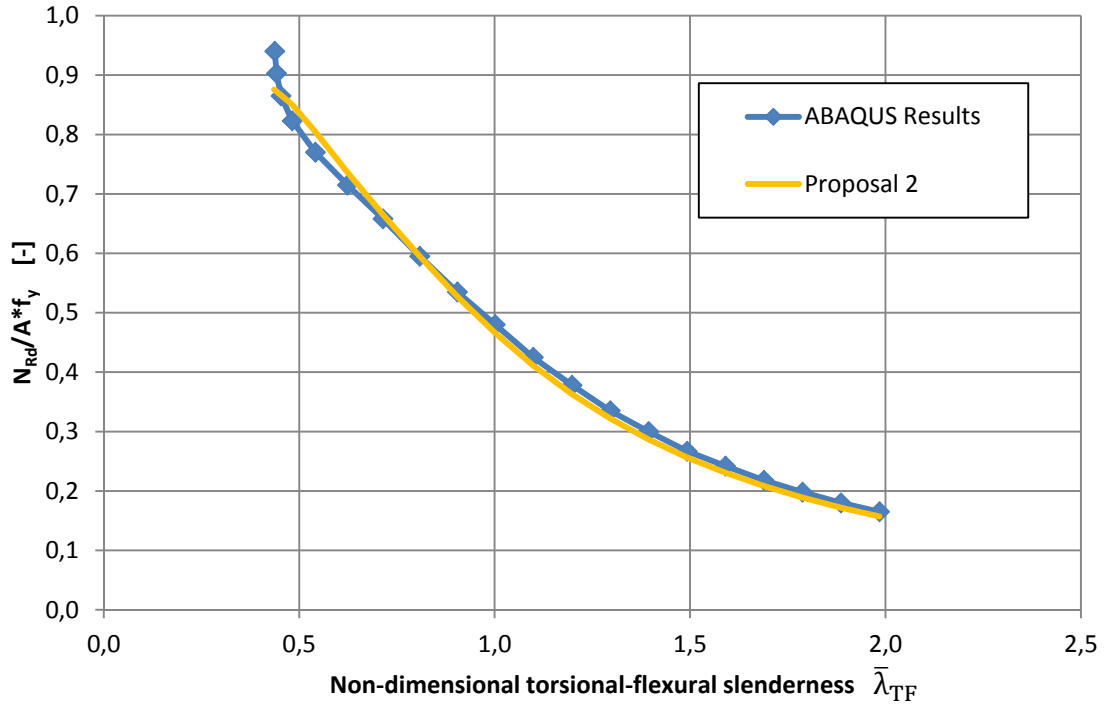


Figure 106: HE-A 500 proposal 2

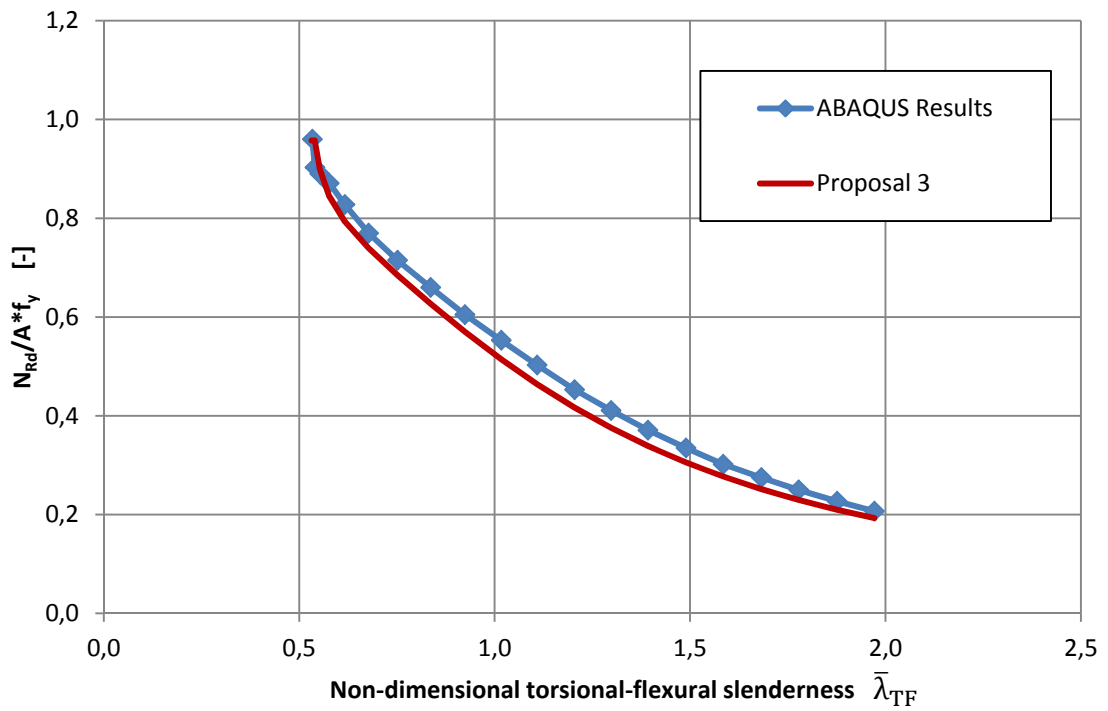


Figure 107: IPE 300 proposal 3

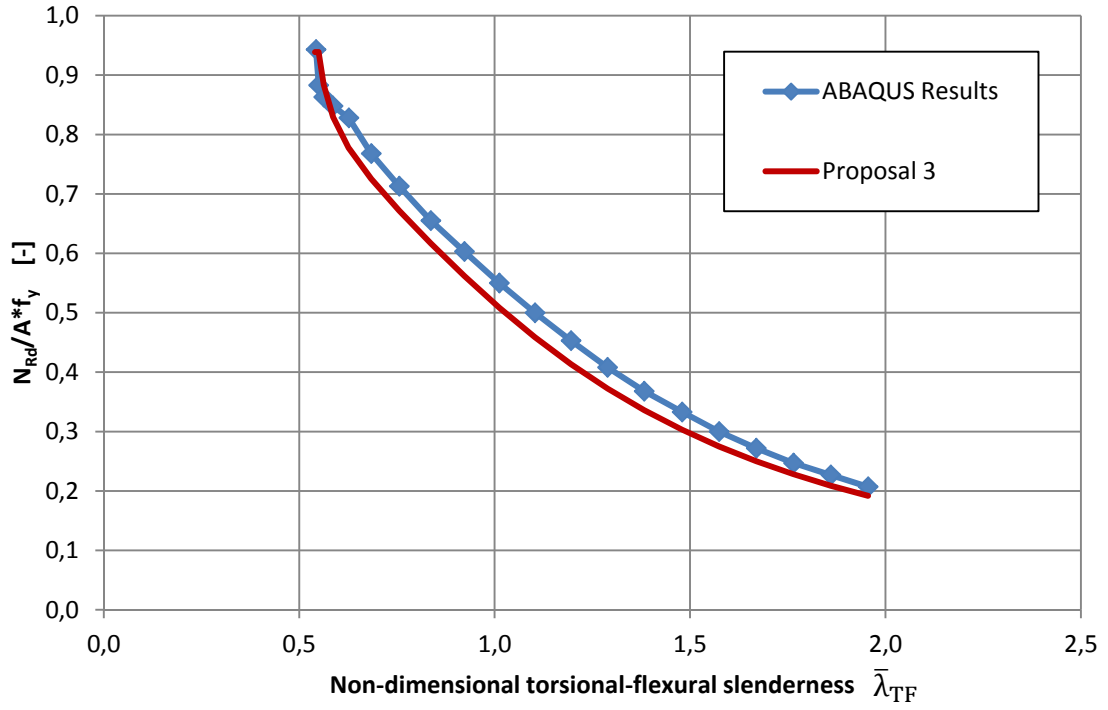


Figure 108: IPE 400 proposal 3

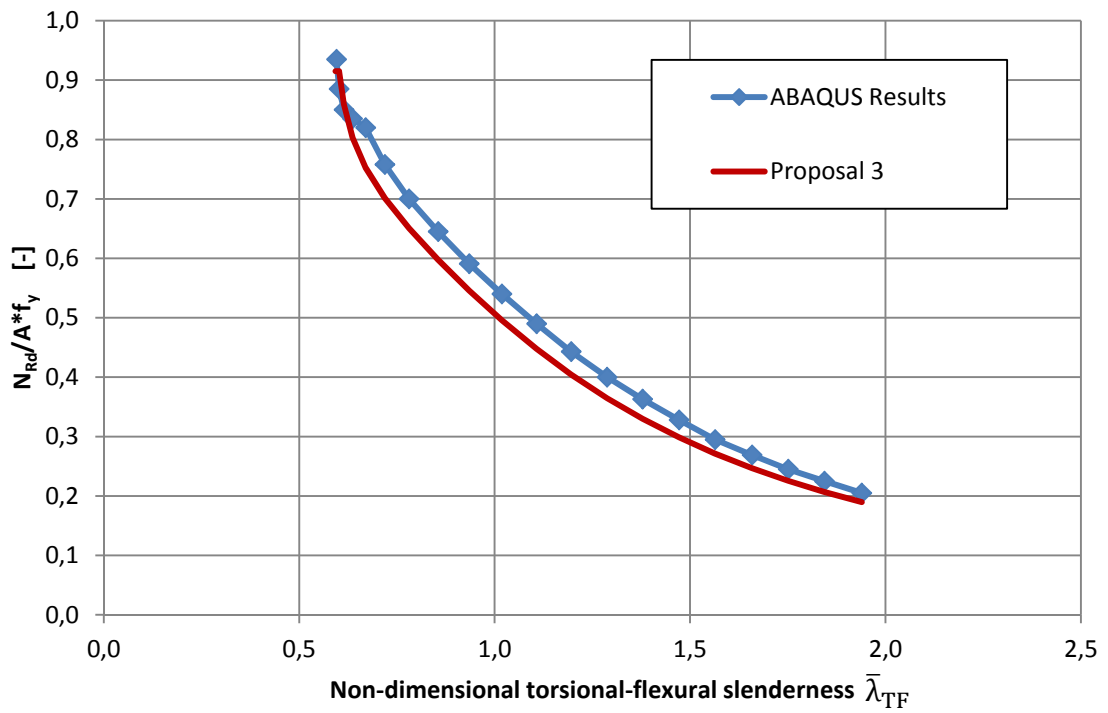


Figure 109: IPE 500 proposal 3

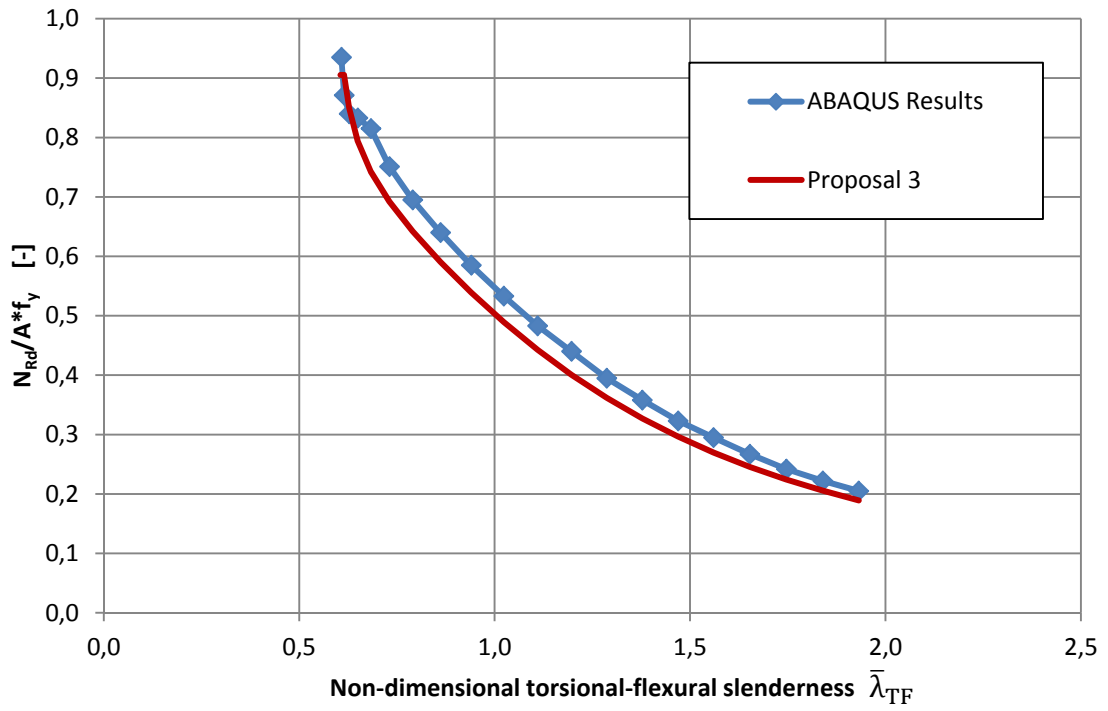


Figure 110: IPE 600 proposal 3

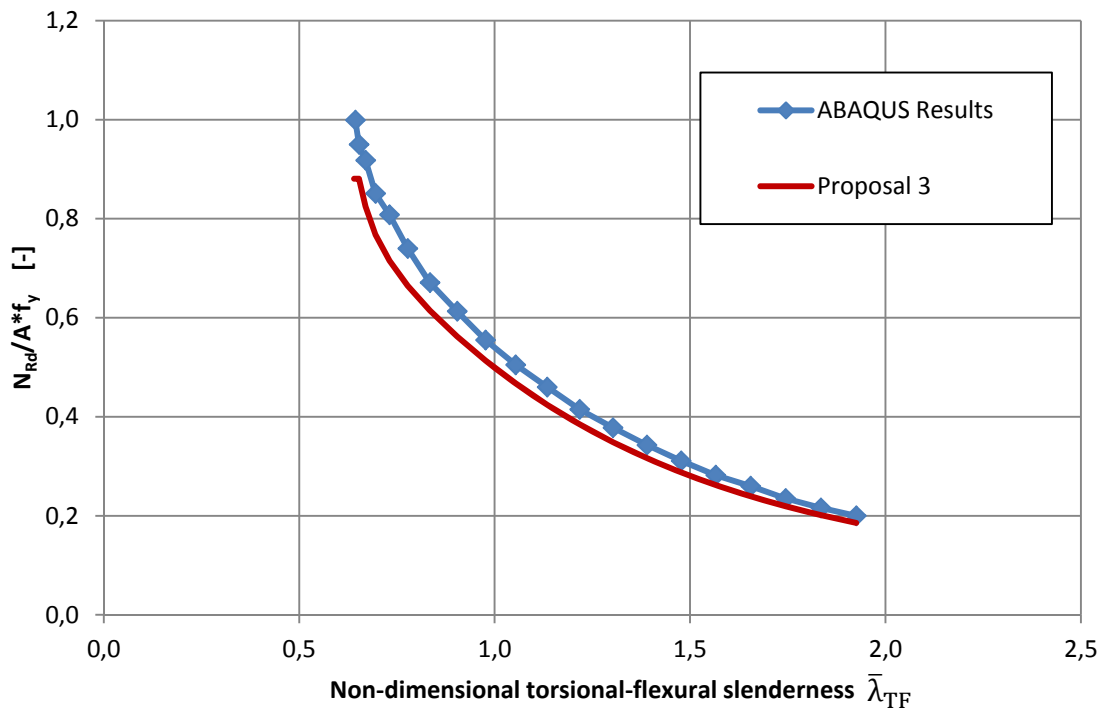


Figure 111: IPE 500-t proposal 3

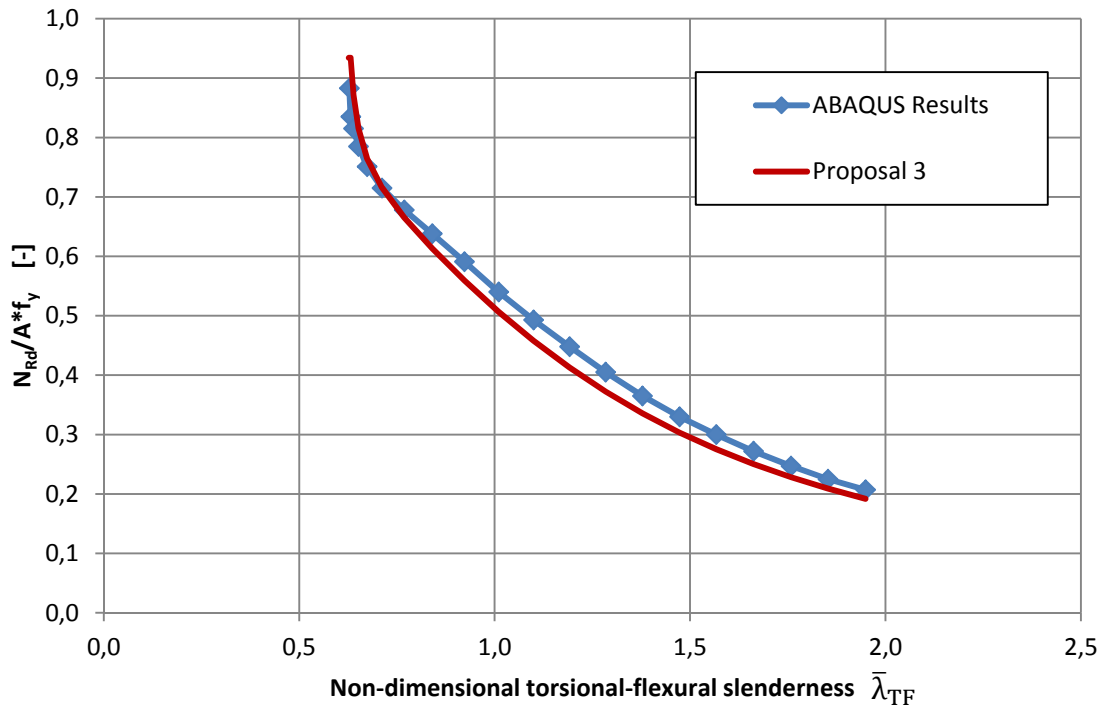


Figure 112: IPE 500-w proposal 3

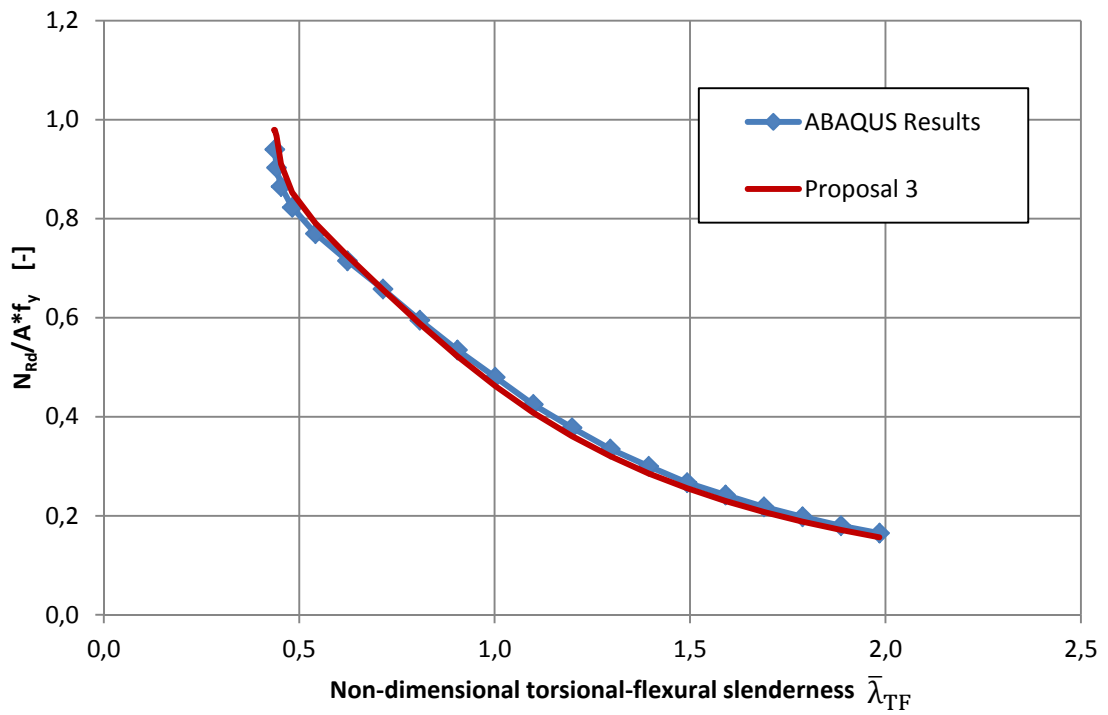


Figure 113: HE-A 500 proposal 3

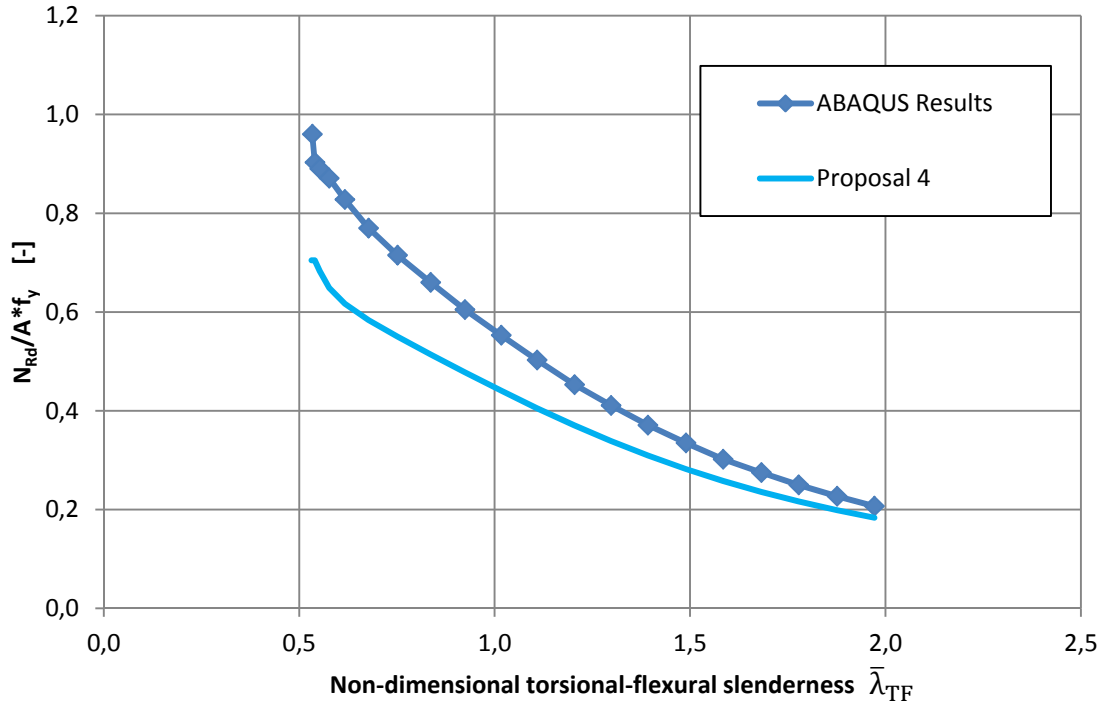


Figure 114: IPE 300 proposal 4

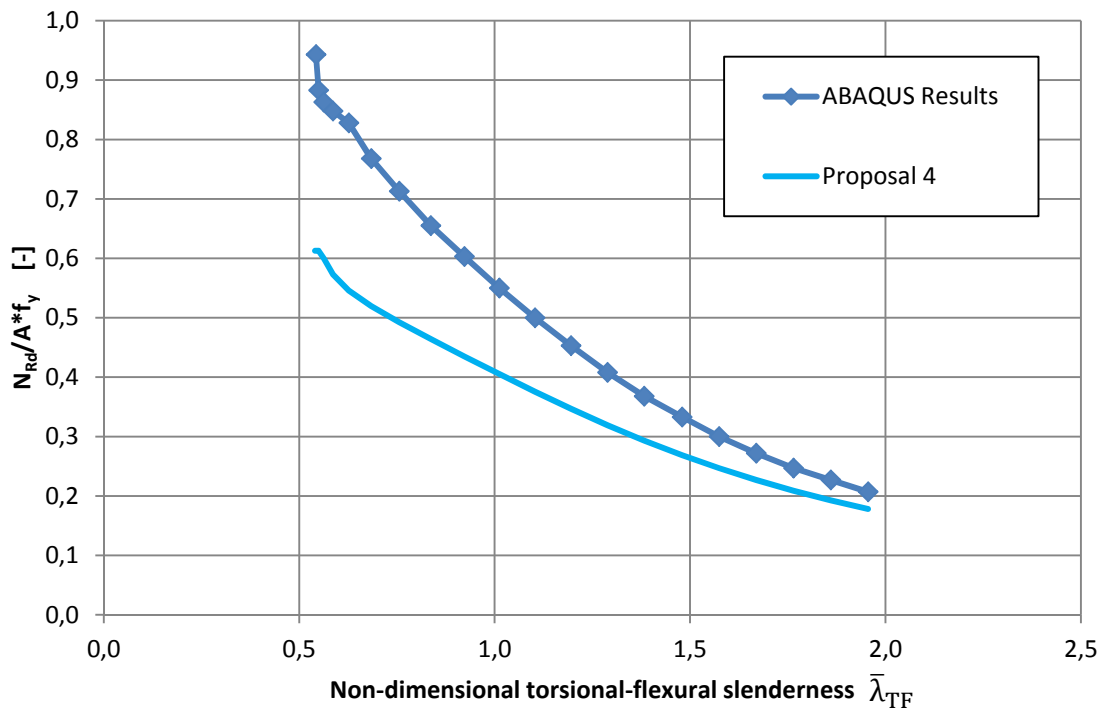


Figure 115: IPE 400 proposal 4

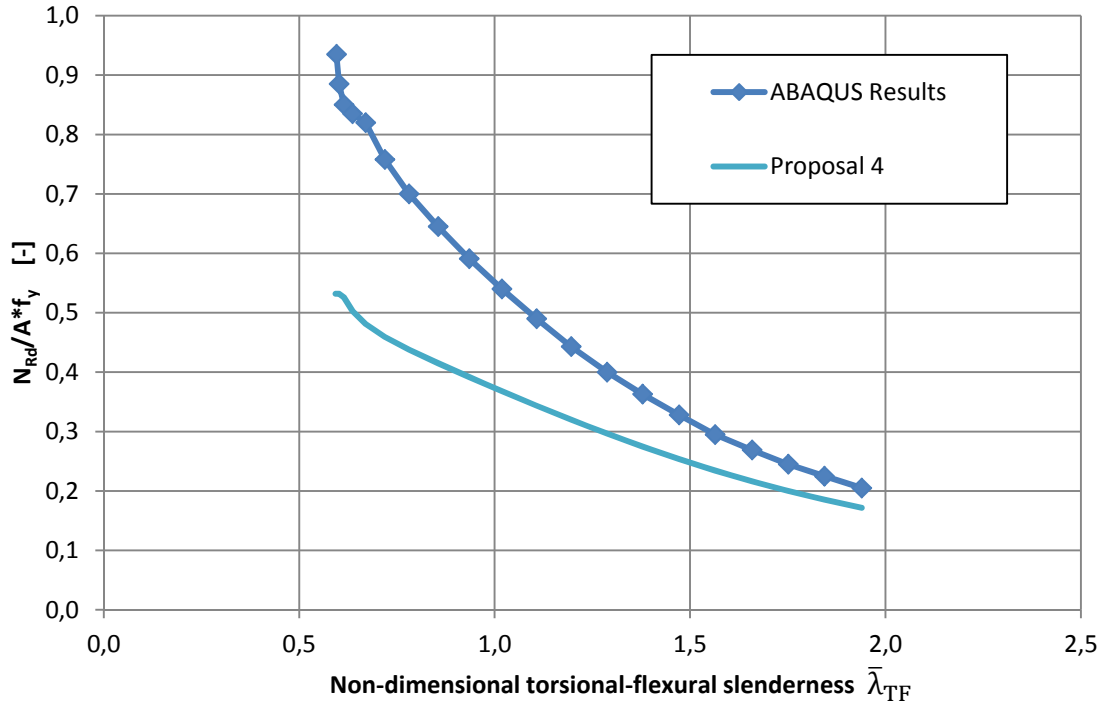


Figure 116: IPE 500 proposal 4

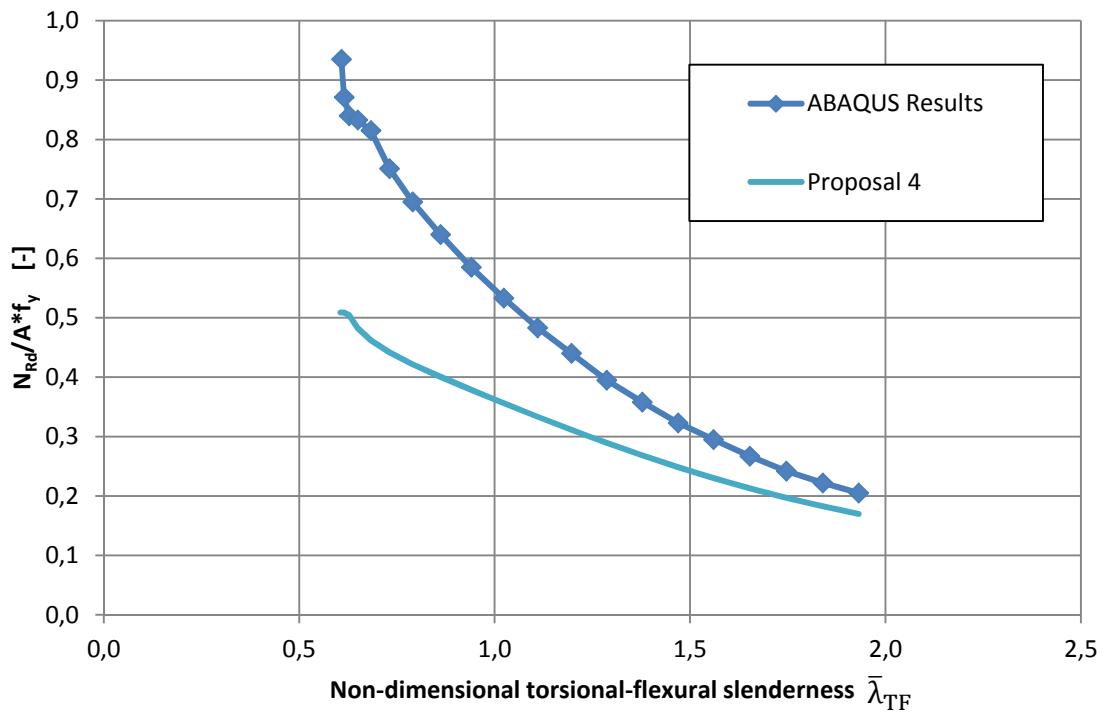


Figure 117: IPE 600 proposal 4

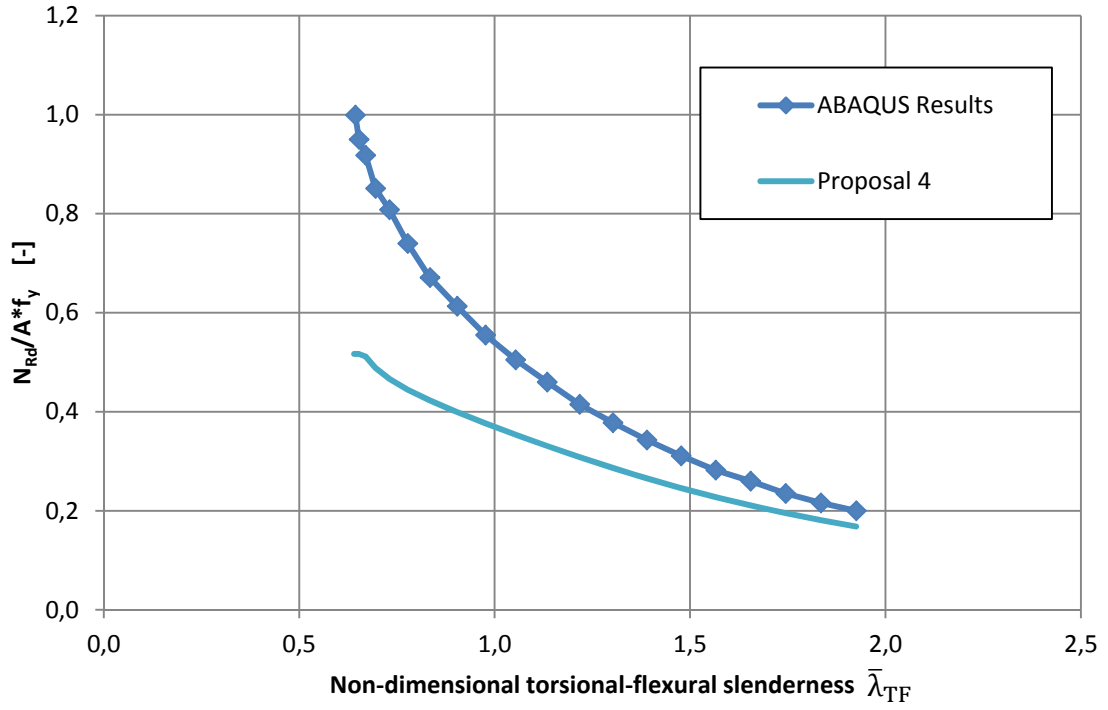


Figure 118: IPE 500-t proposal 4

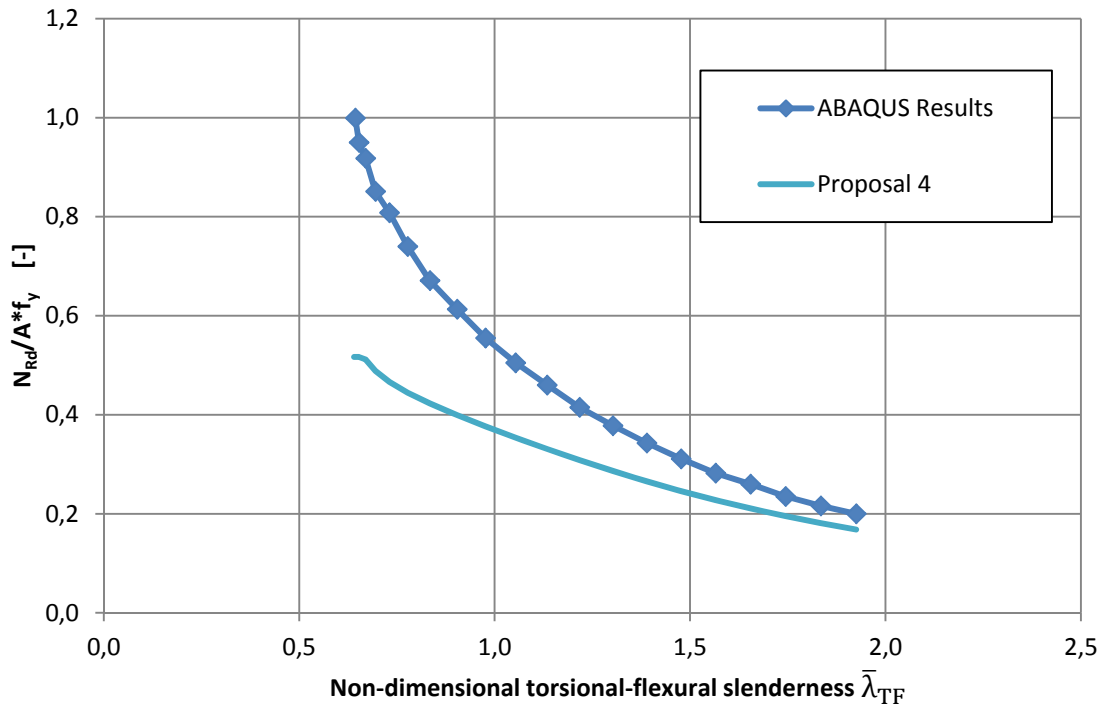


Figure 119: IPE 500-w proposal 4

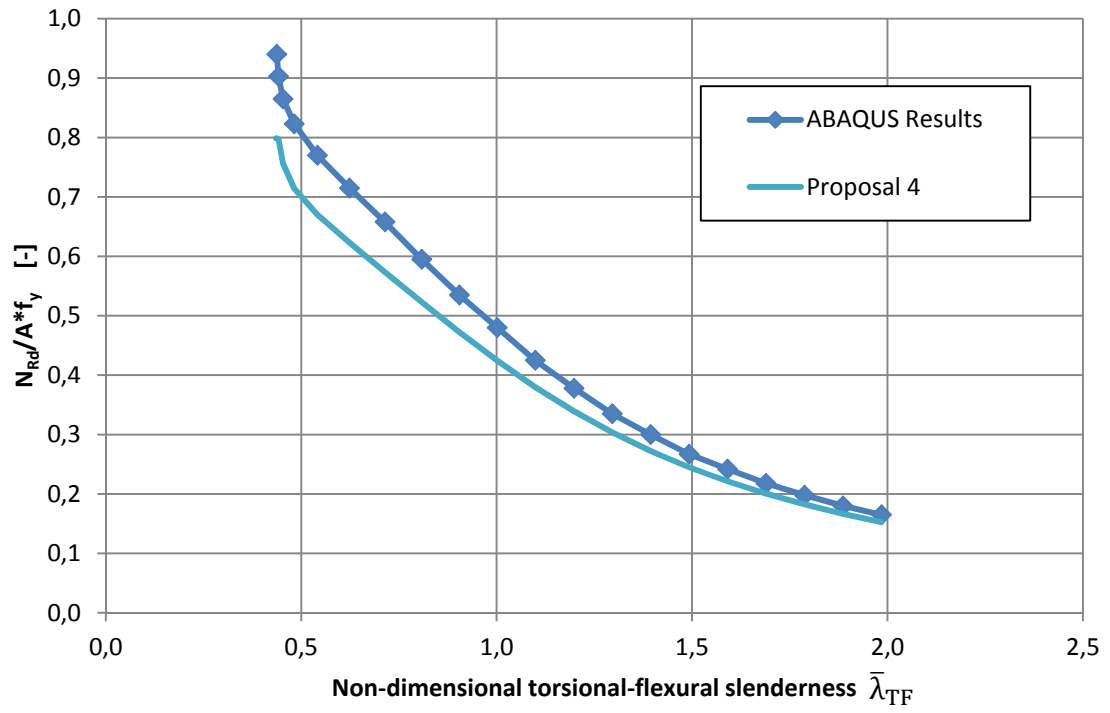


Figure 120: HE-A 500 proposal 4

Bibliography

- [1] European Committee for Standardization, ÖNORM EN 1993-1-1 Eurocode 3: Design of steel structures. Part 1-1: General rules and rules for buildings, Österreichisches Normungsinstitut, 2005.
- [2] A. Taras, R. Greiner and M. G. Puig, “Torsional-Flexural and Lateral-Torsional Buckling Behaviour and Design of Monosymmetric Beam-Columns,” Eurosteel, Hungary, 2011.
- [3] H. Unterweger, “Stahlbau GL,” Institut für Stahlbau, Technische Universität Graz, 2012.
- [4] Austria Standards Institute, ÖNORM EN 1993-1-5 Eurocode 3: Bemessung und Konstruktion von Stahlbauten. Teil 1-5: Plattenförmige Bauteile, Österreichisches Normungsinstitut, 2007.
- [5] Austrian Standards Institute, ÖNORM EN 1993-1-3 Eurocode 3 - Bemessung von Konstruktion von Stahlbauten. Teil 1-3: Allgemeine Regeln - Ergänzende Regeln für kaltgeformte dünnwandige Bauteile und Bleche, Österreichisches Normungsinstitut, 2010.
- [6] PDM Steel, “PDM Steel Service Centers, Inc.,” Thomas Web Solutions, 2012. [Online]. Available: <http://www.pdmsteel.com/steel-beam-splitting-services.html>. [Accessed 27 November 2013].
- [7] P. Kaim, “Spatial Buckling Behaviour of Steel Members under Bending and Compression,” Technische Universität Graz, Graz, 2004.

- [8] SteelConstruction.info, “Steel Construction Products - SteelConstruction.info,” MediaWiki, [Online]. Available: http://www.steelconstruction.info/images/a/a9/Westok_1.png. [Accessed 18 12 2013].
- [9] Wikipedia, 3 December 2013. [Online]. Available: <http://en.wikipedia.org/wiki/Buckling>. [Accessed 7 December 2013].
- [10] Austrian Standards Institute, ÖNORM B 1993-1-1 Eurocode 3: Bemessung und Konstruktion von Stahlbauten Teil 1-1: Allgemeine Bemessungsregeln Nationale Festlegung zu ÖNORM EN 1993-1-1, nationale Erläuterungen und nationale Ergänzungen, Österreichisches Normungsinstitut, 2007.
- [11] Dlubal Software GmbH, “Dlubal Profile,” 2013. [Online]. Available: http://profiles.dlubal.de/App_Forms/Profile_Gewalzte.aspx?iid=4. [Accessed 21 November 2013].